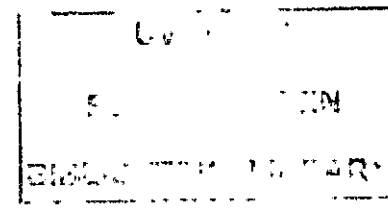

On the evolution of the cataclysmic variable stars from the super soft X-ray sources: AE Aquarii a trial case

Hsien-Chang, Liu

This thesis is submitted to fulfill the requirements
for the qualification Master of Science
in the
Faculty of Natural and Agricultural Sciences,
Department of Physics
of the University of the Free State

Supervisor: Prof. P.J. Meintjes

November
2006

Acknowledgments

Firstly, I sincerely thank the inspirations and gifts from GOD wholeheartedly.

I deeply appreciate Prof. P.J. Meintjes for his initiative and excellent leadership in this study.

I gratefully thank the friendship of Prof. H.C. Swart, Prof. W.D. Roos, Dr. M.J.H. Hoffman, as well as their families.

I also would like to acknowledge the finical support of the NRF.

I appreciate the love of my family, wife and children, also the support of the family of my bosom friend Gevin Haung, as well as too many friends to be mentioned here.

Abstract

It is shown that the wide binary system and short white dwarf spin period of AE Aquarii (AE Aqr), i.e. $P_{spin,1} \sim 33\,\mathrm{s}$, is perfectly reconcilable with a high mass accretion history of the white dwarf. The long orbital period $P_{orb} \sim 9.88\,\mathrm{hr}$ of AE Aqr implies that the binary separation is large enough to accommodate a well-developed accretion disc. The rotation period $P_{spin,1} \sim 33\,\mathrm{s}$ implies that AE Aqr most possibly evolved through a high mass transfer/ accretion phase, where the white dwarf has been spun-up by accretion torques, possibly by an accretion disc. It has also been suggested that in the past AE Aqr could have been a significant X-ray source and possibly even a super soft X-ray source (SSS).

This thesis proposes an investigation of the possible connection between high mass transfer and possible SSS properties. Extending the model calculations related to AE Aqr or cataclysmic variables in general show that the evolved (or slightly evolved), secondary stars filling (or nearly filling) their Roche lobe in systems with large orbital period will drive the highest mass transfer rate, implicitly increasing the probability of potential SSS occurrence. In this situation, the most positive aspect is that the SSS phenomena can be satisfied significantly below the Eddington limit for all filling factors and for all orbital period $P_{orb} \geq 9\,\mathrm{hrs}$.

Concerning the spin-up history of AE Aqr, the results suggest that the spin-up time-scale, rather that the mass transfer time-scale will determine the allowed duration of the run-away mass transfer phase. The model calculations seem also to confirm the magnetic field strength of the white dwarf $B_1 \leq \mathrm{few} \times 10^6\,\mathrm{G}$, which is believed to be the limiting value of the field strength in AE Aqr.

These model calculations readily agree with our conjecture that AE Aqr evolved through a relative brief but violent high mass accretion phase, where the white dwarf has been spun-up to periods $P_{spin,1} \leq 33\,\mathrm{sec}$, during which period the accretion onto the compact white dwarf readily could have sustained stable nuclear burning. In this phase, AE Aqr could have been an extremely bright X-ray source, or SSS. This may be a common phase in the evolution of cataclysmic variables in general.

Contents

Chapter 1

Introduction

1.1 Motivation for this study

Recent developments concerning the evolution of close binaries, in particular the cataclysmic variable AE Aquarii (AE Aqr), seem to suggest that this enigmatic system may have evolved from a high mass transfer (high mass accretion) phase in its past (e.g. Meintjes 2002; Schenker et al. 2002). One consequence of this evolution is that AE Aqr could have been a very luminous Super Soft X-ray Source (SSS) during the high mass accretion phase. It also suggests that this evolution is probably not restricted to AE Aqr alone, but may be common to most cataclysmic variable binary systems. This implies that some SSSs may be, in a way, pre-cataclysmic variable systems. The end-state of each system will depend on the particular initial conditions. This hypothesis will be investigated in detail in this study, especially with respect to AE Aqr.

In order to put this study concerning binary evolution in context, a general introductory discussion concerning the general properties of close binaries will be presented, with emphasis on cataclysmic variables.

1.2 Close Binaries

1.2.1 Binary Separation

Cataclysmic variable (CV) systems consist of two stars: a normal main sequence star of mass M_2 (the secondary star), orbiting a compact companion star of mass M_1 (the primary star) around the system barycentre (or centre-of-mass i.e. CM). The orbital period (P_{orb}) for these systems is usually of the order of $P_{orb} \sim$ few hours. Applying Kepler's law of orbital motion (e.g. Frank, King & Raine 1992, p.47), i.e.

$$4\pi^2 a^3 = G(M_1 + M_2)P_{orb}^2, \qquad (1.1)$$

orbital periods of few hours imply a binary separation a which is (e.g. Frank, King & Raine 1992, p.47)

$$a = 3.53\times10^{10} P_{orb}^{2/3} m_1^{1/3} (1+q)^{1/3} \text{ cm}. \qquad (1.2)$$

In this expression, P_{orb} is the orbital period in hours and $q = m_2 / m_1$ represents the mass ratio of two stars, with m_1 and m_2 representing the primary and secondary mass respectively, in solar mass units ($M_\odot \approx 2\times10^{33}$ g ; i.e. $m_1 = M_1 / M_\odot$, $m_2 = M_2 / M_\odot$). For typical one solar mass stars, binary orbital period $P_{orb} \sim$ few hours, the ratio of the binary separation with respect to the diameter of the sun ($D_\odot \approx 1.4\times10^{11}$ cm) is

$$\frac{a}{D_\odot} \approx 0.7, \qquad (1.3)$$

Hence most of these systems can easily fit into the sun. This results in a significant gravitational interaction between the two stars. This gravitational interaction, in principle, is the driving force behind the peculiar transient emission (outbursts or flares) these systems display, and will be discussed briefly.

1.2.2 Gravitational interaction in close binaries: Roche Geometry

A detailed analysis of the geometry of orbiting stars is complex and requires detailed computer modelling. However, the problem of the gravitational interaction can be simplified (along the lines pioneered by Edouard Roche in the nineteenth century) by assuming that tidal forces have forced the stars into a circular orbit and that the mass of each star can be considered to be concentrated in the star's centre (both of which are reasonable approximations). In terms of the Roche description, the gravitational potential field can be considered as nested potential wells, bounded by surfaces of equal effective gravitational potential energy, i.e. so-called equipotential surfaces (see Figure 1.1). It can be seen that the innermost equipotentials are approximately circular, but on scales comparable to the binary separation the tidal force distorts the outer wells considerably.

We can write the Roche gravitational potential Φ at any point specified by the vector $\bar{r}$ as the sum of the potentials of the two stars (with masses M_1 and M_2 located at $\bar{r}_1$ and $\bar{r}_2$ respectively) and a third term due to the centrifugal force. The Roche potential function with respect to CM is (e.g. Frank, King & Raine 1992, p.48)

$$\Phi = -\frac{GM_1}{|\bar{r}-\bar{r}_1|} - \frac{GM_2}{|\bar{r}-\bar{r}_2|} - \frac{1}{2}(\Omega_{orb} \times \bar{r})^2 \qquad (1.4)$$

where Ω_{orb} is the orbital angular frequency and the first two terms represent the gravitational potential of the primary and secondary star respectively. The third term represents the centrifugal effect of the binary orbiting its centre-of-mass (CM).

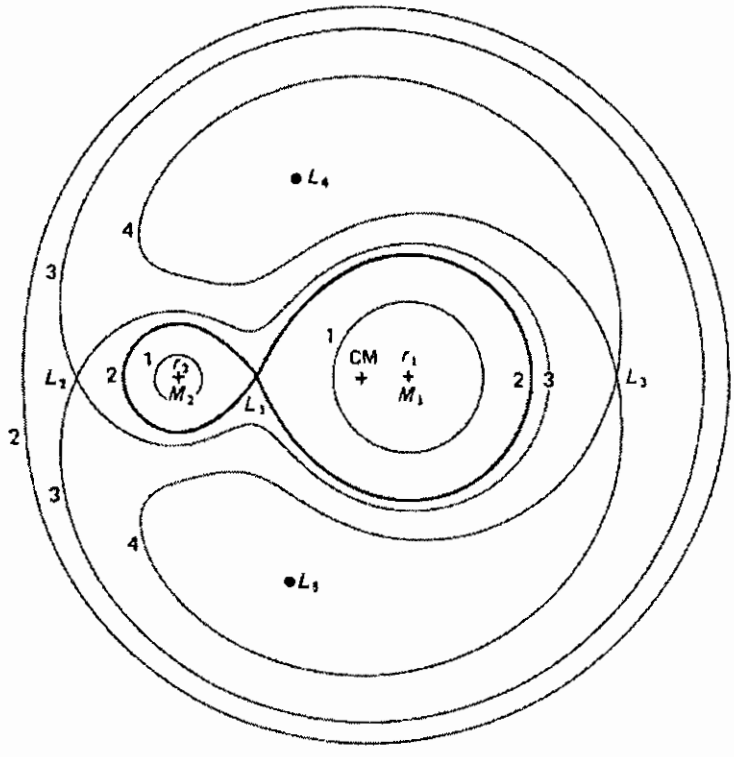

Fig 1.1 A plot of equipotentials of binary stars (Frank, King & Raine 1992, p.49)

The equipotentials for several values of Φ are plotted in Fig 1.1. The innermost critical equipotential surface is called the *Roche lobe*. The point at which they touch is the inner Lagrangian point, or L_1. (There are other Lagrangian points of less significance). The L_1 Lagrangian point defines a point between the two stars, considered as point masses, where the gravity of the two stars, together with the centrifugal force, exactly balances, defining a region of zero effective gravity. If neither star fills its Roche lobe, the binary is described as *detached*. If one star fills its Roche lobe the binary is described as *semi-detached* (all cataclysmic variables are semi-detached systems). If both stars fill or overfill their Roche lobes, the binary is said to be a *contact binary* (e.g. W UMa stars) (Hellier 2001, p.22).

The Roche geometry is completely specified by the mass ratio q ($= m_2 / m_1$) and the binary separation a (obtained from Kepler's law). However, it does not lead to simple formulae for quantities such as the distance to L_1, etc. Instead, one has to model the full Roche geometry numerically, and distil the results empirically into formulae that are accurate to ~1% (see Warner 1995 for a detailed account).

The distance of the L_1 point from the centre of the primary is given by (e.g. Frank, King, Raine 2002, p.54)

$$R_{L1} = a(0.500 - 0.227 \log q) \quad \text{for } 0.1 < q < 10. \tag{1.5}$$

This basically defines the dimension of the Roche lobe of the primary star, shown to be a significant fraction of the orbital separation for most systems.

1.2.3 Roche gravity field

Isolated single stars are spherical, pulled into the most compact configuration possible by gravity. Similarly, stars in a wide binary, where the separation is much greater than their physical sizes, are also approximately spherical. In a close binary, where the primary is a compact star, the same can be said of the compact primary star, but not of the much larger secondary star. Instead, the less dense secondary is distorted by the gravity of its close compact companion, which pulls at the fluffy outer layers. If the two stars are close, the secondary becomes increasingly distorted until the material nearest the primary, close to the L_1 region, experiences a greater gravitational attraction towards the compact object than the material at the back of the star. Thus the secondary star is distorted into a teardrop shape, which will have important consequences for the material in the envelope, close to L_1, as will be discussed later.

By using the effective Roche potential (eqn 1.4), the effective gravitational acceleration anywhere in the binary can be estimated by

$$g_{eff} = -\nabla \Phi_R, \tag{1.6}$$

resulting in

$$g_{eff} = \frac{GM_2}{|\bar{r}_2 - \bar{r}|^2}\bar{e}_2 + \frac{GM_1}{|\bar{r}_1 - \bar{r}|^2}\bar{e}_1 + \Omega_{orb}^2 \bar{R}. \tag{1.7}$$

Here $\bar{r}_1$, $\bar{r}_2$ and $\bar{r}$ represent the coordinate vectors from the centre of mass of the system to the centre of the primary, the secondary and an arbitrary point (P) in the gravity field, respectively. In this expression, $\bar{R}$ represents the horizontal component of $\bar{r}$ in the equatorial plane. The unit vectors $\bar{e}_1$ and $\bar{e}_2$ point from P to the centres of the primary and secondary stars respectively. The coordinate system can be chosen such that the y-axis is directed along the line-of-centres between the two stars (the

positive y-axis extends from the CM of the binary to the centre of the secondary star). As an example we consider only the effective gravitational acceleration along the line of centres between the two stars, i.e. $(x,z)=0$. Here the effective gravity profile can be written as follows (e.g. Meintjes 2004)

$$g_{y,eff} = \frac{GM_2}{(y_2-y)^2}\bar{e}_{y,2} + \frac{GM_1}{(y_1-y)^2}\bar{e}_{y,1} + \Omega_{orb}^2 y\bar{e}_y \qquad (1.8)$$

where y_1, y_2 and y represent the distances from the CM to the centres of the primary, secondary and P_y (projection of P on y-axis), respectively, and where $\bar{e}_{y,1}$, $\bar{e}_{y,2}$ and $\bar{e}_y$ represent the unit vectors pointing from P, to the centres of the primary (negative y-axis) and secondary (positive y-axis) stars, as well as to the CM on the line of the centres.

This can be parameterized in terms of binary parameters (see Meintjes 2004), i.e. the binary separation a (eqn 1.2) and the size of the Roche lobe radius R_{L1} (eqn 1.5). This gives the effective gravity at any arbitrary point on the line of the centres as (Meintjes 2004)

$$g_{y,eff} = \frac{GM_2}{(a-\alpha R_{L1})^2}\bar{e}_{y,2} + \frac{GM_1}{(\alpha R_{L1})^2}\bar{e}_{y,1} + \Omega_{orb}^2(y_1-\alpha R_{L1})\bar{e}_y \qquad (1.9)$$

with α representing the fractional distance of the point P_y with respect to the distance between the centre of the compact object and the L_1 point, i.e. R_{L1}, and a representing the binary separation (see Fig 1.2) (Note that $\alpha = 1$ corresponds to the L_1 point).

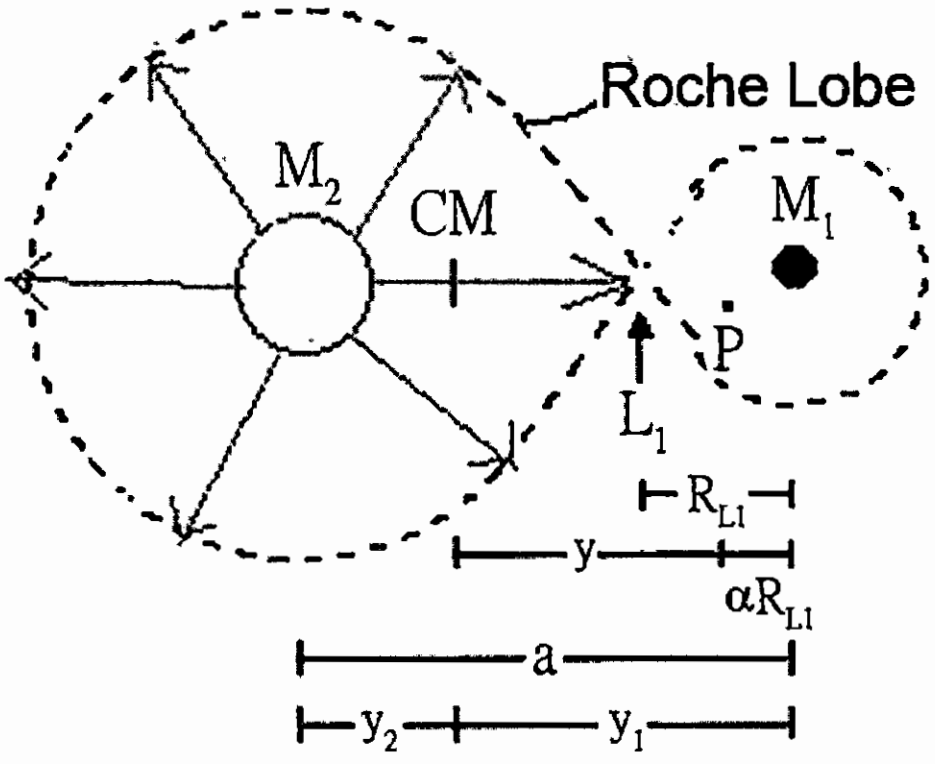

Fig 1.2 The parameters of the binary (with mass ratio $q > 1$)

For illustration purposes, a binary with orbital period $P_{orb} = 9.88\,\mathrm{hr}$, $M_1 = 0.87 M_\odot$ and mass ratio of $q = 0.69$ is selected. The resultant effective gravitational acceleration that material will experience at various points along the line of centres between the two stars are displayed in Table 1.

α	g_{eff} (m s^{-2})
1	0
0.9	60
0.8	110
0.7	190

Table 1: Effective gravity

It can be seen that the effective gravity at L_1 (i.e. $\alpha = 1$) approaches zero. This has important consequences. Thermal motion of particles in the tenuous envelope of secondary star, in the vicinity of L_1, will result in a stream of particles crossing L_1,

resulting in mass transfer from the secondary to the primary. The stream crosses the funnel at L_1 with the speed of sound, i.e. $c_s \sim 10\,\mathrm{km\,s^{-1}}$. After crossing L_1, the stream will rapidly accelerate into the potential well of the white dwarf (WD) (e.g. Table 1). However, since the stream squirts over L_1 from a moving platform (e.g. with velocity of $v_{\phi,L1} \sim 1000\,\mathrm{km\,s^{-1}}$ across L_1 in the binary plane) (e.g. Frank, King & Raine 1992, p.54) the material will follow a ballistic trajectory, passing the white dwarf with a free-fall velocity $v_{ff} \sim 10^5\,\mathrm{km\,s^{-1}}$, and will follow a trajectory that conserves its initial orbital angular momentum.

1.2.4 Mass transfer through L_1

Before the fate of the stream passing the white dwarf is discussed, it is appropriate to highlight some important aspects surrounding the mass transfer through L_1. As a result of the tidal distortion of the secondary star, its tenuous envelope may be close to the L_1 region. Pushed from behind by the pressure of the stellar atmosphere, the material squirts through the L_1 funnel at roughly the speed of sound.

The mass transfer rate $-\dot{M}_2$ through the Lagrangian point L_1 (e.g. Plavec et al. 1973; Lubow and Shu 1975; Meyer and Meyer-Hofmeister 1983; Pringle 1985; D'Antona et al. 1989) can be estimated by employing energy conservation arguments, resulting in

$$-\dot{M}_2 \approx \frac{1}{4\pi}\rho_{L1} c_s^3 P_{orb}^2\ \mathrm{g\,s^{-1}}, \tag{1.10}$$

where ρ_{L1} is the density of the gas flow at L_1, c_s is the isothermal sound speed, and P_{orb} is the orbital period of the system. It has been shown that the density ρ_{L1} of the gas in the secondary star's atmosphere scales as (e.g. Ritter 1988)

$$\rho_{L1} = \frac{1}{\sqrt{e}}\rho_{phot} \exp\frac{-(R_{L2}-R_{p2})}{H_p}\ \mathrm{g\,cm^{-3}}, \tag{1.11}$$

where ρ_{phot} is the photospheric density of the late type star and is of the order of $\rho_{phot} \sim 10^{-6}\,\mathrm{g\,cm^{-3}}$ (e.g. Frank, King, Raine 2002, p.353). Here R_{L2}, R_{p2}, $H_p (= c_s^2 R_{p2}^2 / GM_2)$ represent the Roche lobe radius, the photospheric radius of the

secondary star, and the stellar scale height respectively (e.g. D'Antona et al. 1989; Meintjes 2004). For typical secondary stars with surface temperature $T_2 \sim 4000\,\mathrm{K}$, the isothermal sound speed is (e.g. Frank, King & Raine 1992, p.13; Meintjes 2004)

$$c_s \approx 6\times10^5 (\frac{\varepsilon}{1})^{-1/2} (\frac{T_2}{4000\,\mathrm{K}})^{1/2}\ \mathrm{cm\,s^{-1}} \qquad (1.12)$$

where ε represents the mean molecular mass of the gas and T_2 is the surface temperature of the secondary star.

It can be seen that the mass transfer process depends rather sensitively on the scale height of the secondary star's atmosphere, $\delta = (R_{L2} - R_{p2})/H_p$. This parameter is of fundamental importance in determining the magnitude of the mass transfer from the secondary to the primary star. The mass transfer from the secondary to the primary star on the other hand, in conjunction with angular momentum losses, determine the binary evolution, which in turn feed back to influence the scale height and mass transfer. This intricate feed-back loop is intimately tied to the overall evolution of the binary system and will be discussed in detail in Chapter 3.

1.2.5 Accretion of mass

After the brief discussion of the mass transfer through L_1, the ultimate fate of the ballistic stream accelerated into the Roche lobe of the primary star needs to be considered. In cataclysmic variables there are several vital parameters influencing the ultimate mode of mass accretion onto the compact object, the most important of which are the physical size of the binary, and the magnetosphere of the primary. The physical size of the binary determines the initial specific angular momentum with which material is injected across L_1, i.e.

$$J_{L1} \sim R_{L1} \times v_{\phi,L1} \qquad (1.13)$$

where $R_{L1} \sim f(q)a$ [with $f(q) = 0.5 - 0.227\log q$; $q = m_2/m_1$] and $v_{\phi,L1} \approx R_{L1}\Omega_{orb} \approx (\frac{m_1}{m_1+m_2})a\Omega_{orb}$ (e.g. Frank, King & Raine 1992, p.54). In most binaries $v_{\phi,L1} \sim 1000\,\mathrm{km\,s^{-1}}$ and $R_{L1} \sim \mathrm{few}\times10^{10}\,\mathrm{cm}$, resulting in enormous initial angular momentum, e.g.

$$J_{L1} \sim \text{few} \times 10^{18}\ \text{cm}^2\ \text{s}^{-1}. \qquad (1.14)$$

Accretion of gas onto the white dwarf will only be possible after the material rids itself of this enormous load of angular momentum. The other parameter influencing the mode of interaction of the gas stream with the compact white dwarf is the physical extent of the magnetosphere. The quantity determining the extent of the magnetosphere is the magnetic moment (μ) of the white dwarf, i.e.

$$\mu \sim B_1 R_1^3, \qquad (1.15)$$

where B_1 and R_1 represent respectively the average surface magnetic field strength and the radius of the white dwarf. For cataclysmic variables consisting of a compact white dwarf with size $R_1 \sim 10^9$ cm and magnetic field ranging from $B_1 \sim 10^4 - 10^7$ G, the magnetic moments range between

$$10^{31}\ \text{G cm}^3 \le \mu \le 10^{34}\ \text{G cm}^3. \qquad (1.16)$$

This range of a factor ~ 1000 in magnetic dipole moment has an enormous influence on the various modes of interaction of the stream with the white dwarf and magnetosphere. A stream of material with angular momentum $J \sim 10^{18}\ \text{cm}^2\ \text{s}^{-1}$ approaching a white dwarf with magnetic dipole moment $\mu_{31} \sim 1$ (in unit of $10^{31}\ \text{G cm}^3$) will be able to pass by relatively unhindered, following a path depicted in Fig 1.3 a. Conserving angular momentum, it will eventually settle in a circular orbit at the so-called circularization radius. On the other hand, if the white dwarf has a magnetic moment of $\mu \sim 10^{34}\ \text{G cm}^3$ the stream will most probably ram directly into the magnetosphere, resulting in a mode of accretion inferred from the so-called polars (discussed in Chapter 2).

A physically instructive estimate of the circularization radius is obtained through conservation of the angular momentum of the stream across L_1. The specific angular momentum of material at the L_1 point is $R_{L1} \times v_{\phi,L1}$, where the velocity $v_{\phi,L1}$ at R_{L1} is $2\pi R_{L1} / P_{orb}$. The specific angular momentum after circularization is $R_{circ} \times v_{kep}$, where the Keplerian velocity $v_{kep} = (\frac{GM_1}{R_{circ}})^{1/2}$. Equating the expression for angular momentum then gives (e.g. Hellier 2001 p.24)

$$R_{circ} = \frac{4\pi^2 R_{L1}^4}{G M_1 P_{orb}^2}. \qquad (1.17)$$

Using Kepler's law of orbital motion (eqn 1.1), this expression can be written as (e.g. Frank, King & Raine 1992, p.56)

$$\frac{R_{circ}}{a} = (1+q)(\frac{R_{L1}}{a})^4. \qquad (1.18)$$

For most realistic binary parameters (e.g. Frank, King & Raine 1992, p.56)

$$R_{circ} \geq 3.5\times10^9 P_{hr}^{2/3} \text{ cm}. \qquad (1.19)$$

To understand what follows, three concepts must be kept in mind. First, material in a smaller orbit moves faster (from Kepler's law). Second, material in a smaller orbit has a lower specific angular momentum (the increase in speed is not enough to offset the decrease in radius required to conserve angular momentum). Third, by transferring into a smaller orbit, material liberates gravitational potential energy. Thus, within the ring of material orbiting at the circularization radius, blobs of material slightly nearer the primary will orbit slightly faster, causing friction as they slide past blobs further out. The friction and turbulence heat the gas so that energy is radiated away, resulting in the material losing gravitational potential energy. This means that some of the material has to migrate to smaller orbits in the process. However, to conserve the overall angular momentum, other material must move to larger orbits. Thus overall, the ring spreads out into a thin disc (see Fig 1.3 c). The disc continues to spread until the inner edge meets the primary, in the case of a non-magnetic system, or the white dwarf magnetosphere. The inward ram pressure of the gas and magnetosphere pressure will constitute a boundary, i.e. the so-called Alfvén radius. Material continually flows through the disc, spiralling inwards to ever smaller orbits, and may eventually accrete onto the white dwarf. Angular momentum flows outwards through the disc, enabling the inward flow of material and consequent release of energy. At the outer edge of the disc, tidal interactions with the secondary star transfer the angular momentum to the orbit of the secondary. This limits the outward spread of the disc. The disc is replenished by the mass-transfer stream from the secondary, which brings both fresh material and angular momentum that has to be processed. The thin

disc of circling material, destined to settle onto the compact star lurking at its centre, is called an *accretion disc* (Fig 1.3).

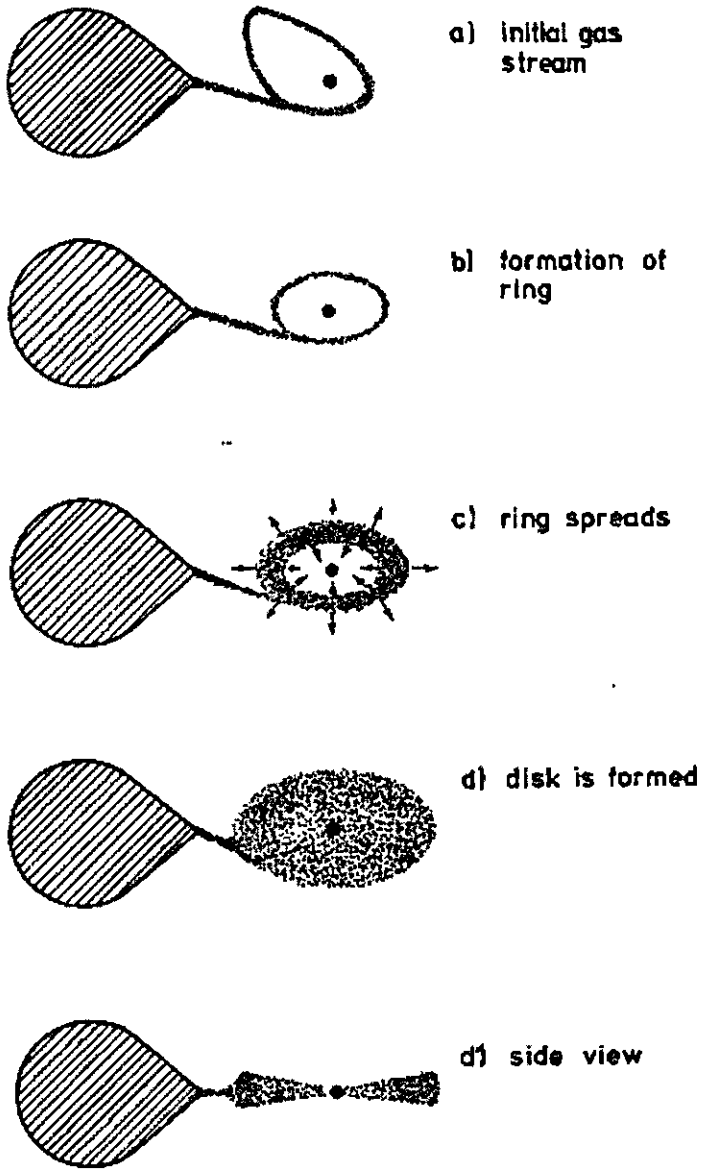

Fig 1.3 Illustration of the formation of the ring and subsequently the disc in a close binary. (Verbunt 1982).

The alternative scenario of the stream interacting with a white dwarf of magnetic moment $\mu_{34} \sim 1$ results in a completely different scenario. In most scenarios the stream will be intersected by the magnetosphere, resulting in the material being channeled by the magnetic field onto the surface, which results in the liberation of gravitational potential energy into heat and radiation energy. Most of the general

properties of CVs - in particular the object of interest, AE Aqr - will be revealed in the next chapter.

1.3 Outline of this study

This thesis will be structured as follows:
In Chapter 2 the general properties of CVs and AE Aqr will be reviewed.

In Chapter 3 the theoretical aspects influencing binary evolution will be reviewed, and will be used to highlight the model calculations, focusing on the object of interest, i.e. AE Aqr.

In Chapter 4 the model calculations and a brief discussion will be presented regarding the possible evolutionary scenarios applicable to the AE Aqr system.

A brief conclusion will be presented in Chapter 5.

Chapter 2

The magnetic cataclysmic variables: Introducing AE Aquarii

Most of the transient emission features in the magnetic cataclysmic variables are driven by the very complex interaction between the mass transfer stream and the secondary star and white dwarf magnetic field. For example, it has been shown (Beardmore & Osborne 1997) that the shot noise behaviour of the X-ray emission in polars can be attributed to blob-like accretion. It has been shown (Meintjes 2004) that the mass transfer stream in the cataclysmic variables can be fragmented by the secondary star magnetic field, explaining the blob-like nature of the mass flow. To put all these in context, a brief theoretical overview of the most relevant magnetohydrodynamic processes will be presented.

2.1 The magnetosphere-flow interaction

Most astrophysical plasmas can be considered as highly conducting fluids. The fields in a highly conducting fluid ($\sigma \to \infty$) governed by low velocity $\bar{v}$ (i.e. $\frac{\bar{v}}{c} \to 0$) are deduced from Maxwell's equations. In a reference frame co-moving with the fluid, Ohm's law states that the relation between the current density ($\bar{J}'$) and electric field is

$$\bar{J}' = \sigma \bar{E}', \tag{2.1}$$

where the Coulomb conductivity $\sigma \approx 3.2 \times 10^6 T^{3/2}$ (esu). The fluids transform to the laboratory system as follows (symbols with ' represent co-moving system with the fluid and symbols without ' represent laboratory system):

$$\bar{E}' = \gamma(\bar{E} + \frac{1}{c}(\bar{v} \times \bar{B})) \text{ and} \tag{2.2}$$

$$\bar{B}' = \gamma(\bar{B} - \frac{1}{c}(\bar{v} \times \bar{E})). \tag{2.3}$$

For non-relativistic fluids $\beta = \frac{\bar{v}}{c} << 1$; we get $\gamma = 1/\sqrt{1-\beta^2} \to 1$ and

$$\bar{E}' = \bar{E} + \frac{1}{c}(\bar{v} \times \bar{B}) \text{ and} \tag{2.4}$$

$$\bar{B}' = \bar{B} - \frac{1}{c}(\bar{v} \times \bar{E}). \tag{2.4}$$

If the conductivity of the medium is very high (i.e. $\sigma \to \infty$), the E-field in the co-moving reference frame $\bar{E}' \to 0$, hence

$$\bar{E} = -\frac{1}{c}\bar{v} \times \bar{B}. \tag{2.5}$$

Similarly for the B-field

$$\begin{aligned}
\bar{B}' &= \bar{B} - \frac{1}{c}[\bar{v} \times \bar{E}] \\
&= \bar{B} + \frac{1}{c^2}[\bar{v} \times (\bar{v} \times \bar{B})] \\
&= \bar{B} + \frac{1}{c^2}[\bar{v}(\bar{v} \cdot \bar{B}) - \bar{B}(\bar{v} \cdot \bar{v})] \\
&= \bar{B} - \bar{B}(\frac{v}{c})^2 \\
&= \bar{B} \text{ (neglecting } (\frac{v}{c})^2 \text{ term).}
\end{aligned} \tag{2.6}$$

If the characteristic scale of the field is L and the characteristic time of change in the fluid is $\tau = \frac{L}{v}$, it follows from Ampere's law, i.e.

$$\bar{\nabla} \times \bar{B} = \frac{4\pi}{c}\bar{J} + \frac{1}{c}\frac{\partial \bar{E}}{\partial t}, \tag{2.7}$$

and

$$c(\bar{\nabla}\times\bar{B}) = 4\pi\bar{J} + \frac{v}{L}\bar{E}. \tag{2.8}$$

On dimensional grounds one can show, by using $\bar{E} = -\frac{1}{c}(\bar{v}\times\bar{B})$, that

$$\frac{cB}{L} \approx 4\pi J - (\frac{v}{c})^2 \frac{cB}{L}. \tag{2.9}$$

Hence it is obvious that the LHS is $\frac{cB}{L}$ and that the magnitude of the second term on the RHS is $(\frac{v}{c})^2 \frac{cB}{L}$, which can safely be ignored. Hence for a highly conducting fluid the $\frac{\partial\bar{E}}{\partial t}$ term can be ignored and Ampere's law states

$$\bar{\nabla}\times\bar{B} = \frac{4\pi}{c}\bar{J} \text{ [for } \sigma\to\infty]. \tag{2.10}$$

From Ohm's law the current density in a fluid is

$$\bar{J}' = \sigma\bar{E}', \tag{2.11}$$

which for slow moving fluids results in

$$\begin{aligned}\bar{J}' = \bar{J} &= \sigma\bar{E}' \\ &= \sigma[\bar{E} + \frac{1}{c}(\bar{v}\times\bar{B})] \\ &= \sigma\bar{E} + \sigma(\frac{\bar{v}}{c}\times\bar{B}).\end{aligned} \tag{2.12}$$

Therefore,

$$\begin{aligned}\bar{E} &= \frac{\bar{J}}{\sigma} - (\frac{\bar{v}}{c}\times\bar{B}) \\ &= \frac{c}{4\pi\sigma}(\bar{\nabla}\times\bar{B}) - (\frac{\bar{v}}{c}\times\bar{B}).\end{aligned} \tag{2.13}$$

Substituting in Maxwell's induction equation

$$\bar{\nabla}\times\bar{E} = -\frac{1}{c}\frac{\partial\bar{B}}{\partial t},$$

gives

$$\begin{aligned}\frac{\partial\bar{B}}{\partial t} &= -c(\bar{\nabla}\times\bar{E}) \\ &= -c[\bar{\nabla}\times(\frac{c}{4\pi\sigma}(\bar{\nabla}\times\bar{B}) - \frac{\bar{v}}{c}\times\bar{B})] \\ &= \bar{\nabla}\times(\bar{v}\times\bar{B}) - \bar{\nabla}\times\eta(\bar{\nabla}\times\bar{B}),\end{aligned} \tag{2.14}$$

where

$$\eta = \frac{c^2}{4\pi\sigma} \tag{2.15}$$

represents the coefficient of resistive diffusion. In the equation (2.14) the second term represents the diffusion of the magnetic field into or out of a fluid with conductivity σ. From dimensional analysis it can be shown that the second term, i.e. the diffusion term, is smaller than the first term by the reciprocal of the so-called magnetic Reynolds number (e.g. Jackson 1975, p.473)

$$R_M = \frac{Lv}{\eta} = \frac{4\pi L v \sigma}{c^2}, \tag{2.16}$$

which gives

$$\begin{aligned} \frac{B}{t} &\approx \frac{vB}{L} - \frac{\eta B}{L^2} \\ &= \frac{vB}{L} - \frac{\eta}{Lv}\frac{vB}{L} \\ &= \frac{vB}{L} - \frac{1}{R_M}\frac{vB}{L}. \end{aligned} \tag{2.17}$$

For highly conducting fluids, which applies to most astrophysical environments $\sigma \to \infty$, the coefficient of resistive diffusion

$$\eta = \frac{c^2}{4\pi\sigma} \to 0. \tag{2.18}$$

Hence for $\sigma \to \infty$, the magnetic Reynolds number $R_M \to \infty$, which implies virtually no diffusion of magnetic field through a highly conducting fluid. Hence the field is frozen into the fluid, implying that the magnetic field and fluid are tied together. A magnetic field frozen into a moving fluid will be carried along by the fluid without resistance as long as the fluid ram pressure dominates the magnetic pressure. To illustrate this, a brief discussion of the basic principles of magnetic advection will be presented (e.g. Jackson 1975, p.475-479), which will provide a handy theoretical framework to explain the plasma-magnetosphere interaction in the magnetic cataclysmic variables.

For simplicity, consider a non-permeable fluid described by matter density $\rho(\bar{x},t)$, velocity $\bar{v}(\bar{x},t)$, pressure $P(\bar{x},t)$, and conductivity σ. Then the force equation of motion of a fluid is given by (e.g. Jackson 1975, p.471)

$$\rho\frac{d\bar{v}}{dt}=-\bar{\nabla}P+\frac{1}{c}(\bar{J}\times\bar{B})+\bar{f}_{v}+\rho\bar{g}\,; \tag{2.19}$$

which in addition to pressure and magnetic forces includes gravitational force, $\rho\bar{g}$ and the viscous force, $\bar{f}_{v}$ given by

$$\bar{f}_{v}=\mu_{k}\nabla^{2}\bar{v}\,, \tag{2.20}$$

in the case of an incompressible fluid, where μ_k represents the coefficient of kinematic viscosity.

In CVs the effective gravity at the L_1 region is zero. In this case the gravitational term in equation (2.19) can be neglected and for a steady state, i.e. $d\bar{v}/dt=0$, it takes the form

$$\bar{\nabla}P=\frac{1}{c}(\bar{J}\times\bar{B})+\mu_{k}\nabla^{2}\bar{v}\,. \tag{2.21}$$

In the following discussion, consider an incompressible, viscous conducting fluid flowing in the x-direction between two non-conducting boundary surfaces at $z = 0$ and $z = L$, representing the edges of the funnel across L_1. Also assume a uniform magnetic field B_0 in the z-direction, acting as a barrier for the flow along the x-direction (see Fig 2.1). In this case the only non-vanishing component of $\bar{J}$ is given by (e.g. Jackson 1975, p.476)

$$J_{y}(z)=\sigma(E_{0}-\frac{1}{c}B_{0}v)\,, \tag{2.22}$$

where E_0 is the only component of the electric field and is in the y-direction, and therefore must be constant. In the expression above v is the flow velocity in the x-direction. The x-component of the equation of motion, eqn (2.21), is therefore given by

$$\frac{\partial P}{\partial x}=\frac{\sigma B_{0}}{c}(E_{0}-\frac{B_{0}}{c}v)+\mu_{k}\frac{\partial^{2}v}{\partial z^{2}}\,. \tag{2.23}$$

Assuming that the pressure gradient in the x-direction, i.e. $\partial P/\partial x\rightarrow 0$ at a localized position (i.e. L_1, if it is significantly removed from the photosphere), eqn (2.23) can be expressed in the form

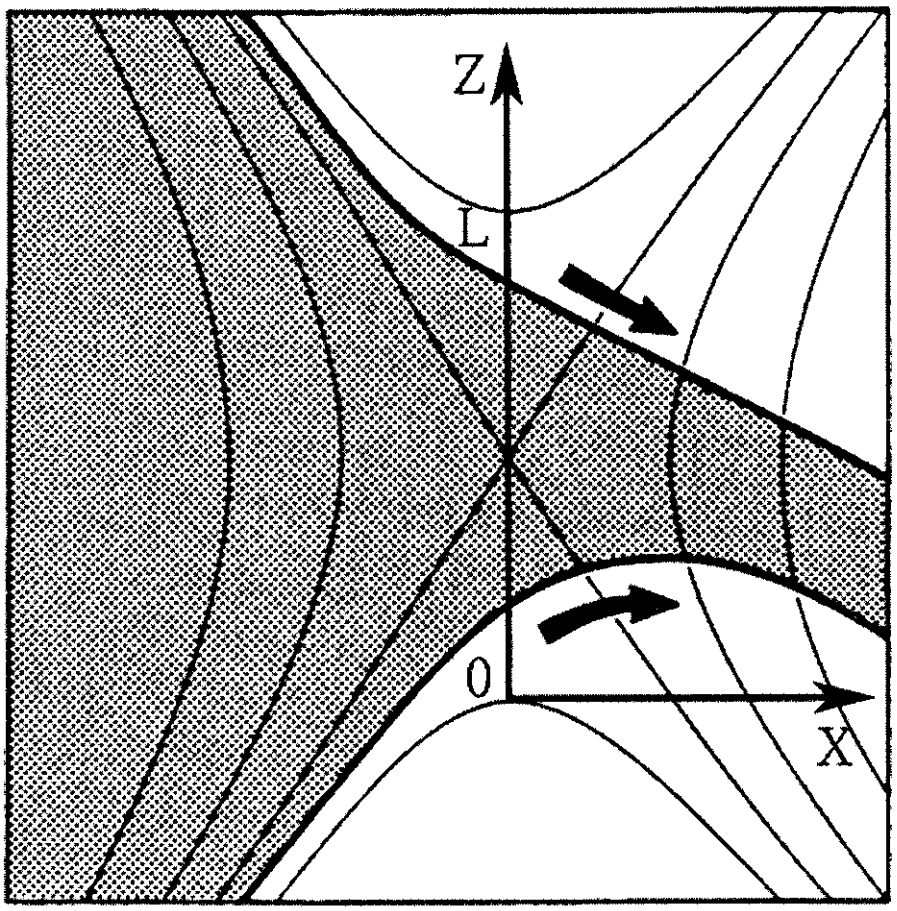

Fig 2.1 Mass flows through L_1 funnel (Pringle 1985)

$$\frac{\partial^2 v}{\partial z^2} - \frac{\sigma B_0^2}{\mu_k c^2} v = -\frac{\sigma B_0}{\mu_k c} E_0$$

$$\frac{\partial^2 v}{\partial z^2} - \frac{\sigma B_0^2 L^2}{\mu_k c^2 L^2} v = -\frac{\sigma B_0^2 L^2}{\mu_k c^2 L^2} \frac{c E_0}{B_0}$$

$$\frac{\partial^2 v}{\partial z^2} - (\frac{M_H}{L})^2 v = -(\frac{M_H}{L})^2 \frac{c E_0}{B_0}, \qquad (2.24)$$

where $M_H = (\frac{\sigma B_0^2 L^2}{\mu_k c^2})^{1/2}$ (2.25)

is the Hartmann number, i.e. the ratio of the magnetic viscosity to the fluid kinematic viscosity (μ_k). If $M_H >> 1$, the flow will ram into a rigid magnetic obstruction, resulting in the fluid experiencing severe effects of magnetic viscosity (e.g. Jackson 1975, p.477), forcing it to decelerate across the field lines.

The solution to eqn (2.24), assuming boundary conditions $v(0) = v_1$ and $v(L) = v_2$ is readily found to be (e.g. Jackson 1975, p.477)

$$v(z) = \frac{v_1}{\sinh M_H}[M_H(\frac{L-z}{L})] + \frac{v_2}{\sinh M_H}(\frac{M_H z}{L}) + \frac{cE_0}{B_0}[1 - \frac{\sinh[M_H(L-z)/L] + \sinh(M_H z/L)}{\sinh M_H}]. \quad (2.26)$$

Since the condition for magnetic viscosity to dominate the flow is $M_H >> 1$, and since from the calculation it is found that $M_H > 1$, the limit of $M_H >> 1$ will therefore be considered, in which case it is expected that the magnetic viscosity will dominate and the flow will be determined almost entirely by the $\overline{E} \times \overline{B}$ drift. Since the flow is considered to be in the x-direction, the magnetic field in the x-direction $B_x(z)$ can be determined from eqn (2.10) and eqn (2.12), i.e.

$$\frac{\partial B_x}{\partial z} = \frac{4\pi\sigma}{c}(E_0 - \frac{B_0 v}{c}). \quad (2.27)$$

Substituting eqn (2.26) for velocity into eqn (2.27), it can be shown (e.g. Jackson 1975, p.478) that

$$B_x(z) = B_0(\frac{4\pi\sigma L^2}{c^2})(\frac{v_2 - v_1}{2L})[\frac{\cosh(M_H/2) - \cosh(M_H/2 - M_H z/L)}{M_H \sinh(M_H/2)}]. \quad (2.28)$$

From eqn (2.28) the term $(v_2 - v_1)/2$ is a typical velocity and L is a typical length. The dimensionless quantity in the square brackets can therefore be identified as the magnetic Reynolds number R_M. Therefore eqn (2.28) reduces to (e.g. Jackson 1975, p.478)

$$\frac{B_x(r)}{B_0} = \frac{R_M}{M_H}(1 - [\exp(-\frac{M_H r}{L}) + \exp(-M_H \frac{L-r}{L})]) \quad \text{for } M_H >> 1 \quad (2.29)$$

$$\frac{B_x(r)}{B_0} = \frac{R_M}{M_H}\frac{r}{L}(1 - \frac{r}{L}) \quad \text{for } M_H << 1, \quad (2.30)$$

where the radial distance $r = z$. Expressing r as a fraction of the funnel width, i.e. r/L where $L = H$, the value of $B_x(r)/B_0$ can be calculated. From this values of the magnetic field at the various radial distances advected into the funnel with the fluid flow can be determined. A graph of $B_x(r)/B_0$ against r/L is shown in Figures 2.2 and 2.3.

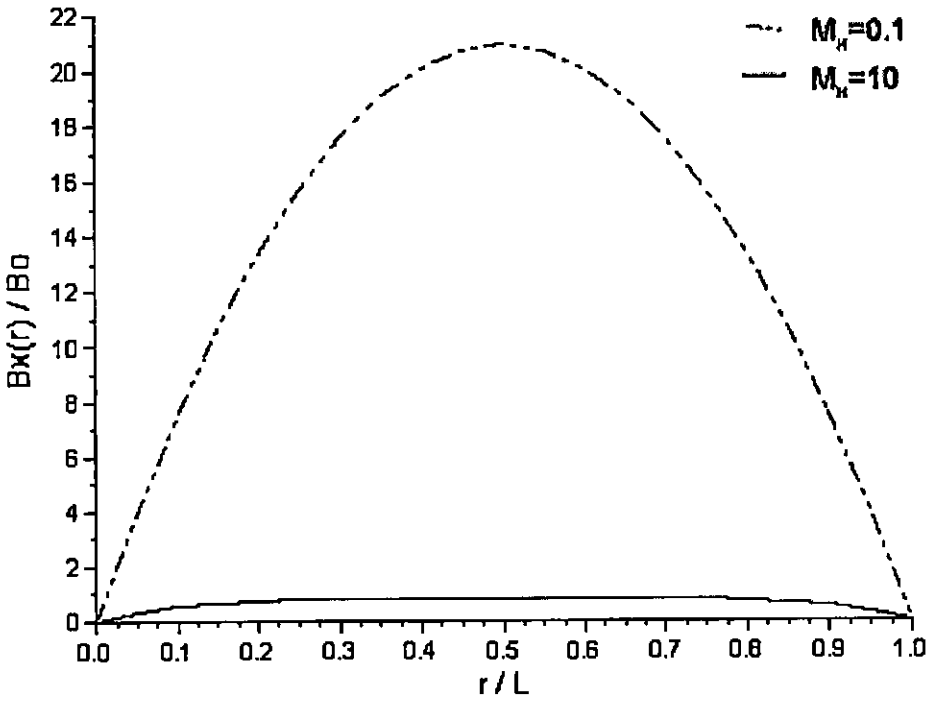

Fig 2.2 Radial component of the magnetic field advected into the funnel [for turbulence $R_M = 8.3$ and different $M_H (= 0.1 \text{ and } 10)$]

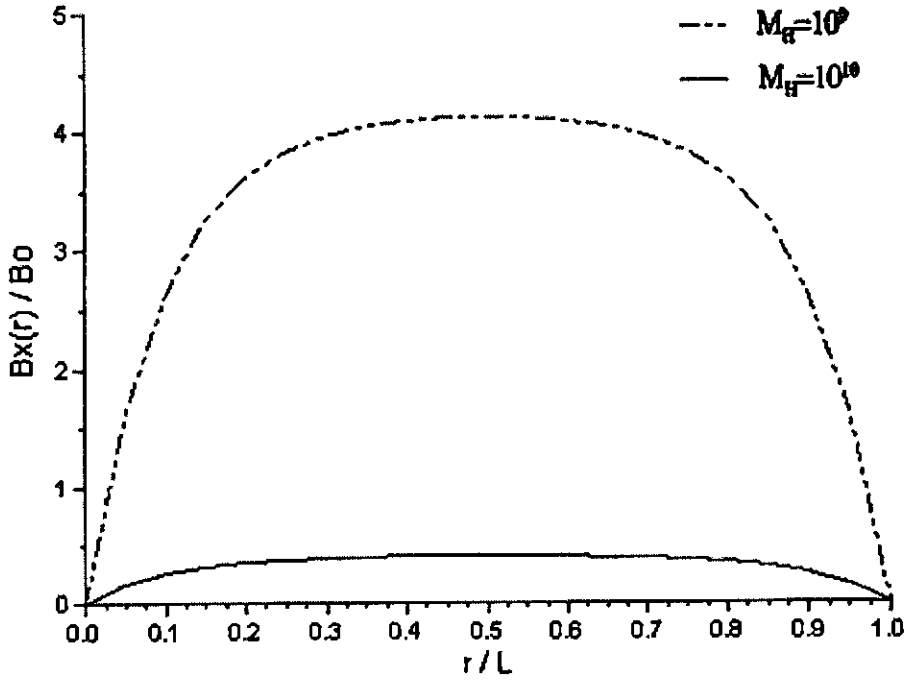

Fig 2.3 Radial component of the magnetic field advected into the funnel [for $R_M = 4.189 \times 10^9$ and different $M_H (= 10^9, 10^{10})$]

Figures 2.2 and 2.3 show the behavior of the lines of the forces for each of the two limits [$M_H = 0.1, 10$ (for $R_M \sim 10$) and $M_H = 10^9, 10^{10}$ (for $R_M \sim 10^9$)]. For a given R_M, the larger the Hartmann number ($M_H >> 1$) the less transport (advection) of the magnetic field occurs.

Within the framework of this discussion, the interaction of a conducting fluid, (i.e. the mass transfer flow from the secondary star) with the magnetosphere of the compact object (the white dwarf) can be evaluated. Since the dipole field of the compact object

$$B = B_1 (\frac{R_1}{R})^3 \tag{2.31}$$

drops off as $B \propto R^{-3}$ there will be virtually no magnetic resistance to the flow where the ram pressure of the bulk flow from the secondary star significantly exceeds the magnetospheric pressure. This will allow the flow to plunge through the magnetosphere relatively unaffected. In this regime the field will be dragged along by the flow since in the limit $\sigma \to \infty$ there will be virtually no diffusion of the field relative to the flow (e.g. Fig 2.3). Closer to the white dwarf the field pressure may become significantly high, dominating the flow ram pressure. In this region, the structure of the magnetosphere field will dominate the flow, determining the path which the flow will follow onto the surface of the white dwarf. In this case, the field lines act as an immovable obstruction to flow ramming into it, the only alternative being flow along flux tubes towards the surface of the accreting star.

The region where the magnetosphere and the flow pressures balance, i.e. the transition region, defines the extent of the magnetosphere of the compact object, i.e. the magnetosphere or Alfvén radius. The basic properties of magnetic cataclysmic variables can then be explained in terms of the magnetic properties of the compact object. A brief discussion is presented in the following sections. Since the strength of a magnetic field declines rapidly with increasing distance, magnetic cataclysmic variables can often be regarded as having a weakly magnetized outer zone which has very little or no influence on the flow ($M_H << 1$), and a magnetically dominated magnetosphere surrounding the white dwarf, totally dominating the flow ($M_H >> 1$)

toward the polar caps where the gravitational potential energy of the material is released in heat and radiation.

The hard X-ray ($>0.5\,\text{keV}$) bremsstrahlung from polars is a characteristic that distinguishes them from non-magnetic CVs. Polars also are spectacular emitters of soft X-rays ($<0.5\,\text{keV}$) , originating from reprocessed bremsstrahlung, and thermalized subphotospheric deposition. (Warner 1995).

Figure 2.4 shows the observed flux distribution of EF Eri in the 70 eV - 2 keV region (Beuermann, Thomas & Pietsch 1991). The dashed curve represents a blackbody spectrum with $kT_{BB}=19\,\text{eV}$ ($T_B=2.1\times10^5\,\text{K}$) combined with a $kT=20\,\text{keV}$ bremsstrahlung spectrum, both absorbed by interstellar absorption with $N_H=1\times10^{19}\,\text{cm}^{-2}$. Because of the large uncertainties in most T_{BB}, the values of the blackbody luminosity L_{BB} are probably uncertain by factors ~4. The estimate of T_{BB} are close to the maximum permitted by stability of a white dwarf atmosphere.

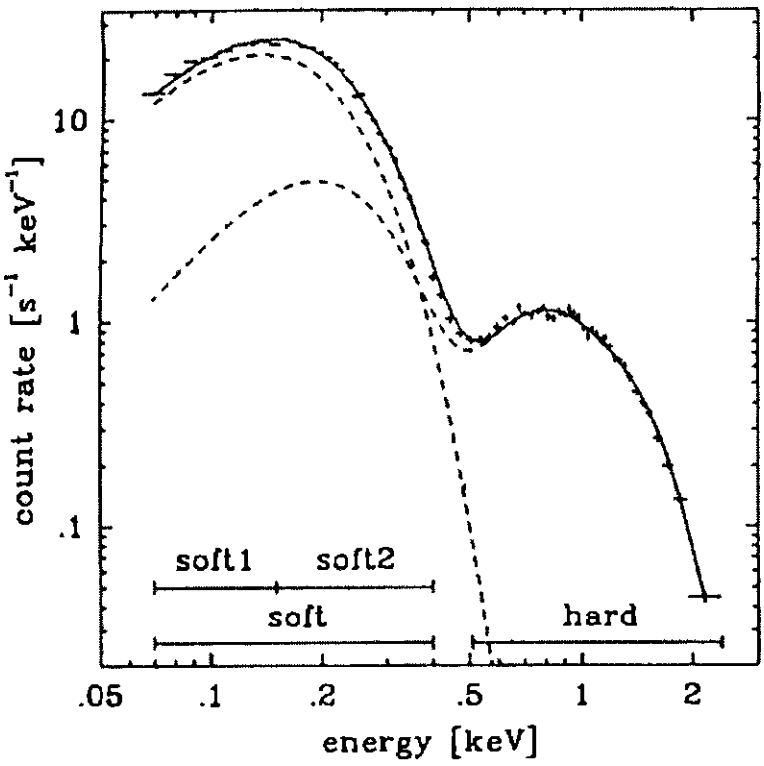

Fig 2.4 X-ray flux distribution in EF Eri, obtained by ROSAT. (Beuermann et al. 1991)

The relative role of the various emitting regions can be judged from the parameters derived for ST LMi in Table 2.1 (Beuermann 1987). It is clear from this that the accretion luminosity is dominated by L_{BB}, which gives $L_{acc} \sim 3\times10^{32}$ erg s^{-1} for polars and implies $\dot{M} \sim 2.5\times10^{15}$ g s^{-1} (Warner 1995).

	Emitting area		Luminosity
	10^{15} cm	Fraction of WD	(erg s^{-1})
Bremsstrahlung	~0.04	$\sim 5\times10^{-6}$	$\sim 5\times10^{31}$
Blackbody	0.04-8	$5\times10^{-6} - 9\times10^{-4}$	$12 - 90\times10^{31}$
Cyclotron	4-32	$5\times10^{-6} - 4\times10^{-3}$	$\sim 1\times10^{31}$

Table 2.1: Energy Budge in St LMi

2.2 The magnetic cataclysmic variables (MCV)

2.2.1 AM Her stars: Polars

These systems are the magnetic cataclysmic variables (mcv) in which the white dwarfs have magnetic fields significantly exceeding 10 Mega Gauss (MG) (e.g. Schmidt 1999), confirmed by Zeeman splitting and polarization measurements. The strong magnetic field of the primary interacts with the smaller magnetic field of the secondary, locking the two stars together into corotation. This has the following two implications:

(i) Polars are synchronously rotating systems (P_{rot}=P_{orb}), with orbital periods lying between ~ 81 and 222 minutes (e.g. Chanmugam & Ray 1984). The phase locked interaction is caused by the strong magnetic interaction between the white dwarf and the low mass magnetic secondary.

(ii) The formation of the disc is prevented (i.e. discless accretion), since the small orbital period ($P \leq 3$ hours) implies small binary separation and an extended magnetosphere, resulting in the mass transfer stream ramming directly into the magnetosphere of the white dwarf. The stream punches

through the magnetosphere until the magnetospheric pressure starts to dominate. From this point the flow is channeled along the field onto one or both poles of the white dwarf.

Evolutionary models (Warner & Wickramasinghe 1991) describe the condition for synchronization and discless accretion which are set by the ratio of the magnetic moment to the mass accretion rate of the white dwarf. For polar systems, the following condition must be satisfied (Warner & Wickramasinghe 1991)

$$0.4(\frac{P_{orb}}{4\,\mathrm{hr}})^{\frac{7}{6}} m_1^{\frac{5}{6}} < \frac{\mu_{34}}{\sqrt{\dot{M}_{18}(\max)}} < 7(\frac{P_{orb}}{4\,\mathrm{hr}})^{\frac{7}{6}} m_1^{\frac{5}{6}}, \qquad (2.32)$$

where m_1 is the mass of the white dwarf in solar mass units, μ_{34} is the magnetic moment of the white dwarf in units of $10^{34}\ \mathrm{G\,cm^3}$, and $\dot{M}_{18}$ represents the mass accretion rate in units of $10^{18}\ \mathrm{g\,s^{-1}}$. This condition implies that for orbital periods $P \leq 4$ hours and mass accretion rates $\dot{M}_{18} \sim 1$, synchronism can be achieved if $0.4 \leq \mu_{34} \leq 7$. This is in fact observed from most polars. For effective synchronization and discless accretion the ratio of the synchronization time-scale to spin-up time-scale must be of the order (e.g. Meintjes 1992)

$$\frac{t_{syn}}{t_{spin-up}} \leq 1. \qquad (2.33)$$

Close to the white dwarf surface, material falling in with supersonic velocities is decelerated and heated to approximately 10^8 K in a stand-off shock (e.g. Frank, King & Raine 1992, p.137) resulting in a release of gravitational potential energy in the accretion column (see Fig 2.5), (Kuijpers & Pringle 1982; Done, Osborne, Beardmore 1995; Beardmore et al. 1995; Gansicke, Beuermann, de Martino 1995). The radiation is characterized by:

(i) Strong polarized emission at optical/IR wavelengths.

(ii) Intense soft, and in some cases, hard X-ray emission.

(iii) An emission line spectrum of excitation which reflects the large streaming motion of accreted material in the magnetosphere of the white dwarf (see e.g. Beuermann 1988).

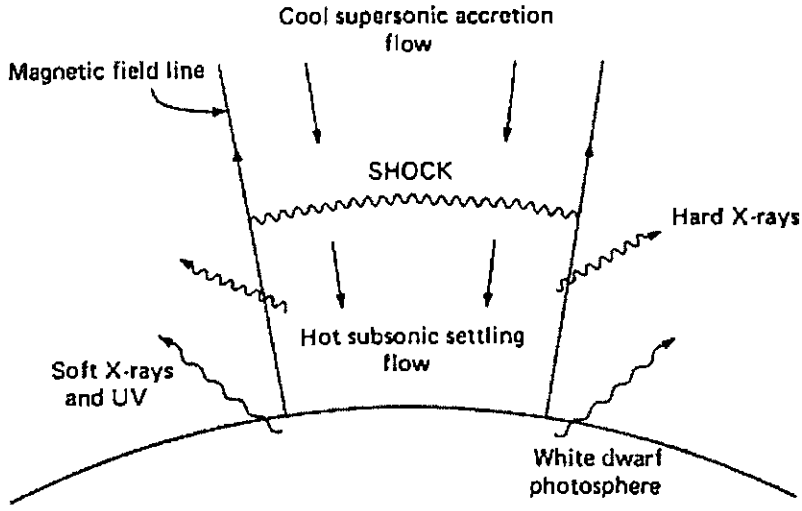

Fig 2.5 Schematic picture of a standard accretion column geometry for a magnetized white dwarf (Watson 1986)

The polars will be presented according to the magnetic field strength of WD as follows: the AR UMa system with the strongest field known among CVs and the typical AM Her systems. The properties of these systems will be discussed briefly.

2.2.1.1 The highest-field systems (i.e. the AR UMa systems)

The white dwarf in AR UMa has the strongest field known among cataclysmic variables, measuring 230 MG at its surface (Schmidt et al 1996; Schmidt 1999; Hellier 2001, p.110). The 230 MG field is strong enough to dominate the flow from the L_1 point. In terms of the earlier discussion, $M_H >> 1$ for the system, resulting in the accretion stream following field lines almost from the start. Thus to follow a field line, the stream must divert out of the orbital plane. The stream splits into two, one part heading towards the 'north' magnetic pole and the other towards the 'south pole' (see Fig 2.6). The field lines converge as they approach the white dwarf, squeezing the streams and funneling them onto tiny accretion spots near the poles.

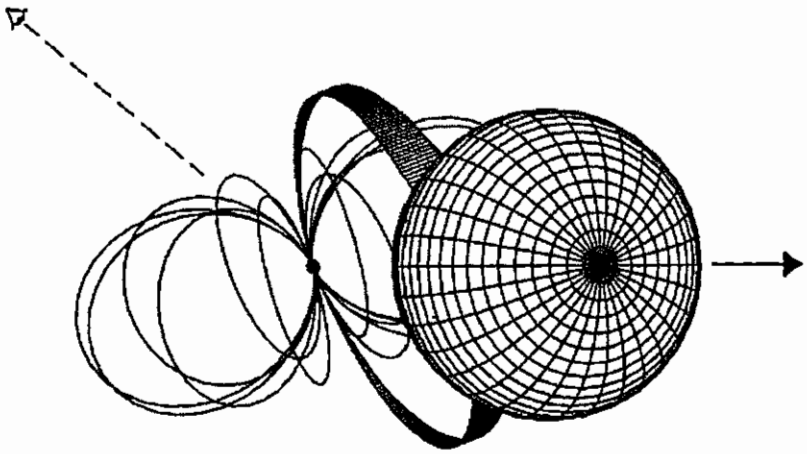

Fig 2.6 The accretion stream in AR UMa (Schmidt 1999)

Being channeled by the field, the stream moves almost radially towards the white dwarf, in virtual free-fall. The potential energy is converted to kinetic energy and the stream slams onto the white dwarf at roughly the 3000 km s^{-1}. In the resulting accretion shock the kinetic energy is converted into X-rays and radiated away. Magnetic cataclysmic variables are thus stronger X-ray sources than their non-magnetic counterparts, emitting most of their energy as X-rays and extreme-ultraviolet photons.

2.2.1.2 The typical AM Her stars

Whereas AR UMa's 230 MG field controls the stream from the L_1 point, in AM Her stars with more typical fields of 10-70 MG (e.g. Cropper 1990; Schmidt et al 1996), the stream is at first unaffected by the field, following a 'ballistic trajectory' until close to the white dwarf. Provided the magnetosphere extends out further than the circularization radius, the ballistic stream rams into the magnetosphere. As the stream approaches the white dwarf, the increasing magnetic pressure of the converging field lines first squeezes the stream, causing it to break up into dense blobs of material (see Fig 2.7).

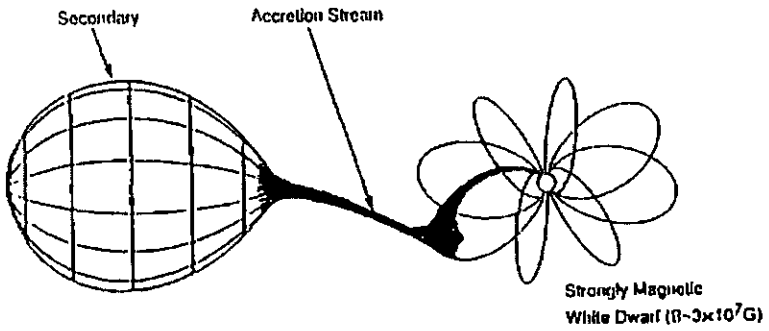

Fig 2.7 The typical accretion flow of polar (Cropper 1990)

The field cannot easily penetrate such blobs because of screening, so they continue ballistically towards the white dwarf surface. As the magnetic pressure increases the clumpy flow is compressed, resulting in collisions in the stream and shock formation. Material stripped from the surface of the blobs will flow along field lines and onto the white dwarf where the gravitational potential energy of the flow is converted into heat and radiation.

2.2.2 Intermediate polars (IPs)

In the majority of CVs the magnetic fields are sufficiently weak so that they can be ignored, whereas in AM Her stars they completely dominate the accretion flow. With a medium-strength field a CV can combine the characteristics of a non-magnetic system (in its outer regions) with those of an AM Her system (nearer to the white dwarf). The AM Her stars can be knocked out of synchronism if the field of the primary is a little too weak, or the stellar separation a little too large. Continuing this trend leads to systems which have lost synchronism entirely (e.g. a nova outburst leading to desynchronisation, a good example is V1500 Cyg, nova Cygni 1975, e.g. Schmidt et al. 1995), in which the white dwarf is spun up by the accretion of material, ending at rotation periods of typically a tenth of the orbital period (e.g. Warner 1995; King 1993; King & Lasota 1991). Such systems are called intermediate polars, to denote a status halfway between AM Her stars (polars) and the non-magnetic CVs.

An interesting question to ponder is under what circumstances does the direct interaction of a stream with a magnetic field give way to the formation of a disc? An

easy case to deal with is when the magnetosphere is smaller than the radius of minimum approach of the free-falling accretion stream ($r_{mag} < r_{min}$). The stream could then orbit the white dwarf, ignoring the feeble magnetic field, spreading as a result of viscosity to form a disc. The disc would then spread inwards and outwards until the inward migration of its inner edge is stopped by the increasing magnetic pressure of the magnetosphere (see Fig 2.8).

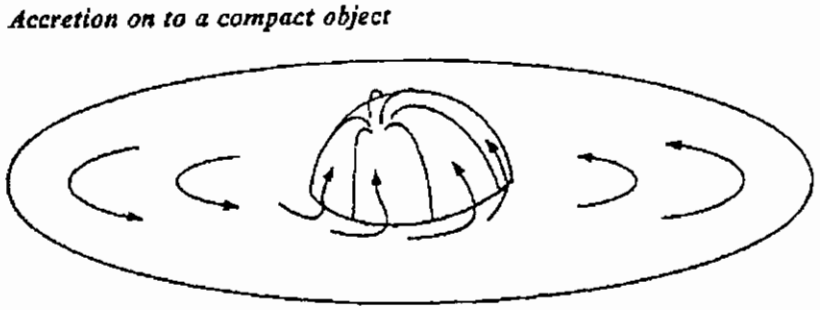

Fig 2.8 Accretion disc around the magnetic primary (Frank, King & Raine 1992, p.122)

In the high mass transfer phase, a well-developed disc should be present that could facilitate mass accretion onto the white dwarf. By inverting the discless accretion argument (Wickramasinghe, Wu & Ferrario 1991; Warner 1995) during the initiation of the high mass transfer phase, an accretion disc will develop if the magnetic moment of the white dwarf does not exceed (e.g. Meintjes 1992)

$$\mu_{34} \leq 0.4\sqrt{\dot{M}_{18}}\left(\frac{P_{orb}}{4\,\mathrm{hr}}\right)^{7/6}\left(\frac{M_1}{M_\odot}\right)^{5/6}\ \mathrm{G\,cm^{-3}} \qquad (2.34)$$

2.2.3 DQ Herculis (DQ Her) systems

The DQ Her binaries are a subset of the intermediate polars. They have short primary rotation periods ($P_{rot} < 100\,\mathrm{s}$) and lack hard X-ray emission. In terms of the standard model, the short rotation period $P_{rot} << P_{orb}$ hints that these systems may be disc accretors. To put the pulsed emission of DQ Her, the prototype of this class, into perspective, the oblique disc rotator model was developed by Bath, Evans & Pringle

(1974), which could be a representative model for all disc accreting mcvs (see Fig 2.9).

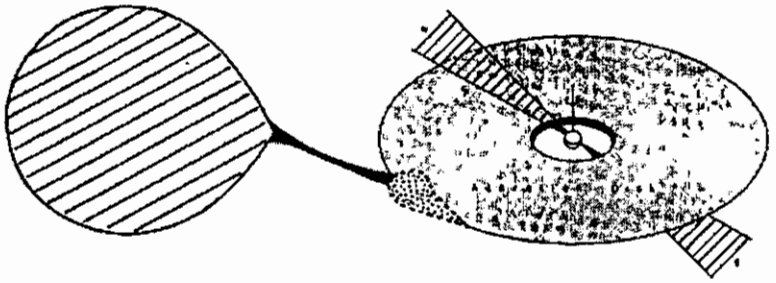

Fig 2.9 The supposed configuration of an oblique rotator (Patterson 1979, 1994)

In this model the pulsed emission from disc accreting DQ Her stars, as well as the intermediate polars, is the direct result of the accretion of gas onto the exposed magnetic pole of a magnetized white dwarf, which is tilted with respect to the rotation axis (see Fig 2.8, 2.9). Rotation of the compact object will cause the pole heated by accretion to continually move into and out of the field of view of an observer, resulting in pulsed emission modulated with the spin period of the magnetized white dwarf.

Traditionally, the subclass contains only three systems, AE Aquarii (AE Aqr), DQ Herculis (DQ Her) and V533 Herculis (V533 Her) as listed in Table 2.2.

Name	P_{orb} (hr)	P_{rot} (min)	$\dot{P}_{rot} / P_{rot}$ (yr^{-1})
AE Aqr	9.88	0.55	5.4×10^{-8}
V533 Her	5.04	1.06	1.5×10^{-7}
DQ Her	4.65	1.18	-3.6×10^{-7}

Table 2.2: The characteristic periods of the three DQ Her systems. (Campbell 1997)

These binaries played an extreme important role in the early pioneering work regarding the development of a general model for the CVs. AE Aqr was shown to be a spectrospic binary by Joy (1954) and was subsequently used by Crawford & Kraft (1956) towards deriving the basic model for the CVs.

Having discussed the various mcvs, with some of their most important properties, AE Aqr can now be considered. This system has a 9.88-hr long orbital period and a 33-s short spin period. The long orbital period and short white dwarf spin period implies that the binary separation is large enough to accommodate a well-developed accretion disc. However recent studies (e.g. Wynn, King & Horne 1997; Meintjes & de Jager 2000; Meintjes 2002) reveal that the AE Aqr system is quite unique since it is ejecting virtually 100% of the mass transfer from the secondary star. It is believed that AE Aqr went through a run-away mass transfer phase when the accretion rate probably was high enough to support surface nuclear burning on the white dwarf and the magnetic torque on the white dwarf, exerted by a well-developed accretion disc in that phase, spinning-up the white dwarf to the current short spin period. The conjecture that AE Aqr, and possibly other CVs went through a high mass accretion, and hence possibly a super soft X-ray source (SSS) phase (e.g. Schenker et al. 2002; Meintjes 2002), can be evaluated quantitatively by scrutinizing the possible evolutions of the system. This will be the topic of investigation in this study. However, it is important firstly to explain some of the properties of the SSS, and of AE Aqr in particular.

2.3 The Super Soft X-ray Sources (SSS)

The first of the luminous Super Soft X-ray Sources (SSS) in the Large Magellanic Cloud (LMC) was discovered around 1980 with the Einstein Observatory (Long et al. 1981). After the discovery of SSSs with the Einstein Observatory observations and later with EXOSAT (Pakull et al. 1985), the detection of an orbital period established the close-binary nature of these sources (Smale et al. 1988). The real proof of their super soft nature was given by observations with ROSAT (Trumper et al. 1991; Greiner et al. 1991), which showed that SSS do not emit detectable X-ray radiation above ~0.5 keV. Typical blackbody parameters of an SSS are temperatures of $T_1 \sim 10^5 - 10^6$ K and a radius of $R_1 \sim (1-3)\times 10^9$ cm. This suggests that the emitting object has the size of a white dwarf and radiates at or above the Eddington limit ($\sim 10^{38}$ erg s^{-1}) of a solar mass object (Heise et al 1994).

The ROSAT satellite with its PSPC detector has discovered about four dozen new SSSs and has thus established luminous SSSs as a new class of object. The new class of soft X-ray IPs are discovered by ROSAT (dominated by a soft black body, e.g. Haberl & Motch). Although many different classes of objects emit super soft X-ray radiation (defined here as emission predominantly below 0.5 keV which corresponds to effective temperatures of the emitting objects of <50 eV), Greiner (2000) considers only sources with bolometric luminosities in the range 10^{36} to 10^{38} erg s^{-1}. Optical observations have revealed the binary nature of several of these objects.

The first thoughts about the nature of SSS included accretion onto black holes (Cowley et al. 1990; Smale et al. 1988) and neutron stars accreting above the Eddington rate (Greiner et al. 1991). Van den Heuvel et al. (1992) proposed as a possible explanation that the super soft X-ray emission was the result of steady nuclear burning of hydrogen accreted onto white dwarfs. Such a close binary system would be a strong source of soft X-rays.

Instead of a hydrogen burning white dwarf, Iben & Tutukov (1993) proposed helium burning on a carbon-oxygen (CO) degenerate dwarf, which accretes helium from a companion that is burning helium shell above a CO core. However, the detection of the Hα line in emission in CAL 83 and CAL87 (e.g. Pakull et al. 1988) supports the scenario in which the mass-donor star in these systems is hydrogen rich.

A white dwarf model, the so-called close-binary super soft source (CBSS) model, is perhaps the most promising (Kahabka & van den Heuvel 1997; Rappaport et al. 1994; van den Heuvel et al. 1992). It invokes steady-nuclear burning on the surface of an accreting white dwarf generating these systems' prodigious flux. Indeed, CBSS sources have temperatures and luminosities, derived from the X-ray data, suggesting an effective radius comparable to that of white dwarfs. Eight super soft X-ray sources have orbital periods between approximately 4-hr and 3.5-d (Greiner 2000). These are the candidates from the CBSS model. Mass transfer rates derived from the CBSS model are in the right range for steady nuclear burning of the accreted matter, which is (Prialnik 1986):

$$\dot{M}_{1(\mathrm{SNB})} \geq 10^{19}\left(\frac{M_1}{0.9M_\odot}\right)^{3/2} \mathrm{g\,s^{-1}} \qquad (2.35)$$

2.4 The AE Aquarii system

The investigation of a possible relation between the AE Aqr system and the SSS justify a detailed discussion of the system in its current state.

2.4.1 Properties of AE Aquarii

The mcv AE Aqr is probably one of the best studied sources in the sky, with observations ranging from radio to TeV gamma-rays. The highly variable binary is a member of the DQ Her type cataclysmic variables, and was discovered by Zinner (1938) on photographic plates and was first classified as a U Gem type variable. Since its discovery in the optical range on photographic plates, the rapidly varying cataclysmic variable AE Aqr has remained a source of continuous observational and theoretical study.

The rapid variability of AE Aqr in the optical range was instrumental in stimulating extensive multi-wavelength (spanning 17 decades) interest. This subsequently led to its detection in frequencies other than the optical range, spanning radio to TeV gamma-rays. The emission from AE Aqr, in both radio and TeV gamma-rays is of non-thermal nature, and extensive reports on, and models of the nature of the non-thermal radio and TeV gamma-rays emission are presented by Bookbinder & Lamb (1987), Bastian, Dulk & Chanmugam (1988), Abada-Simon et al. (1993, 1995a, 1998); Abada-Simon et al. (1995b), Meintjes (1992), Meintjes et al. (1992, 1994), Bowden et al. (1992), de Jager (1994, 1995), de Jager & Meintjes (1993), Ikhsanov (1997, 1998, 1999, 2000), Kuijpers et al. (1997) and Meintjes & de Jager (1995, 2000). An encyclopaedic summary of the overall multi-wavelength properties of the system, and cataclysmic variables in general, is given by Warner (1995).

AE Aqr is one of the most distinctive CVs with a white dwarf primary and a K4-5 type secondary. The secondary star is suspected to be an evolved late-type star. It was first classified as a K0-5 by Joy (1954) but subsequent studies of photometric variability, together with independent spectroscopic studies have shown that this was

too early and these studies support a spectral type in the range K3-K5 (Crawford & Kraft 1956; Tanzi, Chincarini & Tarenghi 1981; Wade 1982; Bruch 1991; Welsh, Horne & Oke 1993; Welsh, Horne & Gomer 1995). The analysis of the absorption features supports a K4 classification for the companion star, which contributes >95 per cent of the total flux in the range 600-700nm (Casares et al. 1996). These studies classified AE Aquarii as a white dwarf that accretes matter from a late type K4-5 secondary star with the two stars orbiting their common centre of mass every 9.88-hr.

A 1978 optical photometric campaign revealed low-amplitude (0.1 – 0.2 percent), but persistent pulsations at 16.54 and 33.08-s, and transient quasi-periodic oscillation (QPOs), which appear to be connected to outbursts (Patterson 1979). The 33-s oscillations were explained in terms of an oblique rotator model (e.g. Bath, Evans & Pringle 1974) as the rotation period of the white dwarf caused by the released gravitational potential energy of gas that is accreted from an accretion disc onto the nearest pole of the white dwarf that sweeps through the line of sight every 33.08-s. The 16.54-s pulse, in the context of the oblique rotator model, was explained as illumination of the disc inner edge by the second pole (Patterson 1979). In this context the outbursts (flares) seen on a regular basis are episodes of enhanced mass accretion onto the poles of the white dwarf. The QPOs associated with flares were explained as self-luminous blobs in the disc orbiting the white dwarf with Keplerian periods. This model placed AE Aqr in the same category as DQ Her.

A detailed pulse timing analysis of the 33-s pulse, using a data set spanning nearly 15-year, de Jager et al. (1994), showed that the white dwarf is spinning down at a rate of

$\dot{P} \sim 5.64 \times 10^{-14}\ \mathrm{s\,s^{-1}}$

yielding a spin-down power of

$$-I\Omega\dot{\Omega} = 6 \times 10^{33} I_{50}\ \mathrm{erg\,s^{-1}} \qquad (2.36)$$

By adopting an orbital inclination of $\sim 55^{\circ}$ (Welsh, Horne & Gomer 1995; also Warner 1995), and using the 15-year baseline of the arrival times of the 33-s oscillation, de Jager et al. (1994) put constraints on the binary parameters, for example, on the mass of the secondary and primary star

$$(\frac{M_2}{M_\odot}) \sim 0.6(\frac{\sin i}{\sin 55^\circ})^{-3} \quad (2.37)$$

$$(\frac{M_1}{M_\odot}) \sim 0.87(\frac{\sin i}{\sin 55^\circ})^{-3} \quad (2.38)$$

with $i \sim 55^\circ$ (e.g. Warner 1995) representing the inclination from which the source is observed above the binary plain. This is based upon the fact that no eclipsing of the compact object by the secondary star has ever been detected, and which results in a mass ratio $q = (M_2 / M_1) \sim 0.69$. These values are in excellent agreement with the q-ratio value of $q = (M_2 / M_1) \sim 0.64$ obtained from a similar pulse timing analysis of two HST observations made in 1992 (by Eracleous et al. 1994), and an independent study of the absorption lines of the secondary (Welsh, Horne & Gomer 1993, 1995; Casares et al. 1996, Meintjes 2002).

2.4.2 Magnetic field of the white dwarf

The orbital period of AE Aqr is $P_{orb} \sim 9.88\,\mathrm{hr}$ (e.g. Welsh, Horne & Gomer 1993, 1998). This implies that the binary separation is large enough to accommodate a well-developed accretion disc. Based upon the accretion torque theory of Ghosh & Lamb (1978, 1979a,b), a study of the spin-up and magnetic field in DQ Her stars (Lamb & Patterson 1983) revealed that the white dwarf may have a surface field of the order of $B_* \sim 6\times10^4\,\mathrm{G}$. However, first Cropper (1986) and later Beskrovnaya et al. (1995) reported circular polarization at the level of (0.05±0.01) and (0.10±0.03) per cent respectively in the optical wavelengths, which, if produced by cyclotron emission, may indicate a magnetic field in excess of $B_* \sim 10^6\,\mathrm{G}$ (Chanmugam & Frank 1987). These levels of circular polarization are consistent with early upper limits of 0.06 % reported by Stockman et al. (1992), from AE Aqr, in a polarimetric survey of magnetic cataclysmic variables. To account for the low level of circular polarization (<1 %) from certain cataclysmic variables, these authors placed an upper limit of $B_* < 5\times10^6\,\mathrm{G}$ on the surface field strength of these white dwarfs (e.g. Meintjes & de Jager 2000).

The estimated magnetic moment (eqn 2.34) is in excellent agreement with the magnetic moments ($\sim \mu_{32}/2$) of the other intermediate polars and DQ Her stars (Warner & Wickramasinghe 1991). This will allow an estimate of an upper limit of the surface magnetic field strength of the white dwarf $B_1 \approx \mu / R_1^3$, if its radius is known. By adopting the white dwarf mass-radius relation (e.g. Hamada & Salpeter 1961; Eracleous & Horne 1996; Meintjes 2002)

$$R_1 = 5.3\times10^8 (\frac{M_1}{0.9M_\odot})^{-0.8} \text{ cm}, \tag{2.39}$$

resulting in a white dwarf surface field which is in the order of (Meintjes 2002)

$$B_1 \approx \mu / R_1^3 \leq 2.4\times10^6 (\frac{\mu_{32}}{3})(\frac{R_\odot}{R_1})^{-3} \text{ G}. \tag{2.40}$$

This is reconciled with an estimated magnetic field strength of $B_1 \leq \text{few}\times10^6$ G, deduced from circulation polarization measurements (e.g. Cropper 1986; Chanmugam & Frank 1987; Stockman et al 1992; Beskrovnaya et al. 1995; Meintjes 2002).

2.4.3 The propeller phase of AE Aquarii

The system has a long orbital period 9.88 hr (Welsh, Horne & Gomer 1993, 1998), and it also has the shortest spin period yet detected, i.e. 33.08 s of intermediate polars. This spin period has been detected over a wide range of frequencies, from the optical (Patterson 1979) to gamma-rays wavelengths (Meintjes et al. 1992). However a controversy on the origin of the 33 s pulsation remained until Welsh, Horne & Gomer (1993, 1998) and also Reinsch & Beuermann (1994) showed that the Hα emission does not track the motion of the white dwarf. Eracleous et al. (1994) studied the double-peak profile of the UV pulses and proposed that they arise directly from the polar caps of the primary.

A 14-year study of the optical oscillation period (de Jager 1994) shows that the white dwarf is spinning down at an alarming rate. Something extracts rotational energy from the white dwarf at a rate $\dot{E} \sim I\Omega\dot{\Omega} \sim 10^{34}$ erg s^{-1} ~ 1000 times the accretion luminosity of the system derived from X-ray data (Eracleous, Patterson & Halpern 1991). It has

been shown (Wynn, King & Horne 1995, 1997; Eracleous & Horne 1996; Meintjes & de Jager 2000; Pearson et al. 2003) that the rapid variability and the spin-down rate of the white dwarf can be explained in terms of a magnetoshperic propeller process. The propeller process is the result of a low mass transfer rate from the secondary star, i.e. $\dot{M}_2 \geq 4\times10^{17}\,\mathrm{g\,s^{-1}}$ (Eracleous & Horne 1996), interacting with the fast rotating magnetosphere. This results in the ejection of the mass flow from the secondary star before it can settle to form an accretion disc. The magnetic propeller efficiently extracts energy and angular momentum from the white dwarf and transports it via magnetic fields to gas stream material, which it ejects from the binary system. Detailed understanding of the magnetic propeller effects may therefore help us to unlock some of the secrets of magnetic viscosity in accretion flows.

Chapter 3

Orbital and magnetic accretion disc evolution

In this chapter a brief discussion is presented regarding the relevant phenomena that influence the mass transfer, mass accretion and hence the evolution of binary systems. The aim of this discussion is to put in context the model calculations that will be presented in the next chapter.

3.1 Important time-scales for mass transfer

If mass transfer from the secondary star to the primary star in a binary system occurs as a result of the secondary star filling its Roche surface, the mass transfer rate is determined by three important time-scales (e.g. Morton 1960; King 1988; Verbunt 1993):

(1) the nuclear time-scale

$$\tau_n = 10^{10}(\frac{M_2}{M_\odot})(\frac{L_\odot}{L_2})\ \text{yr} \qquad (3.1)$$

in which the star expands as a result of hydrogen burning in its core

(2) the thermal time-scale

$$\tau_{th} = 3.1\times10^{7}(\frac{M_2}{M_\Theta})^{2}(\frac{R_\Theta}{R_2})(\frac{L_\Theta}{L_2})\ \text{yr} \qquad (3.2)$$

in which a star attempts to restore its perturbed thermal equilibrium, if its surface luminosity in not balanced by its nuclear energy generation rate, and

(3) the dynamical time-scale (in days)

$$\tau_d = 0.04(\frac{M_\Theta}{M_2})^{1/2}(\frac{R_2}{R_\Theta})^{3/2}\ \text{d} \qquad (3.3)$$

in which a star restores a perturbed hydrostatic equilibrium as a result of losing its surface layers during the mass transfer process. If a star deviates from hydrostatic equilibrium, that is, if the gravitational force is not balanced everywhere by the pressure force, it will periodically expand and contract a few times until equilibrium is established, provided that no external mechanism feeds energy into the star.

Since the mass accretion onto a compact object has a significant influence on binary evolution, it is important to realize that it has a built-in control mechanism, i.e. a control value, which results in temporal shut-down in the mass accretion. This will obviously have an influence on the evolution of these systems. A qualitative discussion of this will now be presented.

3.2 The Eddington limit

The luminosity of an accreting system depends on the compactness, M/R, and the accretion rate. Under certain conditions, the radiation will push away the accreting material and this leads to the existence of a maximum luminosity for a given system which is called the "Eddington luminosity" and this condition is called the Eddington limit.

Considering a steady spherically symmetrical accretion, we assume the accreting material to be mainly fully ionized hydrogen. Under these circumstances, the radiation exerts a force mainly on the free electrons through Thomson scattering since the scattering cross-section for photon-proton interactions is a factor

$(m_e/m_p)^2 \approx (5\times10^{-4})^2$ smaller. If S is the radiant energy flux (erg s^{-1} cm^{-2}) and $\sigma_T = 6.7\times10^{-25}$ cm^2 is the Thomson cross-section, then the outward radial force on each electron equals the rate at which it absorbs momentum, i.e. $\sigma_T S/c$. The attractive electrostatic Coulomb force between the electrons and protons means that as the electrons move out, they drag the protons with them. In effect, the radiation pushes out electron-proton pairs against the total gravitational force $GM_1(m_p+m_e)/r^2 \approx GM_1 m_p/r^2$,

acting on each pair at a radial distance r from the centre. If the luminosity of the accreting source is L (erg s^{-1}), we have $S = L/4\pi r^2$ by spherical symmetry, so the net force on the electron-proton pair (e.g. Frank, King & Raine 1992, p.3) is

$$(GM_1 m_p - \frac{L\sigma_T}{4\pi c})\frac{1}{r^2}. \qquad (3.4)$$

There is a limiting luminosity for which the inward gravitational force is balanced by the outward force, i.e. the so-called Eddington luminosity, which is

$$L_{edd} = 4\pi GM_1 m_p c/\sigma_T \approx 1.3\times10^{38}(M_1/M_\odot)\,\text{erg s}^{-1}. \qquad (3.5)$$

At greater luminosities the outward pressure of radiation would exceed the inward gravitational attraction and accretion would be halted. If all the luminosity of the source were derived from accretion, the source would be 'switched off'. However, if some, or all, of the luminosity exceeding the Eddington limit is produced by other means, for example nuclear burning, then the outer layers of the material would begin to be blown off by a strong radiation driven wind and the source would not be steady. For stars with a given mass-luminosity relation this argument yields a maximum stable mass.

The Eddington limit is derived from the basic assumptions of the accretion flow being steady and spherically symmetric and the accretion material being largely fully ionized hydrogen. These assumptions may not always be true, however, but this can give us a good estimate of the magnitude of the luminosities and the accretion rate responsible for this effect.

For accretion powered objects the Eddington limit implies a limit on the steady accretion rate, $\dot{M}\,(\mathrm{g\,s^{-1}})$. If all the kinetic energy of infalling matter is given up to radiation at the stellar surface, R_1, then the accretion luminosity L_{acc} and $\dot{M}_{edd}$ are:

$$L_{acc} = GM_1\dot{M}/R_1 \tag{3.6}$$

$$\dot{M}_{edd} = 7.5\times10^{20}\left(\frac{L_{edd}}{10^{38}\ \mathrm{erg\,s^{-1}}}\right)\left(\frac{M_1}{M_\odot}\right)^{-1}\left(\frac{R_1}{10^9\ \mathrm{cm}}\right)\mathrm{g\,s^{-1}} \tag{3.7}$$

where $\dot{M}_{edd}$ is the Eddington accretion rate of the primary star. For stable accretion, $\dot{M}_{acc} < \dot{M}_{edd}$ and hence $L_{acc} < L_{edd}$, which gives us the maximum accretion luminosity as well as the maximum accretion rate for a given primary mass-radius combination.

3.3 Secular evolution of binaries

3.3.1 Mass transfer and binary evolution

To put into perspective the influence that mass transfer, mass accretion by the white dwarf, mass and orbital angular momentum loss from the system have on the subsequent orbital evolution of a binary system, logarithmic differentiation of the expression for the orbital angular momentum (e.g. King 1988), i.e.

$$J_{orb} = M_1M_2\left(\frac{Ga}{M}\right)^{1/2}, \tag{3.8}$$

results in (e.g. King 1988)

$$\frac{\dot{a}}{a} = 2\frac{\dot{J}_{orb}}{J_{orb}} + \frac{\dot{M}}{M} - 2\frac{\dot{M}_1}{M_1} - 2\frac{\dot{M}_2}{M_2}. \tag{3.9}$$

Since the Roche lobe radius of the secondary (R_{L2}) depends on the binary separation according to $R_{L2} \propto (a^3M_2/M)^{1/3}$, for $q = \frac{m_2}{m_1} < 1$, it can be shown that (e.g. Wynn & King 1995)

$$\frac{\dot{R}_{L2}}{R_{L2}} = 2\frac{\dot{J}_{orb}}{J_{orb}} + \frac{2}{3}\frac{\dot{M}}{M} - 2\frac{\dot{M}_1}{M_1} - \frac{5}{3}\frac{\dot{M}_2}{M_2}. \tag{3.10}$$

Mass transfer in the form of diamagnetic blobs (e.g. Kuijpers & Pringle 1982; Frank, King & Lasota 1988; King & Lasota 1991; King 1993; Wynn & King 1995) may result in a fraction (η) of the transferred angular momentum across L_1 being lost from the binary entirely (e.g. King 1993; Wynn & King 1995), resulting in

$$\frac{\dot{J}_{loss}}{J_{orb}} = \eta \frac{\dot{J}_{ov}}{J_{orb}} = \eta \dot{M}_2 \frac{(GM_1 R_{circ})^{1/2}}{J_{orb}}. \tag{3.11}$$

This contributes to the total orbital angular momentum loss of the system through other mechanisms

$$\frac{\dot{J}_{orb}}{J_{orb}} = \frac{\dot{J}_{loss}}{J_{orb}} + (\frac{\dot{J}_{wind}}{J_{orb}} + \frac{\dot{J}_{mb}}{J_{orb}} + \frac{\dot{J}_{gr}}{J_{orb}} + X)$$

$$= \frac{\dot{J}_{loss}}{J_{orb}} + \frac{\dot{J}}{J} \tag{3.12}$$

where X represents any other potential mechanism that may drain orbital angular momentum and $\dot{J}/J$ represents all other drains of orbital angular momentum.

It can be shown that the mass loss from the system and the mass that is accreted by the white dwarf are related through (e.g. $\dot{M} < 0; \dot{M}_2 < 0; \dot{M}_1 > 0$)

$$\dot{M} = \alpha \dot{M}_2 \quad ; \quad \dot{M}_1 = (1-\alpha)|\dot{M}_2| \text{ or } \dot{M}_1 = \beta|\dot{M}_2| \tag{3.13 a,b,c}$$

where α is the fraction of the mass overflow from the secondary that escapes from the system and $\beta = (1-\alpha)$ is the fraction of the mass accreted by primary star from the secondary.

Applying eqns (3.11) and (3.13) to (3.10) gives the rate of change of the Roche lobe radius as

$$\frac{\dot{R}_{L2}}{R_{L2}} = 2\frac{\dot{J}}{J} - \frac{\dot{M}_2}{M_2}[\frac{5}{3} - 2(1-\alpha)q - \frac{2}{3}\frac{q\alpha}{1+q} - 2\eta \frac{M_2(GM_1 R_{circ})^{1/2}}{J_{orb}}]. \tag{3.14}$$

It can be shown that when $\alpha = 0$ (i.e. $\beta = 100\%$), $\eta = 0$ (e.g. King 1988; Frank, King, Raine 1992, p.52), the orbital evolution is determined by these two factors according to

$$\frac{\dot{a}}{a} = 2\frac{\dot{J}}{J} + 2(\frac{-\dot{M}_2}{M_2})(1-q). \tag{3.15}$$

It is evident that the binary will shrink for $q > 1$ and expand for $q < 1$, if the mass transfer rate from the secondary to the compact primary dominates the rate at which angular momentum is drained from the binary.

Mass transfer via Roche lobe overflow can be sustained if the Roche surface is kept close to the surface of the mass-donating star, i.e. within a few scale heights. This criterion can be evaluated by noting that the dynamical evolution of the Roche surface of the secondary star is determined by

$$\frac{\dot{R}_{L2}}{R_{L2}} = 2\frac{\dot{J}}{J} + 2\left(\frac{-\dot{M}_2}{M_2}\right)\left(\frac{5}{6} - q\right) \qquad (3.16)$$

which shows that for $q > 5/6$, and $\dot{J} \neq 0$, the Roche surface of the secondary star will probably shrink effectively enough through the atmosphere of the secondary star to drive a substantial mass transfer. For $q < 5/6$, with the secondary still on the main sequence, mass transfer through Roche lobe overflow can only occur if a very effective angular momentum loss mechanism is at work in the binary system.

3.3.2 The response of the secondary star to mass loss

From the equations above, it can be seen that the mass transfer plays a vital role in the secular evolution of these binary systems. However, the reaction of the star to the mass loss is of extreme importance to the mass transfer process and needs to be discussed briefly. The reaction of the star affects the mass transfer on time scales from the dynamical time scale (seconds) to the thermal time scale (10^7 yr).

To evaluate the effect of mass loss from a star, the way in which the star restores its perturbed hydrostatic equilibrium as a result of losing its surface layers during mass transfer needs to be evaluated. For example, a star with a convective envelope (usually low-mass stars) will respond in a different way in order to restore perturbed hydrostatic equilibrium as opposed a star with a radiative envelope (usually heavier stars). The underlying reason for this is that a star with a convective envelope has a

constant entropy profile throughout the envelope, while a star with a radiative envelope has a steep entropy gradient near the surface (e.g. Hjellming & Webbink 1987; King 1988). As mass is lost from the surface, the entropy profile of the gas envelope underneath the surface will determine the way in which the star will re-adjust to restore its perturbed hydrostatic equilibrium. This occurs on the dynamical time-scale. To investigate this (Hjellming & Webbink 1987; King 1988), the secondary can be treated as a polytrope of index n and adiabatic index ζ_{ad}, which results in a response to mass loss of

$$\frac{\dot{R}_2}{R_2} = -\zeta_{ad}\left(\frac{-\dot{M}_2}{M_2}\right). \qquad (3.17)$$

Stars with convective and radiative envelopes have $\zeta_{ad} < 0$ (convective) and $\zeta_{ad} > 0$ (radiative) respectively, which implies that stars with convective and radiative envelopes respectively expand and contract, in an attempt to restore perturbed hydrostatic equilibrium following mass loss (Hjellming & Webbink 1987; King 1988). This has important consequences for the mass transfer process in these stars.

The influence of surface expansion and angular momentum losses on the mass transfer rate in magnetic CVs can be illustrated in the case of AE Aqr (e.g. Meintjes 2002). A brief discussion will be presented.

The low-mass K4-5 secondary star in AE Aqr can be treated as an $n = 3/2$ polytrope with an adiabatic index $\zeta_{ad} < 0$ (Hjellming & Webbink 1987; King 1988; Wynn, King & Horne 1997). It has been shown (Hjellming & Webbink 1987) that for an $n = 3/2$ polytrope the adiabatic index (ζ_{ad}) depends on the core mass. For a non-evolved zero-age main-sequence star (ZAMS) and an evolved main-sequence star, the authors obtained

ZAMS: $m_{core} = 0 \rightarrow \zeta_{ad} = -0.33$

Evolved: $m_{core} > 0 \rightarrow \zeta_{ad} = -0.2$,

respectively. Therefore, unless the Roche lobe expands with the star during mass loss, it can be envisaged that the expanding secondary can overflow its Roche surface, resulting in a run-away mass transfer to the white dwarf. The overflowing of the Roche surface can follow from an expanding secondary (resulting from mass loss)

accompanied by a shrinking (or too slow expanding) Roche lobe resulting from high angular momentum losses. In the quasi-conservative mass transfer case, this will only be prevented if $q < q_{crit}$ (Meintjes 2002). It can be shown that run-away mass transfer ($-\dot{M}_2 / M_2 >> \dot{J} / J$) will probably proceed until the Roche lobe of the secondary (R_{L2}) expands further than the secondary star evolves (inflates) in the same time in response to high mass loss. In the case where ($-\dot{M}_2 / M_2 >> \dot{J} / J$) this occurs when some critical q-ratio is reached, determined by the condition

$$\frac{\dot{R}_{L2}}{R_{L2}} = 2(\frac{-\dot{M}_2}{M_2})(\frac{5}{6} - q_{crit}) \geq \frac{\dot{R}_2}{R_2}. \tag{3.18}$$

This gives

$$(\frac{5}{3} - 2q_{crit} + \zeta_{ad}) > 0 \tag{3.19}$$

and it can be shown that $q_{crit} \sim 2/3$ (ZAMS secondary) and $q_{crit} \sim 0.73$ (evolved secondary), respectively (e.g. Meintjes 2002). This estimate may play an important role in the evolution of the AE Aqr system and will be evaluated in the next chapter.

3.4 The binary separation, the radius of the secondary and the orbital period

An invaluable tool for the study of orbital evolution of binary systems is the Roche lobe dynamics, which determine the properties of lobe-filling stars, which in turn determine the mass transfer. A brief, qualitative discussion, is now presented.

By analyzing data of the radius of the secondary R_2, the binary separation a and the mass ratio q, Eggleton (1983) derived an empirical expression for the ratio of the secondary star's Roche lobe to the binary separation, for all mass ratios, which is

$$R_2 / a = \frac{0.49 q^{2/3}}{0.6 q^{2/3} + \ln(1 + q^{1/3})}. \tag{3.20}$$

For $0.1 \leq q \leq 0.8$ the equation above can be written (Paczynski 1971)

$$R_2 / a = 0.462(\frac{q}{1+q})^{1/3}. \tag{3.21}$$

To drive stable, long-lived mass transfer, the secondary star must fill, or closely fill, its Roche lobe (e.g. Kopal 1959). The scale of the Roche geometry is determined by the binary separation a, and the shapes of the equipotentials by the mass ratio $q = M_2 / M_1$. For lobe-filling secondary stars a reasonable assumption is the $R_2 / a \approx R_{L2} / a$, where R_{L2} represents the Roche-lobe radius of the secondary star.

An interesting case for $q \leq 0.8$ is that the mean density $\bar{\rho}$ of a lobe-filling star is determined solely by the binary period (e.g. Frank King & Raine 1992, p.51)

$$\bar{\rho} = \frac{3m_2 M_\Theta}{4\pi R_2^3} \cong 115 P_{orb}^{-2} \text{ g cm}^{-3}, \tag{3.22}$$

where we have used eqn (1.1) to eliminate the binary separation a in eqn (3.21). This equation shows that for binary periods of a few hours, stars with mean densities typical of the lower main sequence ($\rho \sim 1-100 \text{ g cm}^{-3}$) can fill their Roche lobes. For example, if we assume that the lobe-filling star is close to the lower main sequence we know that its radius and the mass-radius relation determines that (e.g. King 1988; Kippenhann & Weigert 1990).

$$\frac{M_2}{M_\Theta} \approx \frac{R_2}{R_\Theta} \Rightarrow m_2 \approx \frac{R_2}{R_\Theta} \text{ (in solar mass units)}. \tag{3.23}$$

Thus

$$\bar{\rho} = \frac{3m_2 M_\Theta}{4\pi R_2^3} = \frac{3M_\Theta}{4\pi R_\Theta^3} \frac{1}{m_2^2} = \frac{1.4}{m_2^2} \text{ g cm}^{-3}, \tag{3.24}$$

where the solar mean density $\rho_\Theta = 1.4 \text{ g cm}^{-3}$ has been used. This relation, substituted into eqn (3.22) results in a period-mass relation, which is

$$m_2 \cong 0.11 P_{orb}, \tag{3.25}$$

and a corresponding period-radius relation (e.g. Frank, King & Raine 1992, p.51), which is

$$R_2 \cong 0.11 R_\Theta \times P_{orb} = 7.9 \times 10^9 P_{orb} \text{ cm}. \tag{3.26}$$

These expressions are handy paramerizations, allowing reasonably accurate estimates of important binary parameters which are required for modelling the mass transfer and evolution of binary systems.

3.5 Accretion onto the magnetic cataclysmic variables

In the preceding discussions the influence of mass transfer has been explained in the binary system's evolution. However, it has been shown that the fraction $\beta = (1-\alpha)$ of the mass transfer accreted by the primary star also plays an influential role in the binary evolution, as does the fraction η of the angular momentum across the L_1 point being lost by the binary. To discuss these effects more quantitatively, the focus now shifts to the accreting compact object to explain the possible accretion modes and their influence on the evolution of the binary system.

It has been suggested (Wynn, King & Horne 1997) and shown (Meintjes 2002) that the accretion history of AE Aqr is characterized by disc and discless accretion. However, AE Aqr is currently in a propeller phase where the white dwarf accretes hardly any material. These various modes of accretion have different influences on the binary evolution, which will be discussed briefly.

3.5.1 Discless

It has been suggested (e.g. King 1993) that the relative short spin periods of accreting white dwarf in the intermediate polars, i.e. $P_{spin} < P_{orb}$, may be the result of the accretion of large diamagnetic blobs in the accretion stream. It has been mentioned earlier that the conservation of angular momentum of the stream requires that blobs orbit the compact object initially at the so-called circularization radius. If the circularization radius is inside the corotation radius of the magnetized white dwarf, the white dwarf accretes the angular momentum from the circulating stream, resulting in a gradual spin-up to periods $P_{spin} < P_{orb}$ (e.g. King 1993; Wynn, King & Horne 1995). (Apart from AE Aqr,) There is currently only one confirmed discless IP, namely V2400 Oph (Buckley et al. 1997). However, the short spin period of AE Aqr, i.e. $P_{spin} \sim 33\,\mathrm{s}$, suggests that AE Aqr has evolved through a very rapid spin-up phase, possibly via an accretion disc.

3.5.2 Accretion disc

The short spin period $P_{spin} << P_{orb}$ of the white dwarf in AE Aqr suggests that the white dwarf accreted from an accretion disc at some stage of its evolution, resulting in a subsequent spin-up to a short period (e.g. Meintjes 2002). In the disc-accretion phase the accretion process onto the white dwarf was probably much more efficient ($\alpha = 0$), and tidal interaction between the disc and the secondary resulted in very little angular momentum flowing across L_1 escaping from the system. i.e. $\eta \to 0$. The evolution during the accretion disc phase is then quasi-conservative ($\alpha = 0; \eta = 0$) and the spin-up phases for such systems will involve very rapid, dynamically unstable mass transfer, and accordingly be very short-lived (e.g. Wynn & King 1995). Since it is believed that the so-called SSS phase of AE Aqr, and possibly other cataclysmic variables, is facilitated by a disc-accreting process, a more quantitative discussion will be presented in section 3.6.

3.5.3 Propeller outflow

In the disc accreting phase ($\alpha = 0; \eta = 0$), the magnetic white dwarf is spun-up to a period of the order of $P_{spin} \sim 33\,\mathrm{s}$, i.e. it becomes a very fast rotator. The estimated mass transfer rate driven by magnetic braking (Verbunt & Zwaan 1981; King 1988; Meintjes 2002) is of the order of $-\dot{M}_2 \sim 4\times10^{17}(\frac{P_{orb}}{9.88\,\mathrm{hr}})^{5/3}\,\mathrm{g\,s^{-1}}$ and is in excellent agreement with the estimated current mass transfer rates that are in the range (Wynn, King & Horne 1997) $-\dot{M}_2 \sim (1-5)\times10^{17}\,\mathrm{g\,s^{-1}}$. The low mass transfer will result in the inner disc (inside corotation radius) being eroded by accretion onto the white dwarf, resulting in the fast rotating magnetosphere interacting with the disc residue outside the corotation radius. This results in a subsequent decrease in the mass accretion onto the white dwarf. Since the fast rotating magnetosphere will interact with the slower rotating disc or accretion flow outside the corotation radius, a significant mass ejection will occur as the gas is centrifugally driven from the system by the fast rotating magnetosphere, resulting in a spin-down torque that will erode the rotational kinetic energy of the white dwarf with time (e.g. Meintjes 2002).

3.6 The consequences of disc accretion

The short rotation period of AE Aqr can only be reconciled with a period of significant accretion via an accretion disc. As mentioned in section 2.2.2, during the high mass transfer phase, a well-developed disc should be present that can facilitate mass accretion onto the white dwarf if the condition of eqn (2.34) is satisfied. It is under these circumstances that the interaction of a stream with a magnetic field will give way to the formation of a disc.

3.6.1 Magnetic accretion flow

Let us first consider the much simpler case in which the stellar magnetic field disrupts the accretion flow which is quasi-spherical far from the star. For a dipole-like magnetic field, the field strength B varies roughly as $B \sim \frac{\mu}{r^3}$ at radial distance r from the star of radius R_1; hence $\mu_1 = B_1 R_1^3$ is a constant magnetic moment specified by the surface field strength B_1 at $r = R_1$. Thus, there is a magnetic pressure (Frank, King & Raine 1992, p.121)

$$P_{mag} = (\frac{4\pi}{\mu_0})\frac{B^2}{8\pi} = (\frac{4\pi}{\mu_0})\frac{\mu^2}{8\pi r^6} \qquad (3.27)$$

increasing steeply as the matter approaches the stellar surface. This magnetic pressure will begin to control the matter flow and thus disrupt the spherically symmetric infall at a radius r_M where it first exceeds the ram and gas pressures of the matter (see Figure 3.1). For highly supersonic accretion, it is the ram pressure term ρv^2 which is important, with the velocity v close to the free-fall values $v_{ff} = (2GM_1/r)^{1/2}$ and $|\rho v|$ given in terms of the accretion rate $\dot{M}_1$, i.e.

$$|\rho v| = \frac{\dot{M}_1}{4\pi r^2}. \qquad (3.28)$$

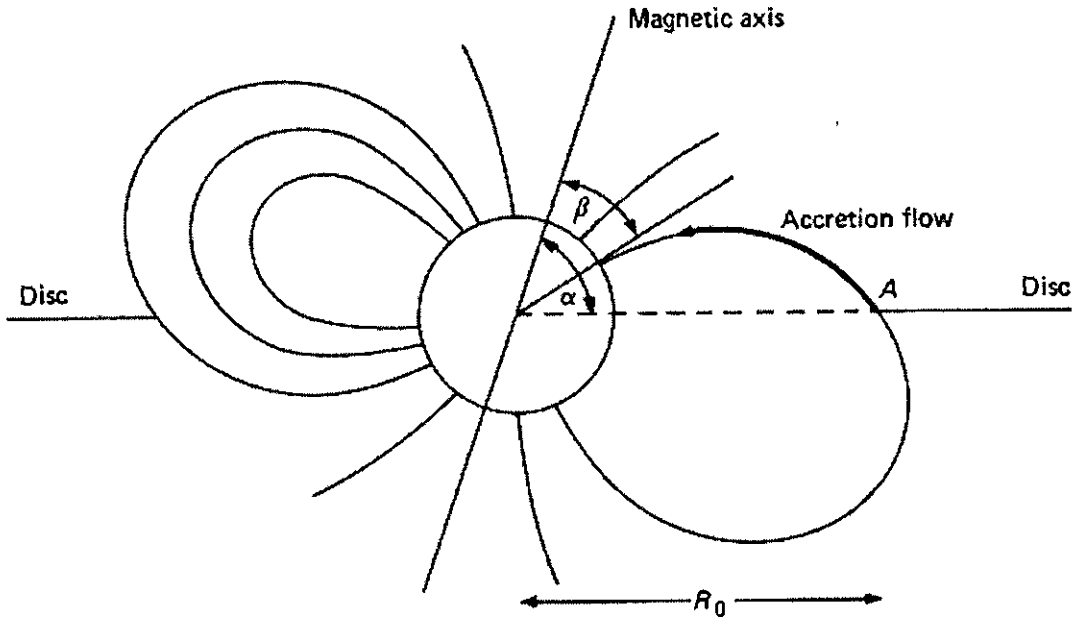

Fig 3.1 The accretion flow of a magnetized neutron or white dwarf (Frank, King & Raine 1992, p.123)

Thus setting $P_{mag}(r_M) = \rho v^2\Big|_{r_M}$ we find (e.g. Frank, King & Raine 1992, p.122)

$$(\frac{4\pi}{\mu_0})\frac{\mu^2}{8\pi r^6} = \frac{(2GM_1)^{1/2}\dot{M}_1}{4\pi r_M^{5/2}}, \tag{3.29}$$

from which the magnetosphere, or pressure balancing radius, can be determined, i.e.

$$r_M = 5.1\times10^8 \dot{M}_{16}^{-2/7} m_1^{-1/7} \mu_{30}^{4/7} \text{ cm}. \tag{3.30}$$

In this expression $\dot{M}_{16}$ is the mass accretion rate of the white dwarf in units of 10^{16} g s^{-1}, μ_{30} is magnetic moment of the white dwarf in units of 10^{30} G cm^3 and R_1 is the radius of the white dwarf, adopting a white dwarf mass-radius relation, i.e. $R_1 = 5.3\times10^8(\frac{M_1}{0.9M_\odot})^{-0.8}$ cm (e.g. Hamada & Salpeter 1961; Eracleous & Horne 1996; Meintjes 2002). It is often convenient to replace $\dot{M}$ in terms of the accretion luminosity, which is more directly related to the observational quantities, especially for X-ray sources, which results in

$$r_M = 5.5\times10^8 m_1^{1/7} R_9^{-2/7} L_{33}^{-2/7} \mu_{30}^{4/7} \text{ cm}. \tag{3.31}$$

The quantity r_M is known as the Alfvén radius. Within the Alfvén radius the matter is expected to flow along field lines. Although derived for spherically symmetric accretion, a good order of magnitude estimate for the inner edge of an accretion disc, supported by the magnetospheric pressure of a magnetized compact objects is (e.g. Frank, King & Raine 1992, p.122):

$$R_0 = 0.5 r_M . \tag{3.32}$$

3.6.2 The spin-up and spin-down of the white dwarf

By adopting the basic framework of the Ghosh & Lamb (1979b) model, but using a different approach to calculate the toroidal magnetic fields induced in the accretion disc, Wang (1987) derived expressions for the spin-up and spin-down torques on a disc-accreting compact object. The spin-up results from angular momentum flux of the accreted matter, and magnetic stresses inside the corotation radius that are transmitted to the compact object, while the spin-down torque results from magnetic stresses outside the corotation radius that are attempting to force disc plasma into corotation with the rotating accreting star. The net torque (N) on the accreting star as a result of spin-up ($N > 0$) and spin-down ($N < 0$) torques is (Wang 1987)

$$N = \dot{M}_1 (G M_1 R_c)^{1/2} f(x_0) \tag{3.33}$$

where the dimensionless function $f(x_0)$ is given by

$$f(x_0) = x_0^{1/2} + \frac{2}{9} x_0^{31/80} [1 - x_0^{3/2} - \frac{x_0^{9/4}}{(1 - x_0^{3/2})^{1/2}}] \tag{3.34}$$

where $x_0 = (R_0 / R_c)$. Here R_0 and R_c represent respectively the radial distance where the gas flow is guided by field lines to the accreting object and the corotation radius.

Here $R_0 \sim 0.5 r_M$ and R_c is

$$R_c = (\frac{G M_1}{\Omega_1^2})^{1/3} \text{ where } \Omega_1 = \frac{2\pi}{P_{spin,s}}, \tag{3.35 a,b}$$

where the $P_{spin,s}$ is the spin period of the white dwarf in seconds.

It has been shown (Wang 1987) that the dimensionless function $f(x_0)$ varies slowly between $0 < f(x_0) < 0.794$ (which is a maximum when $x_0 \sim 0.62$), while it decreases sharply below zero for $x_0 > 0.971$, e.g. see Fig 3.2.

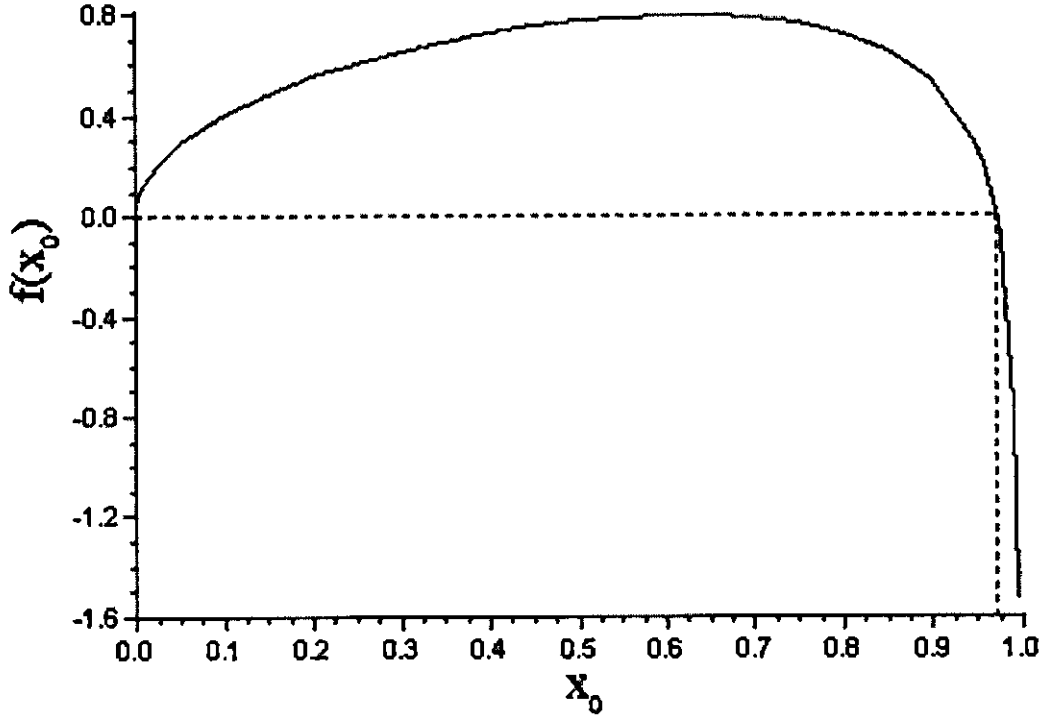

Fig 3.2 Plot of the function $f(x_0)$

It can be seen that $f(x_0) > 0$ for all $x_0 < 0.971$, implying a positive net torque and subsequent spin-up of the compact object. Also $f(x_0) < 0$ for all $x_0 > 0.971$, implying a spin down torque that is applied to the compact object.

The total rate of change of the rotation period of the accreting compact object as a result of the total torque is (Wang 1987)

$$-\frac{\dot{P}_1}{P_1} = \frac{N}{I\Omega_1} \approx \frac{5}{2}\frac{\dot{M}_1}{M_1}\left(\frac{R_c}{R_1}\right)^2 f(x_0)\,\mathrm{s}^{-1}, \tag{3.36}$$

where N is the total torque on the compact object, $I = 2M_1R_1^2/5$ is the compact object's moment of inertia, which is assumed to stay more or less constant. The total spin time-scale in which the spin period of the compact object evolves is $t_{su} \sim P_1/\dot{P}_1$,

which is

$$t_{su} \approx -\frac{P_1}{\dot{P}_1} = \frac{2}{5}\frac{M_1}{\dot{M}_1}\left(\frac{R_1}{R_c}\right)^2 f(x_0)^{-1}\ \mathrm{s}. \tag{3.37}$$

3.6.3 The break-up and equilibrium period

The minimum period to which the white dwarf can be spun-up by disc torques before it obliterates itself under the intense centrifugal forces, is the break-up period

$$P_{bu} \approx 6\left(\frac{R_1}{5\times10^8\,\mathrm{cm}}\right)^{3/2}\left(\frac{M_1}{0.9M_\Theta}\right)^{-1/2}\ \mathrm{s}. \tag{3.38}$$

Using the model of Wang (1987), it can shown that, for a given mass accretion rate and magnetic moment, the equilibrium period of the rotating compact object, where the period of the rotating compact object equals the Keplerian period at R_c, is (Meintjes 2002)

$$P_{eq} \approx 3.5\left(\frac{\varepsilon_{31}}{2}\right)^{180/211}\left(\frac{M_1}{0.9M_\Theta}\right)^{-140/211}\left(\frac{\dot{M}_1}{10^{20}\,\mathrm{g\,s^{-1}}}\right)^{-96/211}\ \mathrm{s} \tag{3.39}$$

In the above equation $\varepsilon = (\gamma/\xi)^{1/3}(\eta\mu/\alpha^{3/20})$ (Wang 1987), with $\eta \sim 0.2$ a screening coefficient (Ghosh & Lamb 1979a), and where $\xi \sim 0.1-1$ determines the rate of annihilation of disc-generated toroidal fields via reconnection with ambient fields on the disc surface, by either diffusing [~0.1 (e.g. Priest 1981)] through disc surface, or rising as a result of buoyancy [~1 (e.g. Wang 1987)]. The symbols μ and α represent the magnetic moment of the white dwarf and the Shakura & Sunyaev (1973) disc α-parameter, respectively. Since the equilibrium period can never be reached before the star breaks up, it shows that the white dwarf and accretion disc are spinning far out of equilibrium, which suggests that spin-up of the white dwarf occurs for $x_0 << x_{eq}$. For these x_0 values, the average value of the dimensionless function is less than the maximum value 0.794, i.e. the average of $f(x_0) \sim 0.57$ (Wang 1987). A resultant spin-up for $x_0 \to 0$ will result in $f(x_0) \to 0$ and since $t_{su} \propto f^{-1}(x_0)$ the spin-up time-scale will increase noticeably as a result of the slow momentum transfer from the accretion disc to the white dwarf. This can be attributed to the short lever arm suggested by an accretion disc of which the inner edge is in the vicinity $x_0 << x_{eq}$.

Therefore, a sustained high mass transfer and accretion is required over periods long enough for effective spin-up to short rotation periods.

By using the Wang (1987) model, different mass transfer and accretion rate scenarios have been investigated in order to determine the possible spin-up history of the white dwarf in AE Aqr to a period of $P_{spin} \sim 33$ s. The results will be presented in Chapter 4.

3.7 Orbital angular momentum loss and mass transfer mechanisms

To end the discussion related to the various aspects that determine the evolution of binary systems, a brief discussion of the main angular momentum loss mechanisms responsible for mass transfer in a binary system will be presented. There are two dominant mechanisms by which cataclysmic binaries lose angular momentum; i.e. gravitational radiation and magnetic braking.

3.7.1 Gravitational radiation

In accordance with the theory of general relativity, matter causes space-time to curve. The repetitive orbiting of two stars causes a rhythmic warping of space which ripples outwards in a periodic wave. This is called *gravitational radiation.* The energy which generates the wave is extracted from the binary orbit, causing a slow inward spiraling.

It can be shown that gravitational radiation results in a rate of change of the binary angular momentum ($\dot{J}$), which is (Kraft, Mathews & Greenstein 1962; Landau, Lifchitz 1975)

$$\left|\frac{\dot{J}}{J}\right| \propto \frac{M_1 M_2 M}{a^4}. \qquad (3.40)$$

Here M_1 ,M_2 ,M and a represent respectively the mass of the primary, secondary, binary and orbital separation. It can be seen that $\dot{J}/J \propto a^{-4}$, resulting in gravitational

radiation being effective for compact binaries (small a), i.e. the short period systems, typically for the close binaries below the period gap, i.e. $P_{orb} < 2 \sim 3$ hrs. It can be shown that for systems below the period gap, gravitational radiation can drive mass transfer rates of the order of $\dot{M}_2 \sim 10^{16}$ g s^{-1} which corresponds well with the inferred mass transfer rates in these systems.

3.7.2 Magnetic braking

Secondary stars in close binaries have convective envelopes (Campbell 1997) which explains the magnetic nature of these stars in terms of internal dynamo processes. The short orbital period of these systems ($P_{orb} \sim$ few hours) implies that the secondaries, which are tidally locked to the orbital period, are rapid rotators. This implies that the thermal plasma with velocity exceeding the escape velocity will be centrifugally expelled along the field lines, into the so-called wind zone. Inside the Alfvén surface, where the magnetic pressure exceeds the wind gas pressure, the magnetic field will enforce corotation. The magnetic torque imparts angular momentum to the flowing material, at the expense of the stellar angular momentum, causing a braking torque on the star. The open field lines, constituting the wind zone, accounts for the main loss of stellar angular momentum. A magnetic wind from a lobe-filling secondary star in a binary system leads to a loss of orbital angular momentum. The mechanism responsible for angular momentum losses is the load on the field lines outside the Alfvén surface which attempts to maintain corotation of the wind with the corotating field. This results in a braking torque being exerted on the star. The loss of angular momentum is intimately tied to the size of the Roche lobe of the secondary (Frank, King & Raine 1992, p.53). Angular momentum losses result in the Roche lobe of the secondary shrinking along with the binary orbit (e.g. Frank, King & Raine 1992, p.53 for a discussion). This process ensures that the L_1 point staying close to the stellar surface, resulting in a steady mass transfer being maintained. This process dominates the mass transfer in binaries for most system with $P_{orb} \geq 3$ hrs.

The theory of a steady axisymmetric magnetic wind was developed by Mestel (1967, 1968) and Weber and Davis (1967). Further work was done by many authors, including Pnuman and Kopp (1971), Okamoto (1974) and Sakurai (1985). The braking of the late-type stars was considered by Mestel and Spruit (1987), including the fast rotator secondary star in binaries.

The above mentioned magnetic braking mechanism can provide a way of removing orbital angular momentum fast enough to explain the higher values of $\dot{M}_2$ in many binaries. Verbunt and Zwaan (1981) estimated the magnetic braking torque by using the Skumanich (1972) spin-down law for single stars, assumed to be due to magnetic braking.

Campbell (1997) applied magnetic braking theory to find expressions for $\dot{M}_2$. The above mentioned fast rotator theory is relevant here, which applies for $\Omega_s \geq 100\,\Omega_\odot$ i.e. for $P \leq 7\,\mathrm{hr}$, where $\Omega_\odot$ is solar angular velocity. Firstly the effect of orbital evolution on the magnetic braking rate must be considered. If the secondary is kept in close orbital corotation by tidal forces then $\dot{L}_{orb} = \dot{J}$ applies, where $\dot{J}$ is the loss rate of stellar angular momentum via magnetic braking. The tidal torque is dissipative and so will only be finite when there is some asynchronism. For a turbulent viscosity the tidal torque can be comparable to the braking torque at small degrees of asynchronism, so Ω_s can be taken to be essentially the same as the orbital angular velocity. This mechanism can typically result in mass transfer rates of the order of $\dot{M}_2 \sim 10^{17}\ \mathrm{g\,s^{-1}}$ ($P_{orb} \geq 3 \sim 7\,\mathrm{hr}$).

The purpose of this discussion is to provide the theoretical framework for the model calculations that will be presented in the next chapter. The main focus of the theoretical investigation is the so-called high mass transfer/ accretion history of AE Aqr and its consequence for possible SSS properties the system could have exhibited. This may then constrain the possible range in orbital period of cataclysmic variables which may have entered the SSS phase, as well as other observational features, such as a systematic spin-up of the compact object during this, supposedly, disc accreting phase.

Chapter 4

A Possible Evolution for AE Aqr

A possible connection between high mass transfer and possible SSS properties is intimately tied to the mass accretion history of the compact object It has been shown (e.g. Chapter 3) that the Roche lobe and orbital dynamics, which are both linked to the mass transfer and accretion process, are determined by the parameters $\alpha = \dot{M} / |\dot{M}_2|$ (mass-loss from binary), $\beta = \dot{M}_1 / |\dot{M}_2| = (1-\alpha)$ (mass accreted by compact object) and $q = M_2 / M_1$ (mass ratio). Therefore these parameters and various additional constraints which lead to the appearance of the binary as an SSS during its high mass accretion phase, need to be investigated.

4.1 The constraints

This SSS conjecture will be investigated more quantitatively and the results are presented in the next two sections. However, first, the following constraints must be satisfied in order to confirm whether AE Aqr was an SSS in the past. These constraints are:

1. The minimum requirement for stable nuclear burning $\dot{M}_{1(\mathrm{SNB})}$, on the surface of an accreting white dwarf (Prialnik 1986), i.e. $\dot{M}_{1(\mathrm{SNB})} \approx 5.4\times10^{18}(M_1/0.6M_\Theta)^{3/2}\,\mathrm{g\,s^{-1}}$. Therefore, the requirement for the possible SSS scenarios is $\dot{M}_1 \geq \dot{M}_{1(\mathrm{SNB})}$.

In order to find the relationship between this and the mass accretion fraction β, both sides of the above equation are divided by $|\dot{M}_2|$ which results in $\dot{M}_1/|\dot{M}_2| \geq \dot{M}_{1(\mathrm{SNB})}/|\dot{M}_2|$. This results in the first constraint, which is: $\beta \geq \gamma$, where $\gamma = \dot{M}_{1(\mathrm{SNB})}/|\dot{M}_2|$.

2. Since the primary accretes from the secondary star, the mass transfer rate from the secondary star should be equal or higher than the mass accretion rate onto the primary, i.e. $|\dot{M}_2| \geq \dot{M}_1$. Both sides are divided by $|\dot{M}_2|$, resulting in $\beta \leq 1$. In addition to the first constraint, this results in the following condition that has to be satisfied, i.e. the second constraint $\gamma \leq \beta \leq 1$.

3. The mass of the white dwarf should not exceed the upper-limit of the mass of the white dwarf, i.e. the so-called Chandrasekhar limit $M_c \sim 1.4M_\Theta$. This results in the third constraint, which is $M_1 \leq 1.4M_\Theta$.

4. For a stable mass transfer at a sustained rate that can drive thermal nuclear burning, the system must avoid the delayed dynamical instabilities (DDI) (e.g. Schenker et al. 2002; King et al. 2001; Hjellming 1989; Webbink 1977), which occurs when the initial mass ratio $q_i > 2.9$. Therefore, for sustained stable thermal time-scale mass transfer, the following condition has to be satisfied, i.e. the fourth constraint, which is the initial mass ratio $q_i \leq 2.9$.

4.2 The SSS conjecture: An investigation

In order to find the possible SSS scenarios applicable to AE Aqr in the past, the first constraint $\beta \geq \gamma$, i.e. $\dot{M}_1 \geq \dot{M}_{1(\mathrm{SNB})}$, must be satisfied; therefore we need to find the mass accretion rate $\dot{M}_1$ and the minimum requirement for stable nuclear burning $\dot{M}_{1(\mathrm{SNB})}$ (Prialnik 1986).

However, the mass accretion rate $\dot{M}_1$ is directly dependent on the mass transfer rate from the secondary $\left|\dot{M}_2\right|$ (e.g. Frank, King & Raine 2002, p.352), i.e.

$$\dot{M}_1 = \beta\left|\dot{M}_2\right|, \text{ with} \tag{4.1}$$

$$-\dot{M}_2 \approx \frac{1}{4\pi}\rho_{L1}c_s^3 P_{orb}^2 \ \mathrm{g\,s^{-1}}, \tag{4.2}$$

where (e.g. Campbell 1997, p.56-58)

$$\rho_{L1} = \frac{1}{\sqrt{e}}\rho_{phot}\exp\frac{-(R_{L2}-R_{p2})}{H_p}\ \mathrm{g\,cm^{-3}} \tag{4.3}$$

$$c_s = \left(\frac{kT_{phot}}{\varepsilon m_H}\right)^{1/2} \tag{4.4}$$

Here $\rho_{phot} \sim 10^{-6}\ \mathrm{g\,cm^{-3}}$ represents the photospheric density (e.g. Frank, King, Raine 2002, p.353), R_{L2} and R_{p2} the Roche lobe and photospheric radius of the secondary, $H_p \sim (c_s^2 R_{p2}^2 / GM_2)$ the photospheric scale height of the secondary, the photospheric temperature T_{phot} and orbital period P_{orb} (e.g. Campbell 1997, p. 56-58), respectively.

Copeland et al. (1970) showed that the photospheric temperature (T_2) of the mass transferring secondary stars is a complicated function of the mean molecular mass ε and the mass of the secondary star M_2. Assuming a solar composition for the secondary, i.e. $\varepsilon = 0.75$ (Meintjes 2004), the photospheric temperature can be obtained for secondaries with various masses, i.e. Table 2 (Copeland et al. 1970).

It has been shown (Meintjes 2002) that secondary stars with convective envelopes can transfer mass at a rapid rate (close to dynamical time-scale) for all $q \geq q_{crit} \approx 0.73$,

after which the mass transfer will proceed at a more gentle rate, over the time-scale comparable to the thermal time-scale. In the present phase, the mass of white dwarf $M_1 \approx 0.87 M_\Theta$ (e.g. Welsh, Horne & Gomer 1995; Warner 1995 and Meintjes 2002) and AE Aqr most probably occupied the propeller phase ($\beta \sim 0$) (e.g. Meintjes 2002; Schenker et al. 2002) for the last $\tau \sim 10^7$ years (e.g. de Jager et al. 1994; Meintjes 2002). Therefore the secondary star's mass at the initial stage of the lower mass transfer phase can be determined from $q_{crit} \approx 0.73$. This results in the secondary star's mass at the end of run-away mass transfer phase being

$$M_2 = q_{crit} M_1 \approx 0.73 \times 0.87 M_\Theta \approx 0.635 M_\Theta, \qquad (4.5)$$

assuming $\beta \sim 0$ during the entire spin-down propeller phase.

This is well reconciled with a mass estimate involving the present propeller spin-down period phase lasting $\tau \sim 10^7$ yr, assuming a constant mass loss rate of the secondary star $|\dot{M}_2| \sim 4 \times 10^{17}\,\mathrm{g\,s^{-1}}$ (e.g. Eracleous & Horne 1996). This results in the mass loss in the propeller phase of $|\Delta M_2| \sim 0.06 M_\Theta$. Therefore, the mass of secondary star at the phase $q_{crit} \approx 0.73$ is approximately $M_{2,crit} \sim (0.6 + 0.06) M_\Theta = 0.66 M_\Theta$, where $M_2 \approx 0.6 M_\Theta$ represents the current inferred mass of the secondary (e.g. Meintjes 2002).

Since $\beta \sim 0$ (e.g. Meintjes 2002; Schenker et al. 2002) during the propeller phase, the primary star virtually accreted nothing since $q \le q_{crit} \approx 0.73$, resulting in the mass of white dwarf to remain at $M_1 \approx 0.87 M_\Theta$ for the past $\tau \sim 10^7$ yr. This may be an underestimate, but it simplifies the calculations somewhat.

Therefore, the average accretion fraction onto the surface of the white dwarf during the high mass transfer/ accretion phase can be estimated by taking the ratio of the mass accumulation onto the surface of the white dwarf ($\Delta M_1 = M_{1f} - M_{1i}$) to the mass loss by the secondary star ($|\Delta M_2| = -\Delta M_2 = M_{2i} - M_{2f}$) i.e.

$$\beta = \frac{\Delta M_1}{|\Delta M_2|} = \frac{0.87 - m_{1i}}{m_{2i} - 0.635}, \qquad (4.6)$$

where $M_{1f} \approx 0.87 M_{\odot}$ and $M_{2f} \approx 0.635 M_{\odot}$ (see our earlier discussion).

Using the expression for the mass transfer $|\dot{M}_2| \propto \rho_{L1} c_s^3 P_{orb}^2$, combined with the main sequence period-mass relation for lobe filling secondary stars, i.e. $m_2 \cong 0.11 P_{orb}$* (e.g. Frank, King & Raine 1992, p.51), orbital period-mass combinations have been selected for $q_i < 2.9$ satisfying $|\dot{M}_2| > \dot{M}_{1(\mathrm{SNB})}$. In this calculation several values for $\delta = (R_{L2} - R_{p2})/H_p$ have been selected $\delta = 3.5$, 2, 1, 0, -1, -2, representing several possible evolutionary scenarios related to the secondary, i.e. $\delta > 0$ corresponding to a secondary slightly underfilling its Roche lobe and $\delta < 0$ corresponding to a secondary overflowing its Roche lobe (for comparison). The photospheric density was kept at $\rho_{phot} \sim 10^{-6}\ \mathrm{g\ cm^{-3}}$ (e.g. Frank, King, Raine 2002, p.353) and the photospheric temperature for a given secondary star mass was obtained from Copeland H. et al. (1970). It should be mentioned that the condition $q_i < 2.9$ depends on the initial mass of the white dwarf in the high mass accretion phase, which obviously depends on the accretion fraction (β)

$$m_{1i} = 0.87 - \beta(m_{2i} - 0.635). \qquad (4.7)$$

The values of β satisfying $q_i < 2.9$ and the constraint $\gamma \le \beta \le 1$ may result in possible SSS scenarios.

*Note: Here, the $P_{orb} - m$ relation is derived from eqn (3.21) which is in general applied to $q \le 0.8$ (e.g. Frank, King & Raine 1992). For a more accurate analysis, eqn (3.20) should be used instead. The difference between these two equations increases when q increases, however, we find that for the maximum $q = 2.9$, the maximum difference is approximately 13%, which is quite acceptable for the current investigation. Therefore, for simplicity, we use the $P_{orb} - m$ relation for all the mass ratio q, even for $q > 0.8$.

4.3 The results & the discussion: AE Aqr Possible SSS Scenarios

The results are displayed as follows:

For each $\delta = (R_{L2} - R_{p2})/H_p$ ($\delta = 3.5$, 2, 1, 0, -1 and -2), the values of γ ($= \dot{M}_{1(\mathrm{SNB})}/|\dot{M}_2|$) are plotted as a function of β ($= \dot{M}_1/|\dot{M}_2|$) and the allowed parameters, satisfying stable nuclear burning on the primary (i.e. $\gamma \leq \beta \leq 1$), are indicated by the hatched area in Figs. 4.1, 4.2a, 4.3a, 4.4a, 4.5a and 4.6a, respectively.

The data is presented as follows: A glossary explaining the relevant parameters associated with the modelling is displayed in Table 4.1. The results associated with the investigation of the SSS conjecture for the filling factor $\delta = 3.5$ is presented in Table 4.2. However, to streamline the presentation, the results associated with $\delta = 2$, 1, 0, -1 and -2 are presented in the Appendix, i.e. Table A1-A5, respectively, and the possible SSS scenarios are highlighted in each Tables.

Additionally for each δ, for the β values satisfying the SSS criteria (i.e. the β values for which the points lie in the shaded area of Figs. 4.1, 4.2a-4.6a), the associated values of $\kappa = \dot{M}_1/\dot{M}_{\mathrm{edd}}$ and β are plotted as a function of orbital period in Figs. 4.2b-4.6b and Figs. 4.2c-4.6c, respectively. This may allow the identification of the orbital period range where AE Aqr could have been an SSS in its high mass accretion history. For sustained accretion onto the surface of the white dwarf, it is also required that $\kappa = \dot{M}_1/\dot{M}_{\mathrm{edd}} < 1$ in conjunction with $\gamma \leq \beta \leq 1$.

For each of the scenarios listed, the spin-up time-scale of the white dwarf, assuming an accretion disc being present, has been determined. By adopting the parameters $B_1 = 10^6$ G (e.g. Cropper 1986; Beskrovnaya et al. 1995; Chanmugam & Frank 1987; Meintjes 2002), $P_{spin,i} = 3600$ s (e.g. Wynn, King & Horne 1995; 1997), the spin-up time-scale is obtained from (eqn 3.7; Wang 1987) (see Section 3.6.2 for a detailed discussion).

$$t_{su} \approx -\frac{P_1}{\dot{P}_1} = \frac{2}{5}\frac{M_1}{\dot{M}_1}\left(\frac{R_1}{R_c}\right)^2 f(x_0)^{-1}\ \mathrm{s},$$

For each δ, the values of t_{su} are plotted as a function of orbital period in Figs. 4.7 a-e.

For each of the scenarios listed, the mass transfer time-scale of the system, assuming a constant mass transfer rate, has been determined by the following:

$$t_{mt} = \Delta M_2 / \dot{M}_{2i} \qquad (4.8)$$

For each δ, the values of t_{su} are plotted as a function of t_{mt} in Figs. 4.8 a-e. This is done mainly to compare the disc spin-up time-scale with the inferred mass transfer time-scale.

To summarize, the results of our model calculations are presented as follows:

$\delta = 3.5$	Table 4.2	Figure 4.1		
$\delta = 2.0$	Table A1	Figure 4.2a, b, c	Figure 4.7a	Figure 4.8a
$\delta = 1.0$	Table A2	Figure 4.3a, b, c	Figure 4.7b	Figure 4.8b
$\delta = 0$	Table A3	Figure 4.4a, b, c	Figure 4.7c	Figure 4.8c
$\delta = -1.0$	Table A4	Figure 4.5a, b, c	Figure 4.7d	Figure 4.8d
$\delta = -2.0$	Table A5	Figure 4.6a, b, c	Figure 4.7e	Figure 4.8e

In order to find the possible reconciliation of mass transfer time-scale t_{mt} and spin-up time-scale t_{su}, the mass of secondary star $M_{2i} = 1.0 M_{\odot}$ and $\delta = -1$ are chosen for different parameter combinations of $P_{spin,i}$, B_1. This is done mainly to illustrate the role of initial spin period and magnetic field strength on the spin-up time-scale. The results of $\lambda = t_{mt} / t_{su}$ as a function of $P_{spin,i}$ and B_1 are presented as follows. To streamline the presentation, only the first Table ($P_{spin,i} = 3600\,\mathrm{s}, B_1 = 10^5$ G) is displayed here and the rest are displayed in Appendix:

$P_{spin,i} = 3600\,\mathrm{s}$, $B_1 = 10^5$ G	Table 4.3	Figure 4.9a
$P_{spin,i} = 3600\,\mathrm{s}$, $B_1 = 10^4$ G	Table A6	Figure 4.9a
$P_{spin,i} = 1000\,\mathrm{s}$, $B_1 = 10^5$ G	Table A7	Figure 4.9b
$P_{spin,i} = 1000\,\mathrm{s}$, $B_1 = 10^4$ G	Table A8	Figure 4.9b
$P_{spin,i} = 500\,\mathrm{s}$, $B_1 = 10^5$ G	Table A9	Figure 4.9c
$P_{spin,i} = 500\,\mathrm{s}$, $B_1 = 10^4$ G	Table A10	Figure 4.9c

$\delta = (R_{L2} - R_{p2})/H_p$	a filling factor, i.e. the ratio of the distance between the surface and L_1 region with respect to the pressure scale height of the secondary star
M_{2i} (M_Θ)	the initial mass of the secondary before the high mass-transfer phase, ranging between 2 and 1 solar mass, in steps of 0.2 solar mass
$\beta = \dot{M}_1/\lvert\dot{M}_2\rvert$	the accretion fraction, ranging between 0 and 1 in steps of 0.1
M_{1i} (M_Θ)	the value of the initial mass of the WD (in solar unit) before the high mass-accretion phase (see Section 4.2)
$q_i = M_2/M_1$	the value of the initial mass ratio of the binary
T_2 (K)	the photospheric temperature of the secondary (in Kelvin) (see Section 4.2, from Copeland et al. 1970)
B_1 (10^6 G)	the magnetic field strength of the WD (in unit of 10^6 G)
P_{orb} (hr)	the orbital period (in unit of hours) of the system before the high mass-transfer phase, as deduced from period relation for secondary stars (see Section 4.2).
$P_{spin,i}$ (s)	the initial spin period of the WD (in unit of seconds)
$\dot{M}_{edd}$ (10^{20} g s^{-1})	the value of the Eddington limit (in unit of 10^{20} g s^{-1}) (see Section 3.2)
$-\dot{M}_{2i}$ (10^{18} g s^{-1})	the value of the mass transfer rate from the secondary star (in unit of 10^{18} g s^{-1}) (see Section 4.2)
$\dot{M}_{1i}$ (10^{17} g s^{-1})	the value of the mass accretion rate onto the WD (in unit of 10^{17} g s^{-1}) (see Section 4.2)
$\dot{M}_{1i(SNB)}$ (10^{18} g s^{-1})	the value of the minimum requirement of stable nuclear burning on the surface of the white dwarf (in unit of 10^{18} g s^{-1}) (see Section 4.1)
$\gamma = \dot{M}_{1(SNB)}/\lvert\dot{M}_2\rvert$	the ratio of $\dot{M}_{1i(SNB)}$ against $\lvert\dot{M}_{2i}\rvert$
$\kappa = \dot{M}_1/\dot{M}_{edd}$	the ratio of $\dot{M}_1$ against $\dot{M}_{edd}$
$x_0 = R_0/R_c$	the ratio of R_0 against R_c (see Section 3.6.2)
$f(x_0)$	the value of the dimensionless function scaling the disc inner edge (see Section 3.6.2)
t_{su} (10^4 yr)	the spin-up time-scale (in unit of 10^4 yr) (see Section 3.6.2)
t_{mt} (10^6 yr) $= \Delta M_2/\dot{M}_{2i}$	the mass transfer time-scale (in unit of 10^6 yr) (see Section 4.3)
$\lambda = t_{mt}/t_{su}$	the time-scale ratio of t_{mt} against t_{su}

Table 4.1: The glossary of the symbols of the model calculations

M_{2i} ($M_\odot$)	β	M_{1i} ($M_\odot$)	q_i	T_2 (K)	P_{orb} (hr)	$\dot{M}_{edd}$ (10^{20} g s^{-1})	$-\dot{M}_{2i}$ (10^{18} g s^{-1})	$\dot{M}_U$ (10^{17} g s^{-1})	$\dot{M}_{1i(SNR)}$ (10^{18} g s^{-1})	γ	t_{su} (10^4 yr)	t_{mt} (10^7 yr)
2.0	0	0.87	2.30	10080	18.2	5.44	8.32	0	9.50	1.1	-	
2.0	0.1	0.73	2.73	10080	18.2	6.24	8.32	8.32	7.36	0.88	2.82	1.04
1.8	0	0.87	2.07	9330	16.4	5.44	6.02	0	9.50	1.6	-	
1.8	0.1	0.75	2.39	9330	16.4	6.11	6.02	6.02	7.66	1.3	3.69	1.22
1.8	0.2	0.64	2.83	9330	16.4	6.99	6.02	12.04	5.96	0.99	2.17	1.22
1.6	0	0.87	1.84	8530	14.5	5.44	4.11	0	9.50	2.3	-	
1.6	0.1	0.77	2.07	8530	14.5	5.98	4.11	4.11	7.97	1.9	5.08	1.48
1.6	0.2	0.67	2.36	8530	14.5	6.65	4.11	8.23	6.52	1.6	2.94	1.48
1.6	0.3	0.58	2.76	8530	14.5	7.53	4.11	12.34	5.18	1.3	2.20	1.48
1.4	0	0.87	1.61	7650	12.7	5.44	2.68	0	9.50	3.5	-	
1.4	0.1	0.79	1.76	7650	12.7	5.86	2.68	2.68	8.28	3.1	7.29	1.80
1.4	0.2	0.72	1.95	7650	12.7	6.36	2.68	5.36	7.11	2.7	4.17	1.80
1.4	0.3	0.64	2.19	7650	12.7	6.96	2.68	8.04	6.00	2.2	3.07	1.80
1.4	0.4	0.56	2.48	7650	12.7	7.70	2.68	10.72	4.96	1.9	2.52	1.80
1.4	0.5	0.49	2.87	7650	12.7	8.65	2.68	13.40	3.99	1.5	2.20	1.80
1.2	0	0.87	1.38	6780	10.9	5.44	1.65	0	9.50	5.8	-	
1.2	0.1	0.81	1.48	6780	10.9	5.75	1.65	1.65	8.59	5.2	11.01	2.17
1.2	0.2	0.76	1.59	6780	10.9	6.09	1.65	3.29	7.71	4.7	6.22	2.17
1.2	0.3	0.70	1.71	6780	10.9	6.48	1.65	4.94	6.87	4.2	4.51	2.17
1.2	0.4	0.64	1.86	6780	10.9	6.93	1.65	6.59	6.05	3.7	3.64	2.17
1.2	0.5	0.59	2.04	6780	10.9	7.45	1.65	8.24	5.27	3.2	3.11	2.17
1.2	0.6	0.53	2.26	6780	10.9	8.08	1.65	9.88	4.53	2.8	2.77	2.17
1.2	0.7	0.48	2.53	6780	10.9	8.84	1.65	11.53	3.83	2.3	2.54	2.17
1.2	0.8	0.42	2.87	6780	10.9	9.79	1.65	13.18	3.17	1.9	2.38	2.17
1.0	0	0.87	1.15	6030	9.1	5.44	0.96	0	9.50	9.9	-	
1.0	0.1	0.83	1.20	6030	9.1	5.63	0.96	0.96	8.91	9.3	17.36	2.39
1.0	0.2	0.80	1.25	6030	9.1	5.84	0.96	1.93	8.33	8.7	9.69	2.39
1.0	0.3	0.76	1.31	6030	9.1	6.06	0.96	2.89	7.77	8.1	6.95	2.39
1.0	0.4	0.72	1.38	6030	9.1	6.31	0.96	3.85	7.22	7.5	5.53	2.39
1.0	0.5	0.69	1.45	6030	9.1	6.57	0.96	4.81	6.68	6.9	4.65	2.39
1.0	0.6	0.65	1.54	6030	9.1	6.87	0.96	5.78	6.15	6.4	4.06	2.39
1.0	0.7	0.62	1.63	6030	9.1	7.19	0.96	6.74	5.64	5.9	3.64	2.39
1.0	0.8	0.58	1.73	6030	9.1	7.55	0.96	7.70	5.15	5.3	3.32	2.39
1.0	0.9	0.54	1.85	6030	9.1	7.96	0.96	8.67	4.67	4.8	3.08	2.39
1.0	1.0	0.51	1.98	6030	9.1	8.41	0.96	9.63	4.20	4.4	2.89	2.39

Table 4.2: The results of the SSS investigation ($\delta = 3.5$)

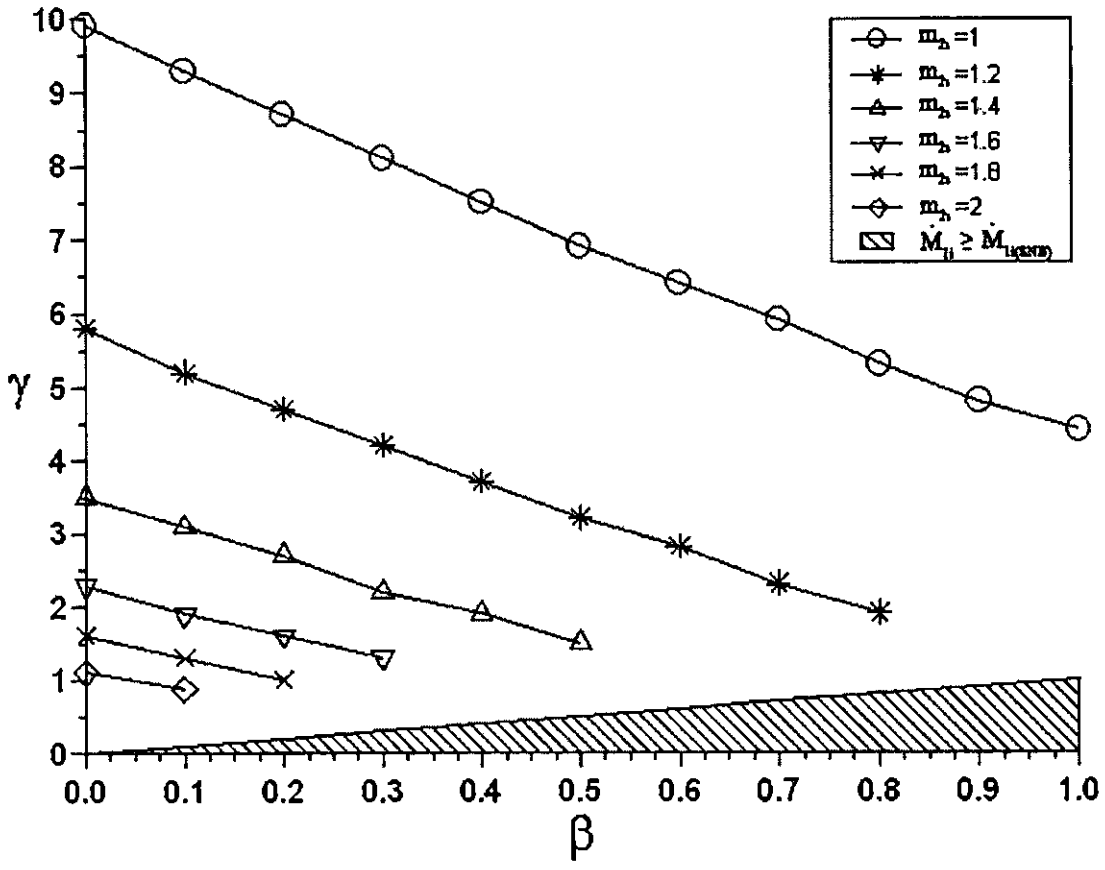

Fig 4.1 The plot of $\gamma = \dot{M}_{1(\mathrm{SNB})} / \left|\dot{M}_2\right|$ v.s. β average accretion fraction ($\delta = 3.5$)

Mentjies (2004) suggested that the ratio of secondary atmosphere scale height $\delta = 3.5$ for the current propeller phase with orbital period $P_{orb} \approx 9.88\,\mathrm{hr}$. The inferred values of $|\dot{M}_2|$, associated with $\delta = 3.5$, corresponds with the minimum inferred mass transfer rate for the current propeller phase (i.e. $|\dot{M}_2| \geq 4\times10^{17}\ \mathrm{g\,s^{-1}}$; Eracleous & Horne 1996).

Close inspection of the Table 4.2, for a given value of accretion fraction β (e.g. 10%), shows the systems with large secondary mass (which implies large orbital period and high photospheric temperature) will drive a higher mass transfer rate $\dot{M}_2$ (since $|\dot{M}_2| \propto c_s^3 P_{orb}^2 \propto T_{phot}^{3/2} P_{orb}^2$) and a higher mass accretion rate onto the white dwarf $\dot{M}_1$ (since $\dot{M}_1 = \beta|\dot{M}_2| \propto |\dot{M}_2|$). On the other hand, the systems with smaller mass of white dwarfs result in a lower the minimum requirement for stable nuclear burning on the surface of the white dwarf $\dot{M}_{1(SNB)}$ (since $\dot{M}_{1(SNB)} \propto M_1^{3/2}$). This results in the plotted curves (in Fig 4.1 and Figs. 4.2a - 4.6a as well) of the systems with large secondary mass being closer to the hatched area (where the requirement of SSS is satisfied).

However, from Table 4.2 (for $\delta = 3.5$), it can be seen that $\dot{M}_1$ is of the order of $10^{17}\ \mathrm{g\,s^{-1}}$ while $\dot{M}_{1(SNB)}$ is of the order of $10^{18}\ \mathrm{g\,s^{-1}}$, for all values of β. Therefore, it can be seen (Fig 4.1) that the mass accretion rate onto the white dwarf $\dot{M}_1$, for all values of β, never satisfies the minimum requirement for stable nuclear burning on the surface of the white dwarf $\dot{M}_{1(SNB)}$ (i.e. $\dot{M}_1 < \dot{M}_{1(SNB)}$ or $\beta < \gamma$). Therefore, for the current state of lobe-filling of the secondary star and accompanying mass transfer, the system will never exhibit SSS properties. This may also apply to semi-detached binaries like the intermediate polars.

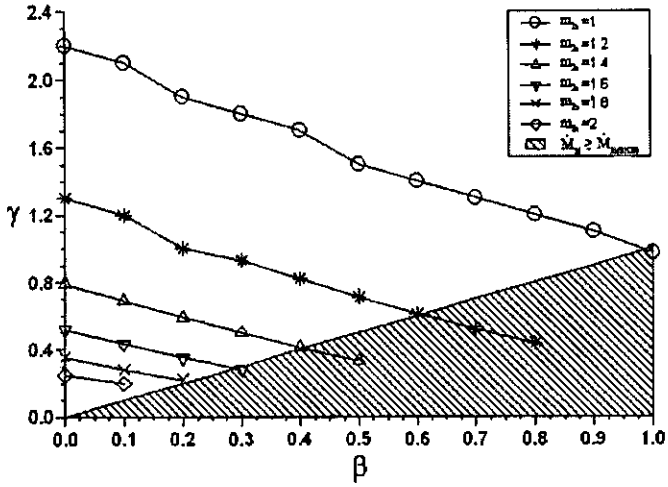

Fig 4.2a The plot of $\gamma = \dot{M}_{1(\mathrm{SNB})} / \left|\dot{M}_2\right|$ v.s. β average accretion fraction ($\delta = 2.0$)

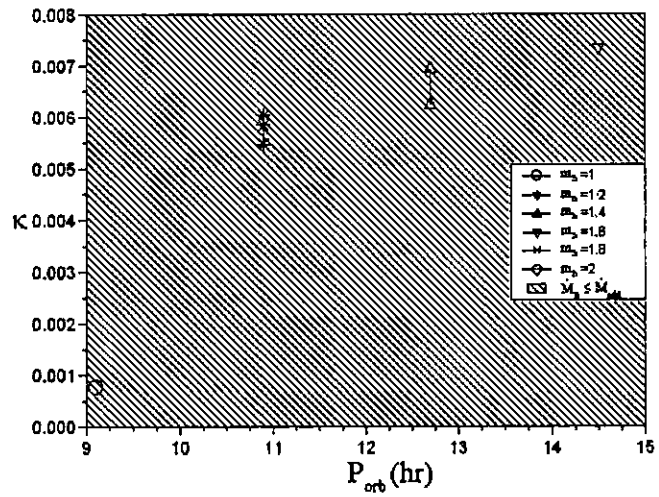

Fig 4.2b The plot of $\kappa = \dot{M}_1 / \dot{M}_{\mathrm{edd}}$ v.s. P_{orb} ($\delta = 2.0$)

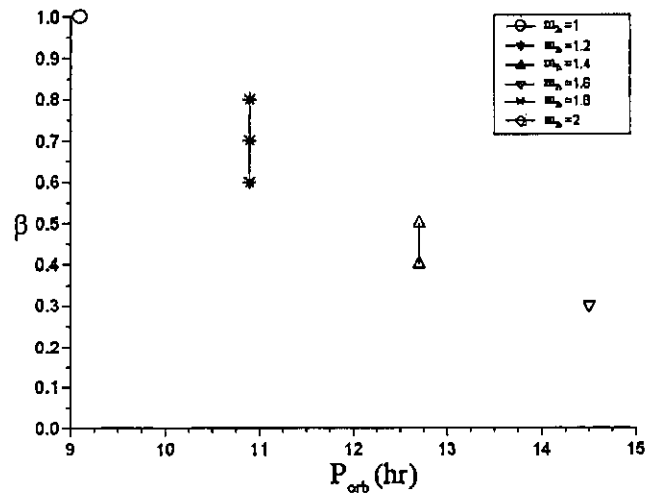

Fig 4.2c The plot of β average accretion fraction v.s. P_{orb} ($\delta = 2.0$)

From Table A1 (and Tables A2-A5 as well), for a given value of the mass of the white dwarf M_1, it can be seen that, the minimum requirement for stable nuclear burning on the surface of the white dwarf $\dot{M}_{1(SNB)}$ remains the same and is independent of the value of δ.

For a given value of β, since $\dot{M}_1 = \beta|\dot{M}_2|$, $\dot{M}_1$ increases with increasing $|\dot{M}_2|$. Also, since $|\dot{M}_2| \propto \rho_{L1} c_s^3 P_{orb}^2$ and $\rho_{L1} \propto \rho_{phot} \exp^{-\delta}$, the decrease of δ will result in the increase of $|\dot{M}_2|$ and hence $\dot{M}_1$. This can be understood that, the secondary comes closer to fill the Roche lobe with decreasing δ, which results in the increase of the stream density ρ_{L1} at L_1 point, subsequently the mass transfer rate $|\dot{M}_2|$ and hence the mass accretion rate $\dot{M}_1$.

Therefore, this results in that, in Fig 4.2a (for $\delta = 2$), there are some allowed parameters in the hatched area (and these are highlighted in Tables A1 in Appendix), which satisfy the SSS criteria (i.e. the second constraint $\gamma \leq \beta \leq 1$).

This is further supported by Fig 4.2b (for $\delta = 2$) (only those β values satisfying the SSS criteria are plotted), and it can be seen that the values of $\kappa = \dot{M}_1 / \dot{M}_{edd}$ are less than 0.008, resulting in the accretion rate onto the WD being much less than the Eddington accretion rate (i.e. $\dot{M}_1 << \dot{M}_{edd}$). This is a very positive result which implies that these possible SSS scenarios can be achieved below the Eddington limit.

The Fig 4.2c indicates the possible orbital periods, satisfying the SSS requirement, which may lie in the range between 15 hour and 9 hour.

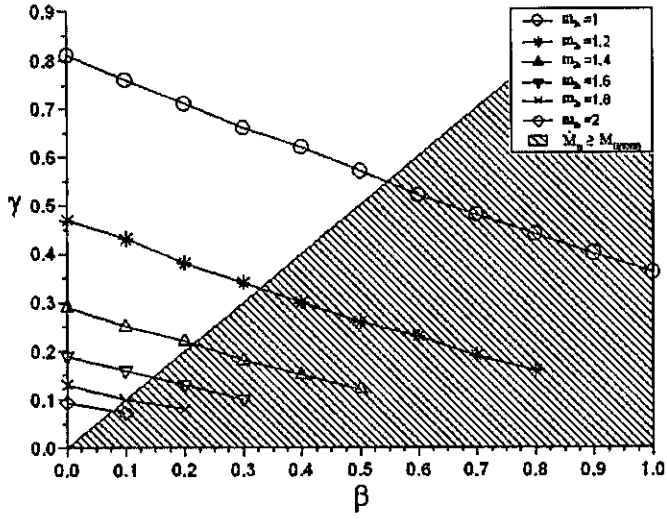

Fig 4.3a The plot of $\gamma = \dot{M}_{1(\mathrm{SNB})} / \left|\dot{M}_2\right|$ v.s. β average accretion fraction ($\delta = 1.0$)

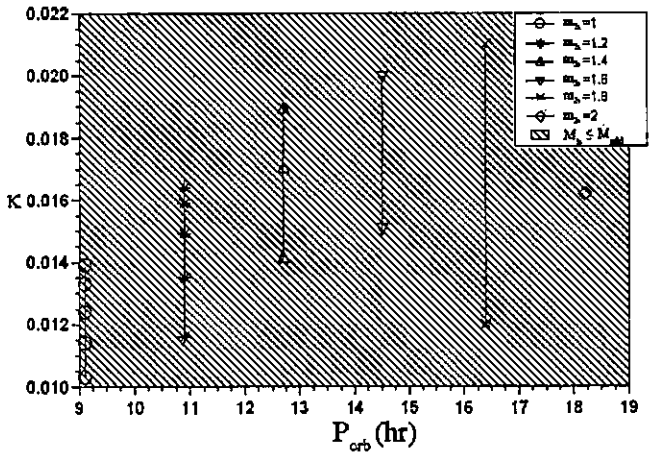

Fig 4.3b The plot of $\kappa = \dot{M}_1 / \dot{M}_{\mathrm{edd}}$ v.s. P_{orb} ($\delta = 1.0$)

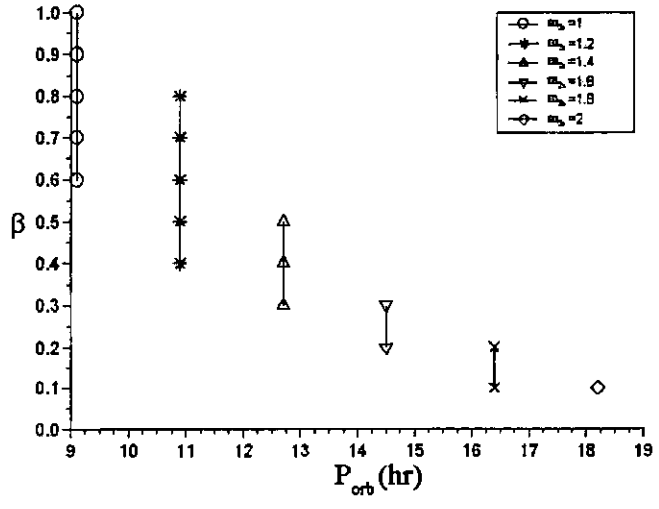

Fig 4.3c The plot of β average accretion fraction v.s. P_{orb} ($\delta = 1.0$)

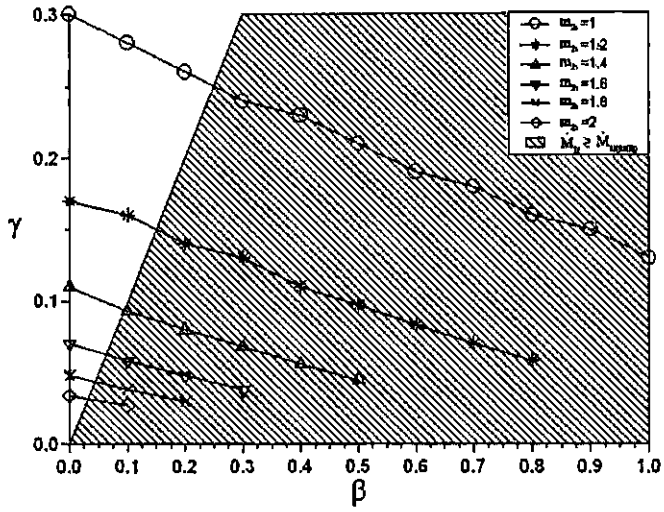

Fig 4.4a The plot of $\gamma = \dot{M}_{1(\mathrm{SNB})} / \left|\dot{M}_2\right|$ v.s. β average accretion fraction ($\delta = 0$)

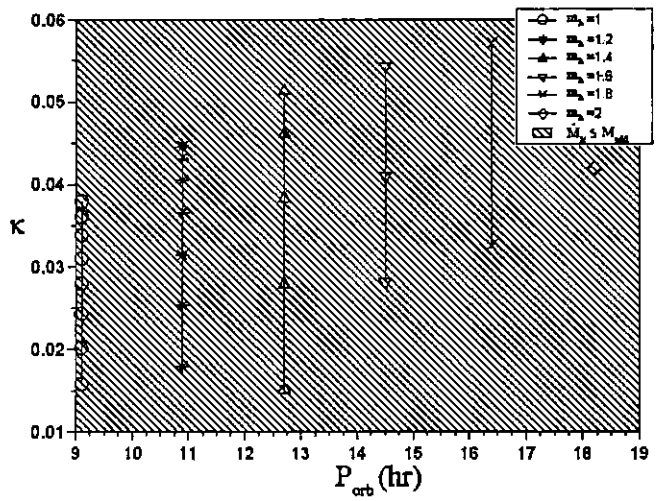

Fig 4.4b The plot of $\kappa = \dot{M}_1 / \dot{M}_{\mathrm{edd}}$ v.s. P_{orb} ($\delta = 0$)

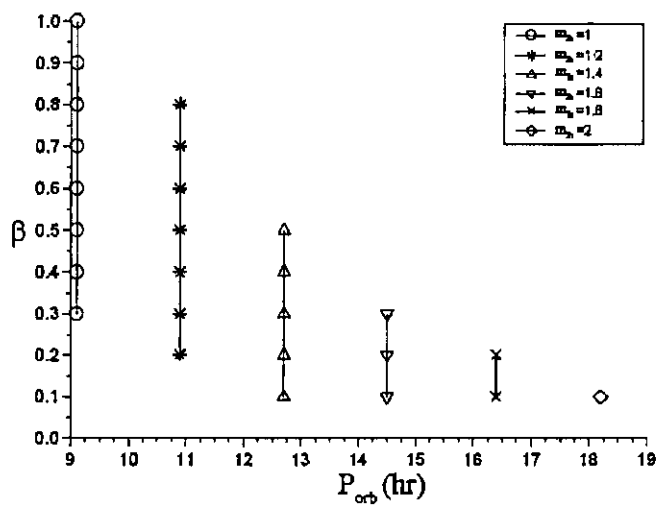

Fig 4.4c The plot of β average accretion fraction v.s. P_{orb} ($\delta = 0$)

From Figs. 4.3a and 4.4a, for $\delta = 1$ (the secondary star slightly underfilling the Roche lobe) and $\delta = 0$ (the secondary star just filling the Roche lobe) respectively, it can be seen that the number of the possible scenarios satisfying the SSS criteria increase significantly.

From Figs. 4.3b and 4.4b, it can seen that the value of $\kappa = \dot{M}_1 / \dot{M}_{edd}$ gradually increases with the increased Roche lobe filling of the secondary star, however, κ is still less than 0.06, i.e. $\dot{M}_1 << \dot{M}_{edd}$. This means the SSS criteria can be achieved, when the mass accretion rate onto the WD is significantly below the Eddington limit.

The Figs. 4.3c and 4.4c show that the possible SSS scenarios seem to be found for the orbital period P_{orb} in the range of 9 hour to 18 hour.

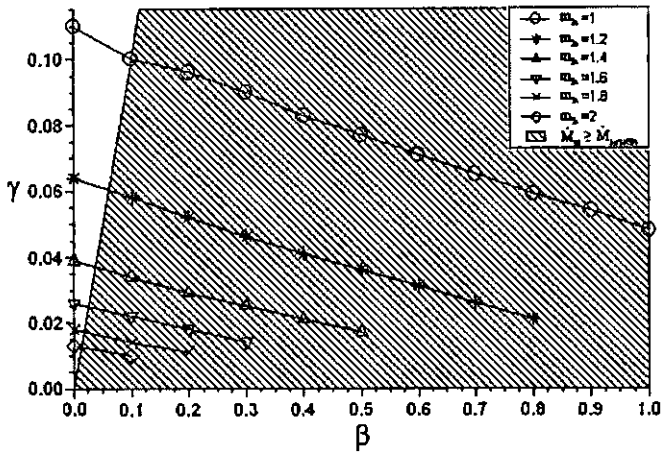

Fig 4.5a The plot of $\gamma = \dot{M}_{1(\mathrm{SNB})} / \left|\dot{M}_2\right|$ v.s. β average accretion fraction ($\delta = -1.0$)

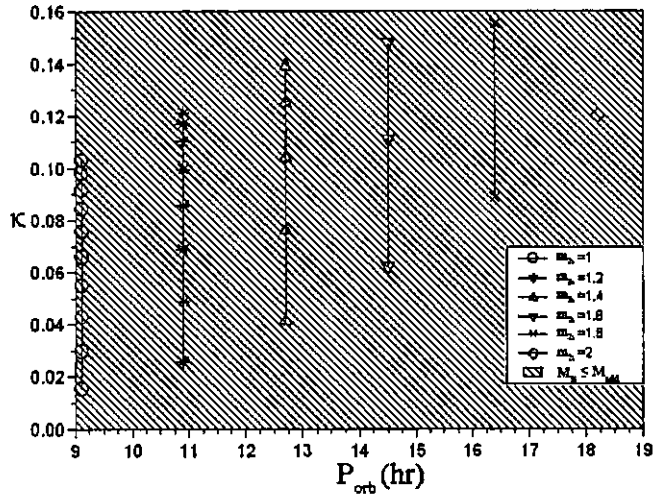

Fig 4.5b The plot of $\kappa = \dot{M}_1 / \dot{M}_{\mathrm{edd}}$ v.s. P_{orb} ($\delta = -1.0$)

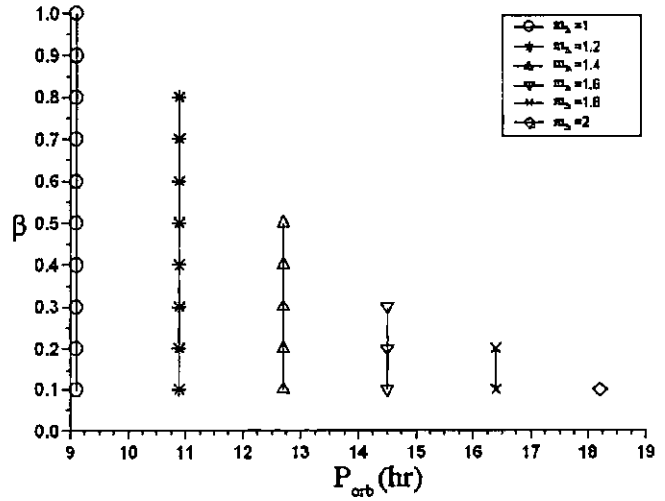

Fig 4.5c The plot of β average accretion fraction v.s. P_{orb} ($\delta = -1.0$)

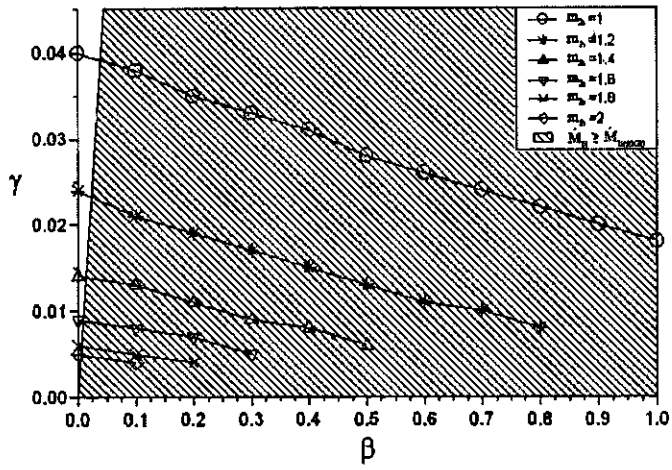

Fig 4.6a The plot of $\gamma = \dot{M}_{1(\mathrm{SNB})} / \left|\dot{M}_2\right|$ v.s. β average accretion fraction ($\delta = -2.0$)

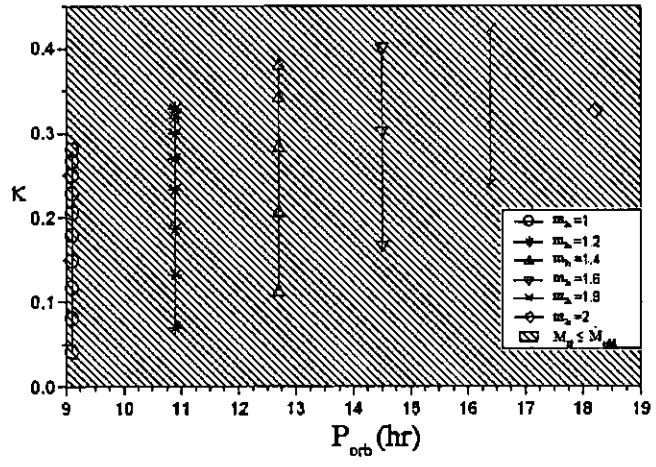

Fig 4.6b The plot of $\kappa = \dot{M}_1 / \dot{M}_{\mathrm{edd}}$ v.s. P_{orb} ($\delta = -2.0$)

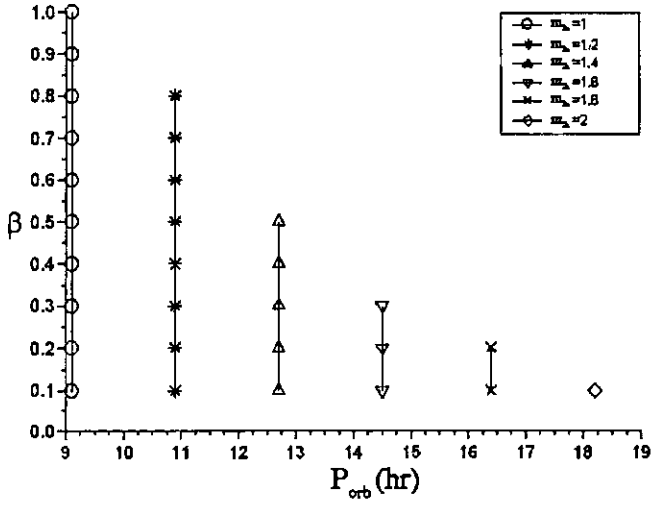

Fig 4.6c The plot of β average accretion fraction v.s. P_{orb} ($\delta = -2.0$)

From Figs. 4.5a and 4.6a, for $\delta = -1$ and $\delta = -2$ (the secondary star overflowing the Roche lobe) respectively, it can be seen that the number of the possible scenarios, satisfying the SSS criteria, increase even more. A close inspection of these figures shows that the SSS requirement can be achieved, almost for all the values of β (except $\beta = 0$), even if β is only 0.1. This is a very exciting result, because it implies that once the secondary (slightly) overflows the Roche lobe, the possible SSS activity can inevitably be achieved, even if the average accretion rate β is the quite small (i.e. even β is very small $\rightarrow 10\%$).

Table A5 shows that, for extreme overfilling of the secondary's Roche lobe ($\delta = -2$), the mass transfer rate from the secondary is of the same order as the Eddignton limit (i.e. $|\dot{M}_2| \sim \dot{M}_{edd}$). For this reason, $\delta = -2$ respects the cut-off value of our model calculations.

From Figs. 4.5b and 4.6b, for these possible SSS scenarios, we can see that the value of $\kappa = \dot{M}_1 / \dot{M}_{edd}$ gradually increases with the decrease of δ; however κ is still less than 0.45, i.e. $\dot{M}_1$ is still smaller than $\dot{M}_{edd}$. This is also a very positive result which means the possible SSS scenarios can be achieved, even if the mass accretion rate onto the WD is much less than the Eddington limit.

The Figs. 4.5c and 4.6c suggest that the possible SSS scenarios for AE Aqr seem to be found for the orbital period P_{orb} in the range between 9 hour and 18 hour. Extending of these model calculations, which may apply to other pre-intermediate polar systems, results in interesting observable consequences, where the possible SSS scenarios could be found with the certain range of the orbital period, if the constraint $1 \leq \beta \leq \gamma$ can be satisfied and the high mass accretion rate can be sustained for a period of time.

An important constrain for the duration of the high mass accretion phase is the spin-up time-scale t_{su} of the white dwarf. By adopting the parameters $B_1 = 10^6$ G (e.g. Cropper 1986; Beskrovnaya et al. 1995; Chanmugam & Frank 1987; Meintjes 2002),

$P_{spin,i} = 3600\,\mathrm{s}$ (e.g. Wynn, King & Horne 1995; 1997), the spin-up time-scales, for all scenarios satisfying the SSS constraints, have been plotted as a function of orbital period, i.e. Figs. 4.7a - e.

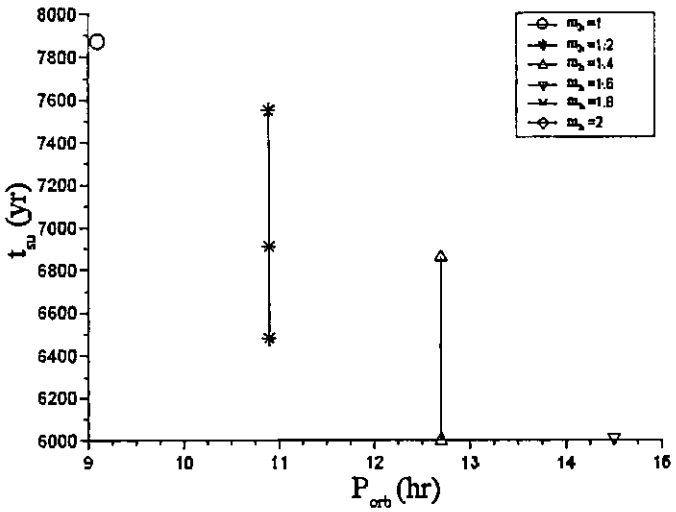

Fig 4.7a The plot of t_{su} v.s. P_{orb} ($\delta = 2.0$, $B_1 = 10^6$ G and $P_{spin,i} = 3600$ s)

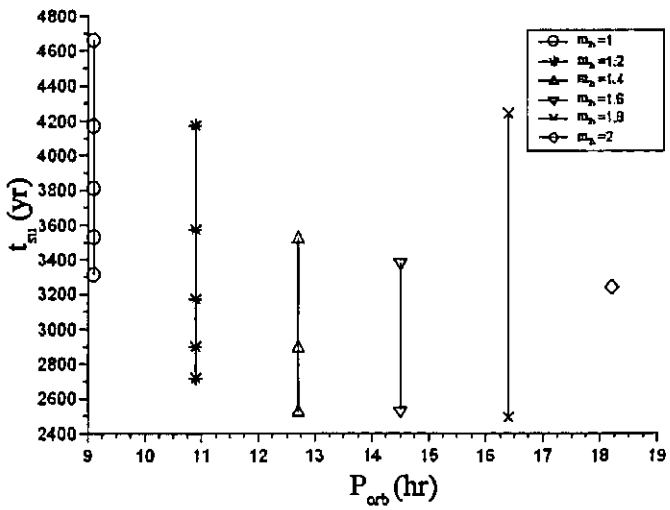

Fig 4.7b The plot of t_{su} v.s. P_{orb} ($\delta = 1.0$, $B_1 = 10^6$ G and $P_{spin,i} = 3600$ s)

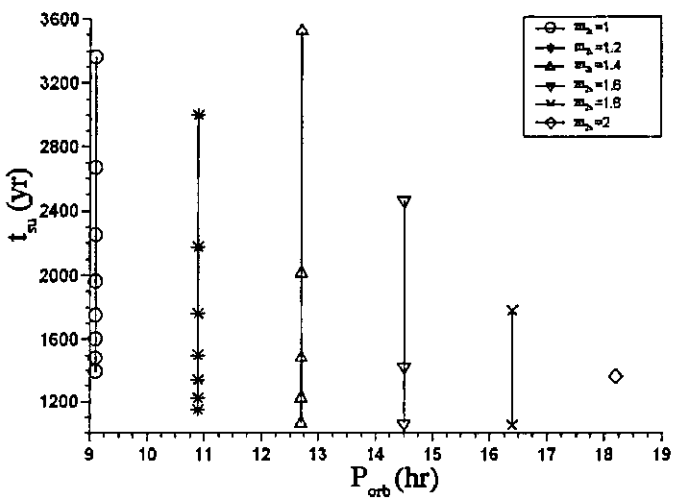

Fig 4.7c The plot of t_{su} v.s. P_{orb} ($\delta = 0$, $B_1 = 10^6$ G and $P_{spin,i} = 3600$ s)

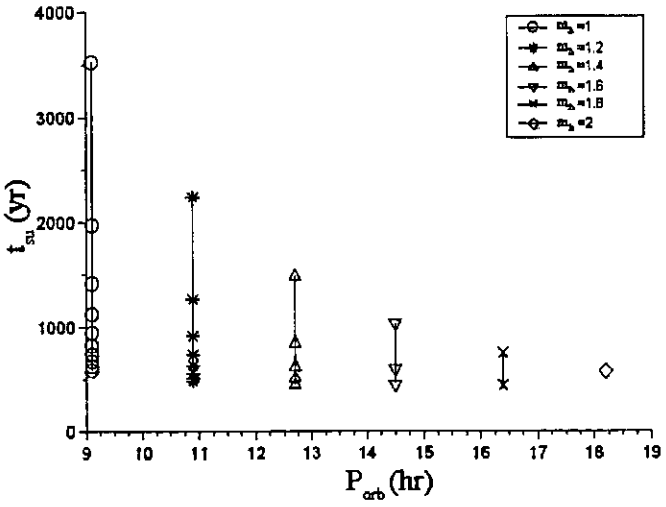

Fig 4.7d The plot of t_{su} v.s. P_{orb} ($\delta = -1.0, B_1 = 10^6$ G and $P_{spin,i} = 3600$ s)

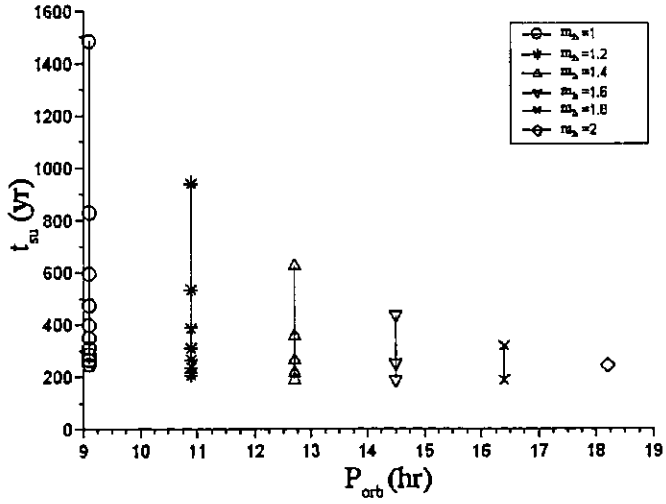

Fig 4.7e The plot of t_{su} v.s. P_{orb} ($\delta = -2.0, B_1 = 10^6$ G and $P_{spin,i} = 3600$ s)

For the given values of M_2, β (hence M_1), it can be seen that when the secondary star gradually overflows the Roche lobe (i.e. δ gradually decreases), the spin-up time-scale t_{su} decreases (from $\sim 8{,}000$ yr to ~ 200 yr) significantly. This is because a gradual decrease in δ results in a significant increase of $\dot{M}_2$, and subsequently $\dot{M}_1$ (from $\sim 10^{18}\,\mathrm{g\,s^{-1}}$ to $\sim 10^{21}\,\mathrm{g\,s^{-1}}$). However $t_{su} \propto (\dot{M}_1)^{-1}$, which results in a significant decrease of t_{su}.

It can be seen that for all filling factors the spin-up time-scales are noticeably short, i.e. $200\,\mathrm{yr} < t_{su} < 8{,}000\,\mathrm{yr}$. Meintjes (2002) showed that the white dwarf in AE Aqr could have been spun-up to a rotation period within a time-scale $t_{su} \sim 10^4$ yr for mass transfer rate $|\dot{M}_2| \sim 10^{20}\,\mathrm{g\,s^{-1}}$. However, it has to be mentioned that Meintjes (2002) considered an inflationary bottom-up (short $\rightarrow$ long orbital period) evolution where the high run-away mass transfer was initiated at $P_{orb,i} \approx 9$ hrs. The current study considers a more conventional top-down (long $\rightarrow$ short orbital period) evolution.

The current study confirms earlier results (Meintjes 2002; Schenker et al. 2002) that AE Aqr most possibly evolved through a high mass transfer/ accretion phase, where the white dwarf has been spun-up by accretion torques, possibly by an accretion disc. In the high mass accretion phase, the WD is spun-up out of equilibrium (i.e. $x_0 = R_0 / R_c \rightarrow 0$, significantly below $x_{eq} \approx 0.971$, see Table A1-A5 for details) and the spin-up time-scales are significantly short, suggesting that the possible SSS activity may, for AE Aqr, be restricted to orbital periods $P_{orb} \geq 9$ hrs (when a well developed disc was presented). This confirms the notion that SSS activity being associated with a pre-cataclysmic variable phase, or alternatively, for young CVs with orbital periods $P_{orb} \geq 9$ hrs.

In order to compare the spin-up time-scale t_{su} and the mass transfer time-scale t_{mt}, t_{su} is plotted as a function of t_{mt} in Figs. 4.8 a–e, for each $\delta = 2$, 1, 0, -1 and 2 respectively.

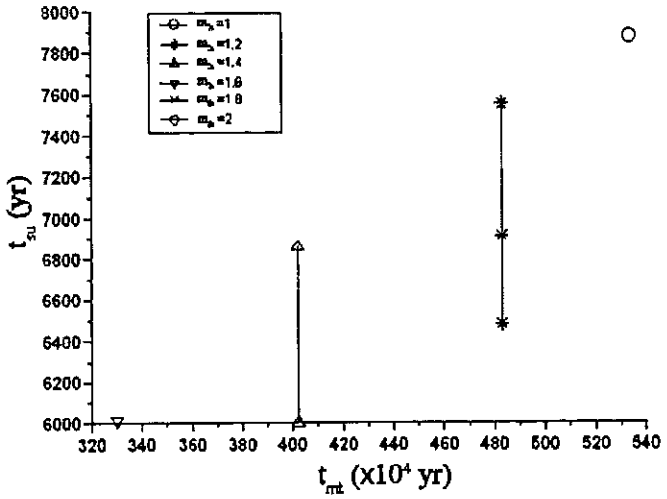

Fig 4.8a The plot of t_{su} v.s. t_{mt} ($\delta = 2.0$, $B_1 = 10^6$ G and $P_{spin,i} = 3600$ s)

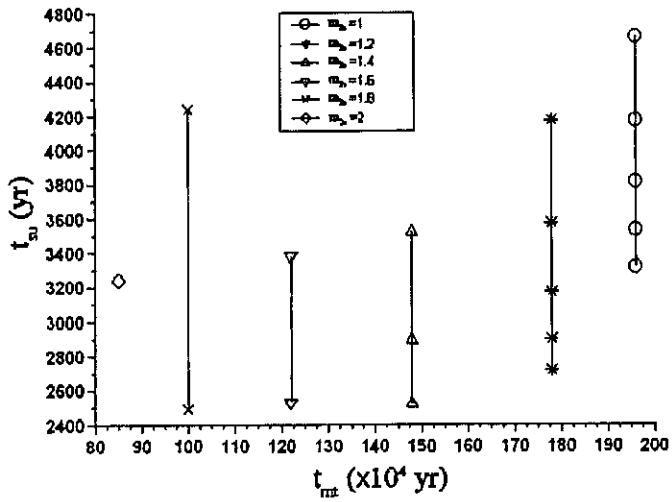

Fig 4.8b The plot of t_{su} v.s. t_{mt} ($\delta = 1.0$, $B_1 = 10^6$ G and $P_{spin,i} = 3600$ s)

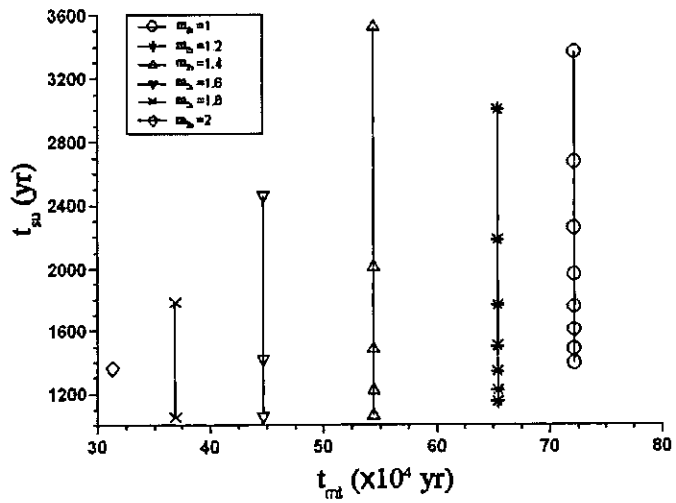

Fig 4.8c The plot of t_{su} v.s. t_{mt} ($\delta = 0$, $B_1 = 10^6$ G and $P_{spin,i} = 3600$ s)

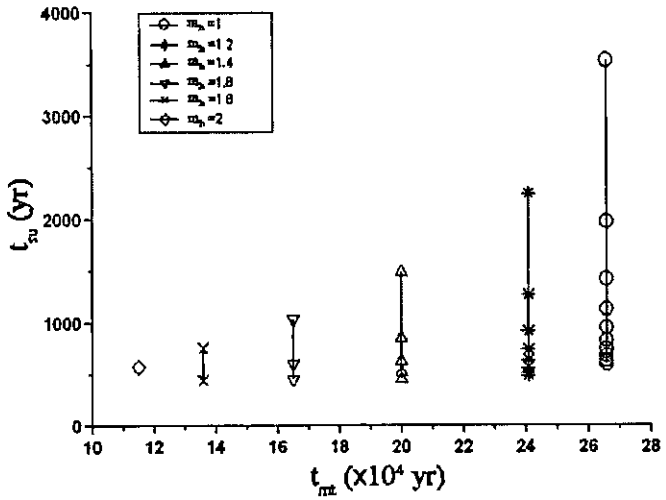

Fig 4.8d The plot of t_{su} v.s. t_{mt} ($\delta = -1.0$, $B_1 = 10^6$ G and $P_{spin,i} = 3600$ s)

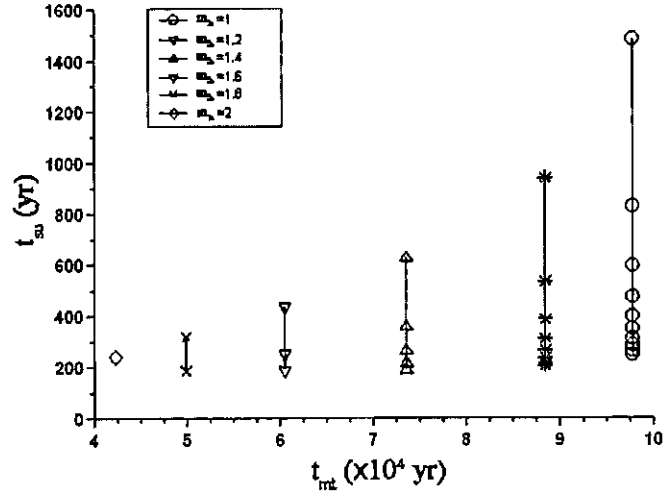

Fig 4.8e The plot of t_{su} v.s. t_{mt} ($\delta = -2.0$, $B_1 = 10^6$ G and $P_{spin,i} = 3600$ s)

As the previous discussion, the t_{su} decreases with decreasing δ. Meanwhile, the decrease of δ results in the increase of the $\dot{M}_2$ and hence the decrease of t_{mt} (since $t_{mt} \propto (\dot{M}_2)^{-1}$).

It can be seen that the spin-up time-scale ($200\ \text{yr} < t_{su} < 8{,}000\ \text{yr}$) is much shorter than the mass transfer time-scale ($4\times10^4\ \text{yr} < t_{mt} < 540\times10^4\ \text{yr}$). These results (Figs. 4.8 a-e) seem to suggest that the spin-up time-scale, rather that the mass transfer time-scale will determine the allowed duration of the run-away mass transfer phase. This is evident from the fact that $t_{su} << t_{mt}$ for most initial conditions.

However, in order for the WD to survive (i.e. to avoid the WD will be spun-up too fast and obliterate itself under intense centrifugal forces), it is necessary to find the possible reconciliation of the mass transfer time-scale t_{mt} and the spin-up time-scale t_{su}. This is investigated by considering different initial conditions concerning the initial white dwarf spin period $P_{spin,i}$ and magnetic field B_1. The mass of secondary star $M_{2i} = 1.0 M_\Theta$ and $\delta = -1$ are chosen for different parameter combinations of initial spin period $P_{spin,i}$ ($= 3600\ \text{s}, 1000\ \text{s}$ and $500\ \text{s}$) and the magnetic field strength of the white dwarf B_1 ($= 10^4\ \text{G}, 10^5\ \text{G}$ and $10^6\ \text{G}$). The results of $\lambda = t_{mt} / t_{su}$ as a function of $P_{spin,i}$ and B_1 are plotted in Figs. 4.9a-c.

β	M_{1i} ($M_\odot$)	q_i	$\dot{M}_{edd}$ (10^{20} g s^{-1})	$-\dot{M}_{2i}$ (10^{20} g s^{-1})	$\dot{M}_{1i}$ (10^{19} g s^{-1})	$\dot{M}_{1i(SNB)}$ (10^{18} g s^{-1})	γ	x_0	$f(x_0)$	t_{su} (10^3 yr)	t_{mt} (10^5 yr)	λ
0	0.87	1.15	5.44	0.87	0	9.50	0.11			-		
0.1	0.83	1.20	5.63	0.87	0.87	8.91	0.10	0.006	0.108	6.53	2.66	40.7
0.2	0.80	1.25	5.84	0.87	1.73	8.33	0.096	0.005	0.102	3.65	2.66	72.8
0.3	0.76	1.31	6.06	0.87	2.60	7.77	0.090	0.005	0.101	2.62	2.66	101.6
0.4	0.72	1.38	6.31	0.87	3.47	7.22	0.083	0.005	0.101	2.08	2.66	127.7
0.5	0.69	1.45	6.57	0.87	4.33	6.68	0.077	0.005	0.102	1.75	2.66	151.8
0.6	0.65	1.54	6.87	0.87	5.20	6.15	0.071	0.006	0.105	1.53	2.66	173.9
0.7	0.62	1.63	7.19	0.87	6.07	5.64	0.065	0.006	0.108	1.37	2.66	194.2
0.8	0.58	1.73	7.55	0.87	6.93	5.15	0.059	0.006	0.112	1.25	2.66	212.7
0.9	0.54	1.85	7.96	0.87	7.80	4.67	0.054	0.007	0.116	1.16	2.66	229.5
1.0	0.51	1.98	8.41	0.87	8.67	4.20	0.048	0.008	0.122	1.09	2.66	244.5

Table 4.7a: The time-scale ratio $\lambda = t_{mt} / t_{su}$ for $m_{2i} = 1.0$, $\delta = -1.0$, $P_{spin,i} = 3600\,\mathrm{s}$ and $B_1 = 10^5$ G

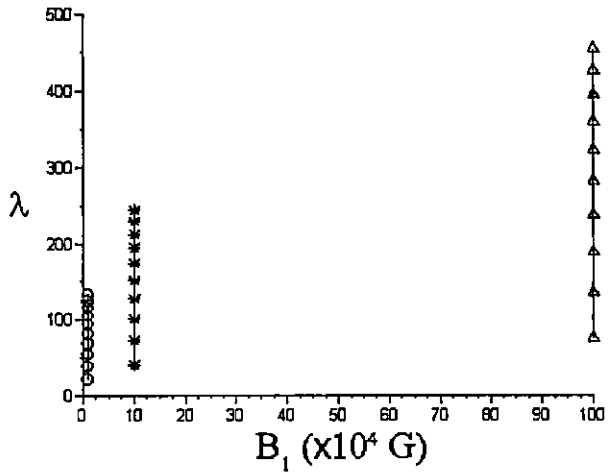

Figure 4.9a: The plot of $\lambda = t_{mt} / t_{su}$ v.s. B_1 ($m_{2i} = 1.0$, $\delta = -1.0$, $P_{spin,i} = 3600\,\mathrm{s}$)

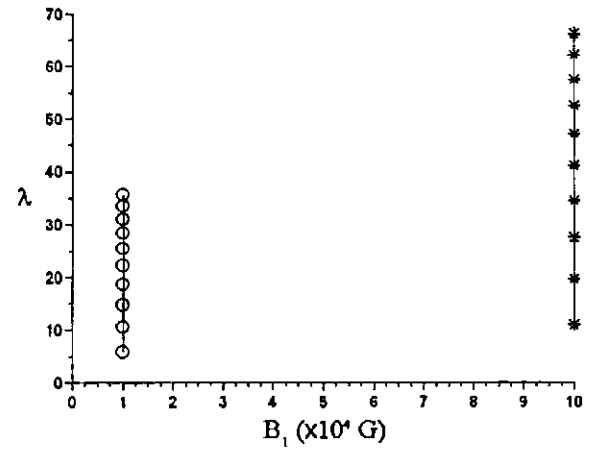

Figure 4.9b: The plot of $\lambda = t_{mt} / t_{su}$ v.s. B_1 ($m_{2i} = 1.0$, $\delta = -1.0$, $P_{spin,i} = 1000\,\mathrm{s}$)

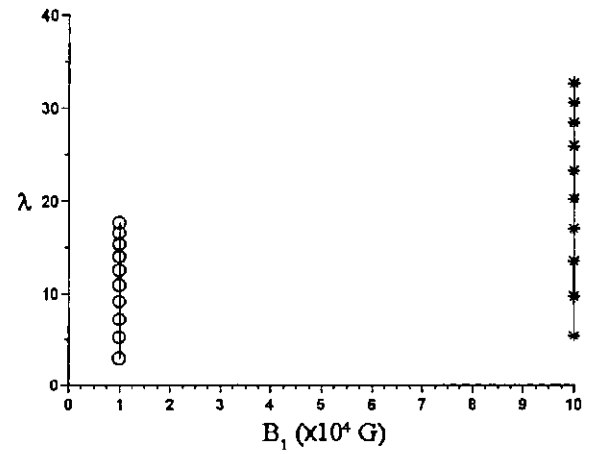

Figure 4.9c: The plot of $\lambda = t_{mt} / t_{su}$ v.s. B_1 ($m_{2i} = 1.0$, $\delta = -1.0$, $P_{spin,i} = 500\,\mathrm{s}$)

It can be seen that for all these various magnetic field values, i.e. $B_1 \sim 10^4$ G, 10^5 G or 10^6 G, the white dwarf is spun-up out of equilibrium, i.e. $x_0 = R_0 / R_c \rightarrow 0$ and $f(x_0) \rightarrow 0$.

From Figs. 4.9 a-c, for various initial periods, it can be seen that the disc spin-up time-scale decreases with increasing magnetic field strength. This can be understood in context of a strong magnetosphere field resulting in an increasing moment arm facilitating angular momentum transport to the compact object from the disc.

This is evident from these figures that $\lambda = t_{mt} / t_{su} >> 1$ for $B_1 > 10^4$ G. This seems to suggest that the spin-up time-scale for $B_1 >> 1$ MG will be unacceptably short, which cast doubt whether the surface field strength of the white dwarf in AE Aqr exceeds $B_1 \sim 1$ MG. Therefore, the model calculations seem to confirm $B_1 \leq \text{few} \times 10^6$ G (see Section 2.4.2 for details), which is believed to be the upper limiting value of the field strength in AE Aqr (e.g. Meintjes & de Jager 2000).

A scenario may be depicted where periods of enhanced run-away mass transfer is followed by a mass transfer at more gentle rate, upon which $x_0 = R_0 / R_c \rightarrow 1$ and $f(x_0) < 0$. This will result in a more significant contribution from the spin-down torque, which may significantly increase the net spin-up time-scale.

It should be emphasized that the lower boundary of the mass transfer time-scale is determined by $q_{crit} \approx 0.73$. This constraint is mainly attributed to the fact that real stars are modelled using idealized fluid models of certain polytropic index $n = 3/2$ (Hjellming & Webbink 1987; King 1988). Real stars may behave differently.

This model calculations readily agree with our conjecture that AE Aqr evolved through a relative brief but violent high mass accretion phase (with $P_{orb} > 9$ hrs) where the white dwarf has been spun-up to periods $P_{spin} \leq 33$ sec, during which period the accretion onto the compact white dwarf readily could have sustained stable nuclear burning. In this phase, AE Aqr could have been an extremely bright X-ray

source, or SSS. The fact that SSS activity is mainly restricted to $P_{orb} > 9$ hrs seems to confirm the notion that SSS activity may be associated with very young evolving IPs or pre-cataclysmic variables.

Chapter 5

Conclusions

It has been shown that the wide binary system and short white dwarf spin period of AE Aqr, i.e. $P_{spin,1} \approx 33\,\mathrm{s}$, is perfectly reconciled with a high mass accretion history of the white dwarf. It has also been suggested that in that phase AE Aqr had been a significant X-ray source (its close proximity of $d \sim 100\,pc$) and possibly even an SSS. This seems to be confirmed by this study, when $P_{orb} \approx 9-18\,\mathrm{hrs}$ and the mass ratio of the binary $q > 1$.

The results presented in this study, albeit somewhat simplistic, showed that the SSS phenomena in AE Aqr (and possibly CVs in general), as expected, is intimately tied to the

i) mass transfer rate from the secondary star, and

ii) the mass accretion rate onto the surface of a white dwarf, presumably in a disc accreting phase. This is however not a requirement for all systems and probably depends on the magnetosphere strength of the white dwarf as well as the orbital separation and mass transfer rate.

These two conditions can be summarized in a single constraint, namely $\gamma \leq \beta \leq 1$.

It has been shown in chapter 3, for the mass ratio $q > 1$ and angular momentum loss $\dot{J} \neq 0$, the Roche lobe will shrink, resulting in the secondary star overflowing its Roche lobe ($R_2 \geq R_{L2}$), thus triggering a run-away mass transfer phase. In other words, for $q > 1$, $R_2 \geq R_{L2}$ resulting in scale height $\delta = (R_{L2} - R_{p2})/H_p \leq 0$.

This is reconciled with the fact that the secondary star of AE Aqr is a somewhat evolved late K4-5 star (e.g. Casares et al. 1996). Since the secondary star had already somewhat evolved, it inflated ($\dot{R}_2 \geq 0$) upon mass loss for $q > 1$, which is amplified by angular momentum loss $\dot{J}_{orb} < 0$, resulting in $\dot{R}_{L2} \leq 0$. This process results in the secondary star probably overflowing its Roche lobe surface, $R_{L2} \leq R_2$, (i.e. $\delta < 0$). This will trigger a run-away mass transfer which will also be associated with enhanced accretion onto the surface of the white dwarf.

Such phenomena will definitely result in interesting observable consequences, especially if it occurs over an extended period of time. The only limiting factor that will determine whether sustained nuclear burning can be achieved is whether the mass accretion exceeds the minimum requirement for stable nuclear burning, and whether it is below the Eddington limit.

For example, Table 4.6 shows that, even for extreme overfilling of the secondary's Roche lobe ($\delta = -2$), the mass transfer rate from the secondary is of the same order as the Eddington limit (i.e. $|\dot{M}_2| \sim \dot{M}_{\rm edd}$). However, for most of the parameters, the average accretion fraction, β, is ≤ 0.5, resulting in the initial mass accretion rate onto WD being less than the Eddington mass accretion rate ($\kappa = \dot{M}_1 / \dot{M}_{\rm edd} < 0.45$ and hence $\dot{M}_{1i} < \dot{M}_{\rm edd}$).

These results are extremely positive, since it shows that the SSS phenomena in AE Aqr can be driven effectively even if the limit where the effectivity of the accretion process onto the surface of the white dwarf $\beta \leq 0.5$. This implies a process of significant mass loss from the binary system, when the secondary star enters a phase

of run-away mass transfer. This may be the result of mass outflow from an accretion disc.

The long orbital period $P_{orb} \sim 9.88\,\mathrm{hr}$ of AE Aqr implies that the binary separation is large enough to accommodate a well-developed accretion disc. The rotation period $P_{spin} \sim 33\,\mathrm{s}$ implies that AE Aqr most possibly evolved through a high mass transfer/ accretion phase, where the white dwarf has been spun-up by accretion torques (e.g. Meintjes 2002), possibly by an accretion disc. This seems to be confirmed by the model calculations performed, which suggest that possible SSS activity may, for AE Aqr, be restricted to orbital periods $P_{orb} \geq 9\,\mathrm{hrs}$. The most positive aspect is that the SSS phenomena can be satisfied significantly below the Eddington limit for all filling factors and for all orbital period $P_{orb} \geq 9\,\mathrm{hrs}$. These seems to confirm the notion that SSS activity being associated with pre-cataclysmic variables, or very young systems with orbital periods $P_{orb} \geq 9\,\mathrm{hrs}$.

Concerning the spin-up history, as the primary star of AE Aqr is a magnetic WD, the deduced results from circular polarization measurements shows the magnetic field strength of the white dwarf $B_1 \sim 10^6$ G (e.g. Cropper 1986; Beskrovnaya et al. 1995; Chanmugam & Frank 1987; Meintjes 2002). In order for the white dwarf to survive, $t_{su} << t_{mt}$ should be avoided; otherwise the white dwarf would be spun-up too fast, obliterating itself eventually under the intense centrifugal forces. Tables (4.1-4.6) show that the disc spin-up time-scale $t_{su} \approx 10^4 - 10^2$ yrs, in contrast to the mass transfer time-scale $t_{mt} \approx 10^6 - 10^4$ yrs. Here, the mass transfer time-scale t_{mt}, for various filling factors, places an upper limit on the allowed duration of the high mass transfer phase. The results (Fig 4.8 a-e) seem to suggest that the spin-up time-scale, rather that the mass transfer time-scale will determine the allowed duration of the run-away mass transfer phase. This is evident from the fact that $t_{su} << t_{mt}$ for most initial conditions. However, these results are in general consistent with earlier findings (Meintjes 2002) predicting a brief but furious mass accretion phase which resulted in a rapid spin-up of the white dwarf to periods of $P_{spin} \sim 33\,\mathrm{sec}$.

To conclude, it has been shown that a relative brief high mass transfer/ accretion phase, where the white dwarf accreted from a well developed disc can indeed explain the peculiar $\chi = P_{spin} / P_{orb} \approx 10^{-3}$ ratio of AE Aqr. Most of the scenarios considered show that in the high mass transfer/ accretion phase, AE Aqr could have been an SSS. This may in fact also apply to other pre-intermediate polar systems, with the exception that white dwarfs with magnetic moment $\mu_{34} \geq 1$ would probably inhibit the development of an accretion disc for a range in orbital periods, preventing too rapid spin-up. However, for significant accretion onto the white dwarf, the SSS conjecture may be satisfied for these systems as well.

Appendix

To streamline the presentation, each $\delta = (R_{L2} - R_{p2})/H_p$, the allowed parameters, satisfying the SSS criteria, are highlighted. Some Tables of our model calculations are displayed in Appendix as the followings:

The results of our model calculations are presented as follows:

$\delta = 2.0$ Table A1

$\delta = 1.0$ Table A2

$\delta = 0$ Table A3

$\delta = -1.0$ Table A4

$\delta = -2.0$ Table A5

The results of $\lambda = t_{ml}/t_{su}$ as a function of $P_{spin,i}$ and B_1 are presented as follows:

$P_{spin,i} = 3600\,\mathrm{s}$, $B_1 = 10^4$ G Table A6

$P_{spin,i} = 1000\,\mathrm{s}$, $B_1 = 10^5$ G Table A7

$P_{spin,i} = 1000\,\mathrm{s}$, $B_1 = 10^4$ G Table A8

$P_{spin,i} = 500\,\mathrm{s}$, $B_1 = 10^5$ G Table A9

$P_{spin,i} = 500\,\mathrm{s}$, $B_1 = 10^4$ G Table A10

M_{2i} ($M_\odot$)	β	M_{1i} ($M_\odot$)	q_i	T_2 (K)	P_{orb} (hr)	$\dot{M}_{edd}$ (10^{20} g s^{-1})	$-\dot{M}_{2i}$ (10^{19} g s^{-1})	$\dot{M}_{1i}$ (10^{18} g s^{-1})	$\dot{M}_{1i(SNB)}$ (10^{18} g s^{-1})	γ	x_0	$f(x_0)$	t_{su} (10^3 yr)	t_{mt} (10^6 yr)
2.0	0	0.87	2.30	10080	18.2	5.44	3.73	0	9.50	0.25			-	
2.0	0.1	0.73	2.73	10080	18.2	6.24	3.73	3.73	7.36	0.20	0.036	0.250	7.69	2.31
1.8	0	0.87	2.07	9330	16.4	5.44	2.70	0	9.50	0.35			-	
1.8	0.1	0.75	2.39	9330	16.4	6.11	2.70	2.70	7.66	0.28	0.037	0.255	10.08	2.73
1.8	0.2	0.64	2.83	9330	16.4	6.99	2.70	5.40	5.96	0.22	0.042	0.269	5.91	2.73
1.6	0	0.87	1.84	8530	14.5	5.44	1.84	0	9.50	0.52			-	
1.6	0.1	0.77	2.07	8530	14.5	5.98	1.84	1.84	7.97	0.43	0.040	0.262	13.86	3.30
1.6	0.2	0.67	2.36	8530	14.5	6.65	1.84	3.69	6.52	0.35	0.042	0.268	8.02	3.30
1.6	0.3	0.58	2.76	8530	14.5	7.53	1.84	5.53	5.18	0.28	0.049	0.290	6.01	3.30
1.4	0	0.87	1.61	7650	12.7	5.44	1.20	0	9.50	0.79			-	
1.4	0.1	0.79	1.76	7650	12.7	5.86	1.20	1.20	8.28	0.69	0.043	0.271	19.89	4.02
1.4	0.2	0.72	1.95	7650	12.7	6.36	1.20	2.40	7.11	0.59	0.042	0.270	11.36	4.02
1.4	0.3	0.64	2.19	7650	12.7	6.96	1.20	3.60	6.00	0.50	0.046	0.282	8.37	4.02
1.4	0.4	0.56	2.48	7650	12.7	7.70	1.20	4.80	4.96	0.41	0.054	0.303	6.86	4.02
1.4	0.5	0.49	2.87	7650	12.7	8.65	1.20	6.01	3.99	0.33	0.066	0.334	6.00	4.02
1.2	0	0.87	1.38	6780	10.9	5.44	0.74	0	9.50	1.3			-	
1.2	0.1	0.81	1.48	6780	10.9	5.75	0.74	0.74	8.59	1.2	0.047	0.284	30.01	4.83
1.2	0.2	0.76	1.59	6780	10.9	6.09	0.74	1.48	7.71	1.0	0.044	0.275	16.95	4.83
1.2	0.3	0.70	1.71	6780	10.9	6.48	0.74	2.21	6.87	0.93	0.045	0.279	12.31	4.83
1.2	0.4	0.64	1.86	6780	10.9	6.93	0.74	2.95	6.05	0.82	0.049	0.288	9.92	4.83
1.2	0.5	0.59	2.04	6780	10.9	7.45	0.74	3.69	5.27	0.71	0.054	0.303	8.48	4.83
1.2	0.6	0.53	2.26	6780	10.9	8.08	0.74	4.43	4.53	0.61	0.062	0.323	7.55	4.83
1.2	0.7	0.48	2.53	6780	10.9	8.84	0.74	5.17	3.83	0.52	0.073	0.348	6.91	4.83
1.2	0.8	0.42	2.87	6780	10.9	9.79	0.74	5.91	3.17	0.43	0.089	0.382	6.48	4.83
1.0	0	0.87	1.15	6030	9.1	5.44	0.43	0	9.50	2.2			-	
1.0	0.1	0.83	1.20	6030	9.1	5.63	0.43	0.43	8.91	2.1	0.052	0.298	47.32	5.34
1.0	0.2	0.80	1.25	6030	9.1	5.84	0.43	0.86	8.33	1.9	0.047	0.283	26.43	5.34
1.0	0.3	0.76	1.31	6030	9.1	6.06	0.43	1.30	7.77	1.8	0.045	0.279	18.96	5.34
1.0	0.4	0.72	1.38	6030	9.1	6.31	0.43	1.73	7.22	1.7	0.046	0.280	15.07	5.34
1.0	0.5	0.69	1.45	6030	9.1	6.57	0.43	2.16	6.68	1.5	0.047	0.284	12.68	5.34
1.0	0.6	0.65	1.54	6030	9.1	6.87	0.43	2.59	6.15	1.4	0.049	0.291	11.07	5.34
1.0	0.7	0.62	1.63	6030	9.1	7.19	0.43	3.02	5.64	1.3	0.053	0.299	9.91	5.34
1.0	0.8	0.58	1.73	6030	9.1	7.55	0.43	3.45	5.15	1.2	0.057	0.310	9.05	5.34
1.0	0.9	0.54	1.85	6030	9.1	7.96	0.43	3.88	4.67	1.1	0.062	0.323	8.39	5.34
1.0	1.0	0.51	1.98	6030	9.1	8.41	0.43	4.32	4.20	0.97	0.068	0.338	7.87	5.34

Table A1: The results of the SSS investigation ($\delta = 2.0$)

M_{2i} ($M_\odot$)	β	M_{1i} ($M_\odot$)	q_i	T_2 (K)	P_{orb} (hr)	$\dot{M}_{edd}$ (10^{20} g s^{-1})	$-\dot{M}_{2i}$ (10^{19} g s^{-1})	$\dot{M}_{1i}$ (10^{18} g s^{-1})	$\dot{M}_{1i(SNB)}$ (10^{18} g s^{-1})	γ	x_0	$f(x_0)$	t_{su} (10^3 yr)	t_{mt} (10^6 yr)
2.0	0	0.87	2.30	10080	18.2	5.44	10.14	0	9.50	0.094			-	
2.0	0.1	0.73	2.73	10080	18.2	6.24	10.14	10.14	7.36	0.073	0.027	0.218	3.24	0.85
1.8	0	0.87	2.07	9330	16.4	5.44	7.33	0	9.50	0.13			-	
1.8	0.1	0.75	2.39	9330	16.4	6.11	7.33	7.33	7.66	0.10	0.028	0.223	4.24	1.00
1.8	0.2	0.64	2.83	9330	16.4	6.99	7.33	14.66	5.96	0.081	0.031	0.235	2.49	1.00
1.6	0	0.87	1.84	8530	14.5	5.44	5.01	0	9.50	0.19			-	
1.6	0.1	0.77	2.07	8530	14.5	5.98	5.01	5.01	7.97	0.16	0.030	0.229	5.83	1.22
1.6	0.2	0.67	2.36	8530	14.5	6.65	5.01	10.02	6.52	0.13	0.031	0.234	3.38	1.22
1.6	0.3	0.58	2.76	8530	14.5	7.53	5.01	15.03	5.18	0.10	0.037	0.254	2.53	1.22
1.4	0	0.87	1.61	7650	12.7	5.44	3.27	0	9.50	0.29			-	
1.4	0.1	0.79	1.76	7650	12.7	5.86	3.27	3.27	8.28	0.25	0.032	0.237	8.37	1.48
1.4	0.2	0.72	1.95	7650	12.7	6.36	3.27	6.53	7.11	0.22	0.032	0.236	4.78	1.48
1.4	0.3	0.64	2.19	7650	12.7	6.96	3.27	9.79	6.00	0.18	0.035	0.247	3.52	1.48
1.4	0.4	0.56	2.48	7650	12.7	7.70	3.27	13.06	4.96	0.15	0.041	0.265	2.89	1.48
1.4	0.5	0.49	2.87	7650	12.7	8.65	3.27	16.32	3.99	0.12	0.050	0.292	2.52	1.48
1.2	0	0.87	1.38	6780	10.9	5.44	2.01	0	9.50	0.47			-	
1.2	0.1	0.81	1.48	6780	10.9	5.75	2.01	2.01	8.59	0.43	0.035	0.248	12.63	1.78
1.2	0.2	0.76	1.59	6780	10.9	6.09	2.01	4.01	7.71	0.38	0.033	0.241	7.13	1.78
1.2	0.3	0.70	1.71	6780	10.9	6.48	2.01	60.2	6.87	0.34	0.034	0.244	5.18	1.78
1.2	0.4	0.64	1.86	6780	10.9	6.93	2.01	8.03	6.05	0.30	0.036	0.252	4.17	1.78
1.2	0.5	0.59	2.04	6780	10.9	7.45	2.01	10.03	5.27	0.26	0.041	0.265	3.57	1.78
1.2	0.6	0.53	2.26	6780	10.9	8.08	2.01	12.04	4.53	0.23	0.046	0.282	3.17	1.78
1.2	0.7	0.48	2.53	6780	10.9	8.84	2.01	14.04	3.83	0.19	0.055	0.305	2.90	1.78
1.2	0.8	0.42	2.87	6780	10.9	9.79	2.01	16.05	3.17	0.16	0.067	0.334	2.72	1.78
1.0	0	0.87	1.15	6030	9.1	5.44	1.17	0	9.50	0.81			-	
1.0	0.1	0.83	1.20	6030	9.1	5.63	1.17	1.17	8.91	0.76	0.039	0.261	19.90	1.96
1.0	0.2	0.80	1.25	6030	9.1	5.84	1.17	2.35	8.33	0.71	0.035	0.247	11.12	1.96
1.0	0.3	0.76	1.31	6030	9.1	6.06	1.17	3.52	7.77	0.66	0.034	0.244	7.98	1.96
1.0	0.4	0.72	1.38	6030	9.1	6.31	1.17	4.69	7.22	0.62	0.034	0.245	6.34	1.96
1.0	0.5	0.69	1.45	6030	9.1	6.57	1.17	5.87	6.68	0.57	0.035	0.249	5.33	1.96
1.0	0.6	0.65	1.54	6030	9.1	6.87	1.17	7.04	6.15	0.52	0.037	0.254	4.66	1.96
1.0	0.7	0.62	1.63	6030	9.1	7.19	1.17	8.21	5.64	0.48	0.040	0.262	4.17	1.96
1.0	0.8	0.58	1.73	6030	9.1	7.55	1.17	9.38	5.15	0.44	0.043	0.271	3.81	1.96
1.0	0.9	0.54	1.85	6030	9.1	7.96	1.17	10.56	4.67	0.40	0.046	0.283	3.53	1.96
1.0	1.0	0.51	1.98	6030	9.1	8.41	1.17	11.73	4.20	0.36	0.051	0.296	3.31	1.96

Table A2: The results of the SSS investigation ($\delta = 1.0$)

M_{2i} (M_Θ)	β	M_{1i} (M_Θ)	q_i	T_2 (K)	P_{orb} (hr)	$\dot{M}_{edd}$ (10^{20} g s^{-1})	$-\dot{M}_{2i}$ (10^{19} g s^{-1})	$\dot{M}_{1i}$ (10^{19} g s^{-1})	$\dot{M}_{1i(SNB)}$ (10^{18} g s^{-1})	γ	x_0	$f(x_0)$	t_{su} (10^3 yr)	t_{mt} (10^5 yr)
2.0	0	0.87	2.30	10080	18.2	5.44	27.56	0	9.50	0.034			-	
2.0	0.1	0.73	2.73	10080	18.2	6.24	27.56	2.76	7.36	0.027	0.020	0.191	1.36	3.13
1.8	0	0.87	2.07	9330	16.4	5.44	19.93	0	9.50	0.048			-	
1.8	0.1	0.75	2.39	9330	16.4	6.11	19.93	1.99	7.66	0.038	0.021	0.195	1.78	3.69
1.8	0.2	0.64	2.83	9330	16.4	6.99	19.93	3.99	5.96	0.030	0.024	0.205	1.05	3.69
1.6	0	0.87	1.84	8530	14.5	5.44	13.62	0	9.50	0.070			-	
1.6	0.1	0.77	2.07	8530	14.5	5.98	13.62	1.36	7.97	0.058	0.022	0.200	2.46	4.47
1.6	0.2	0.67	2.36	8530	14.5	6.65	13.62	2.72	6.52	0.048	0.023	0.205	1.42	4.47
1.6	0.3	0.58	2.76	8530	14.5	7.53	13.62	4.09	5.18	0.038	0.028	0.222	1.06	4.47
1.4	0	0.87	1.61	7650	12.7	5.44	8.87	0	9.50	0.11			-	
1.4	0.1	0.79	1.76	7650	12.7	5.86	8.87	0.89	8.28	0.093	0.024	0.208	3.52	5.44
1.4	0.2	0.72	1.95	7650	12.7	6.36	8.87	1.78	7.11	0.080	0.024	0.207	2.01	5.44
1.4	0.3	0.64	2.19	7650	12.7	6.96	8.87	2.66	6.00	0.068	0.026	0.216	1.48	5.44
1.4	0.4	0.56	2.48	7650	12.7	7.70	8.87	3.55	4.96	0.056	0.030	0.232	1.22	5.44
1.4	0.5	0.49	2.87	7650	12.7	8.65	8.87	4.44	3.99	0.045	0.037	0.255	1.06	5.44
1.2	0	0.87	1.38	6780	10.9	5.44	5.45	0	9.50	0.17			-	
1.2	0.1	0.81	1.48	6780	10.9	5.75	5.45	0.55	8.59	0.16	0.026	0.217	5.31	6.54
1.2	0.2	0.76	1.59	6780	10.9	6.09	5.45	1.09	7.71	0.14	0.025	0.210	3.00	6.54
1.2	0.3	0.70	1.71	6780	10.9	6.48	5.45	1.64	6.87	0.13	0.025	0.213	2.18	6.54
1.2	0.4	0.64	1.86	6780	10.9	6.93	5.45	2.18	6.05	0.11	0.027	0.220	1.76	6.54
1.2	0.5	0.59	2.04	6780	10.9	7.45	5.45	2.73	5.27	0.097	0.030	0.232	1.50	6.54
1.2	0.6	0.53	2.26	6780	10.9	8.08	5.45	3.27	4.53	0.083	0.035	0.247	1.34	6.54
1.2	0.7	0.48	2.53	6780	10.9	8.84	5.45	3.82	3.83	0.070	0.041	0.267	1.22	6.54
1.2	0.8	0.42	2.87	6780	10.9	9.79	5.45	4.36	3.17	0.058	0.050	0.292	1.15	6.54
1.0	0	0.87	1.15	6030	9.1	5.44	3.19	0	9.50	0.30			-	
1.0	0.1	0.83	1.20	6030	9.1	5.63	3.19	0.32	8.91	0.28	0.030	0.228	8.37	7.22
1.0	0.2	0.80	1.25	6030	9.1	5.84	3.19	0.64	8.33	0.26	0.026	0.216	4.68	7.22
1.0	0.3	0.76	1.31	6030	9.1	6.06	3.19	0.96	7.77	0.24	0.026	0.213	3.36	7.22
1.0	0.4	0.72	1.38	6030	9.1	6.31	3.19	1.28	7.22	0.23	0.026	0.214	2.67	7.22
1.0	0.5	0.69	1.45	6030	9.1	6.57	3.19	1.59	6.68	0.21	0.027	0.217	2.25	7.22
1.0	0.6	0.65	1.54	6030	9.1	6.87	3.19	1.91	6.15	0.19	0.028	0.222	1.96	7.22
1.0	0.7	0.62	1.63	6030	9.1	7.19	3.19	2.23	5.64	0.18	0.030	0.229	1.75	7.22
1.0	0.8	0.58	1.73	6030	9.1	7.55	3.19	2.55	5.15	0.16	0.032	0.237	1.60	7.22
1.0	0.9	0.54	1.85	6030	9.1	7.96	3.19	2.87	4.67	0.15	0.035	0.247	1.48	7.22
1.0	1.0	0.51	1.98	6030	9.1	8.41	3.19	3.19	4.20	0.13	0.039	0.259	1.39	7.22

Table A3: The results of the SSS investigation ($\delta = 0$)

M_{2i} (M_Θ)	β	M_{1i} (M_Θ)	q_i	T_2 (K)	P_{orb} (hr)	$\dot{M}_{edd}$ (10^{20} g s^{-1})	$-\dot{M}_{2i}$ (10^{20} g s^{-1})	$\dot{M}_{1i}$ (10^{19} g s^{-1})	$\dot{M}_{1i(SNB)}$ (10^{18} g s^{-1})	γ	x_0	$f(x_0)$	t_{su} (10^2 yr)	t_{mt} (10^5 yr)
2.0	0	0.87	2.30	10080	18.2	5.44	7.49	0	9.50	0.013			-	
2.0	0.1	0.73	2.73	10080	18.2	6.24	7.49	7.49	7.36	0.010	0.015	0.167	5.73	1.15
1.8	0	0.87	2.07	9330	16.4	5.44	5.42	0	9.50	0.018			-	
1.8	0.1	0.75	2.39	9330	16.4	6.11	5.42	5.42	7.66	0.014	0.016	0.170	7.51	1.36
1.8	0.2	0.64	2.83	9330	16.4	6.99	5.42	10.84	5.96	0.011	0.018	0.179	4.40	1.36
1.6	0	0.87	1.84	8530	14.5	5.44	3.70	0	9.50	0.026			-	
1.6	0.1	0.77	2.07	8530	14.5	5.98	3.70	3.70	7.97	0.022	0.017	0.175	10.33	1.65
1.6	0.2	0.67	2.36	8530	14.5	6.65	3.70	7.41	6.52	0.018	0.018	0.179	5.98	1.65
1.6	0.3	0.58	2.76	8530	14.5	7.53	3.70	11.10	5.18	0.014	0.021	0.194	4.47	1.65
1.4	0	0.87	1.61	7650	12.7	5.44	2.41	0	9.50	0.039			-	
1.4	0.1	0.79	1.76	7650	12.7	5.86	2.41	2.41	8.28	0.034	0.018	0.181	14.81	2.00
1.4	0.2	0.72	1.95	7650	12.7	6.36	2.41	4.82	7.11	0.029	0.018	0.181	8.46	2.00
1.4	0.3	0.64	2.19	7650	12.7	6.96	2.41	7.24	6.00	0.025	0.020	0.189	6.23	2.00
1.4	0.4	0.56	2.48	7650	12.7	7.70	2.41	9.65	4.96	0.021	0.023	0.203	5.11	2.00
1.4	0.5	0.49	2.87	7650	12.7	8.65	2.41	12.06	3.99	0.017	0.028	0.223	4.47	2.00
1.2	0	0.87	1.38	6780	10.9	5.44	1.48	0	9.50	0.064			-	
1.2	0.1	0.81	1.48	6780	10.9	5.75	1.48	1.48	8.59	0.058	0.020	0.190	22.35	2.41
1.2	0.2	0.76	1.59	6780	10.9	6.09	1.48	2.97	7.71	0.052	0.019	0.184	12.63	2.41
1.2	0.3	0.70	1.71	6780	10.9	6.48	1.48	4.45	6.87	0.046	0.019	0.186	9.17	2.41
1.2	0.4	0.64	1.86	6780	10.9	6.93	1.48	5.93	6.05	0.041	0.021	0.193	7.39	2.41
1.2	0.5	0.59	2.04	6780	10.9	7.45	1.48	7.41	5.27	0.036	0.023	0.203	6.32	2.41
1.2	0.6	0.53	2.26	6780	10.9	8.08	1.48	8.90	4.53	0.031	0.026	0.216	5.62	2.41
1.2	0.7	0.48	2.53	6780	10.9	8.84	1.48	10.38	3.83	0.026	0.031	0.233	5.14	2.41
1.2	0.8	0.42	2.87	6780	10.9	9.79	1.48	11.86	3.17	0.021	0.038	0.256	4.82	2.41
1.0	0	0.87	1.15	6030	9.1	5.44	0.87	0	9.50	0.11			-	
1.0	0.1	0.83	1.20	6030	9.1	5.63	0.87	0.87	8.91	0.10	0.022	0.200	35.24	2.66
1.0	0.2	0.80	1.25	6030	9.1	5.84	0.87	1.73	8.33	0.096	0.020	0.189	19.69	2.66
1.0	0.3	0.76	1.31	6030	9.1	6.06	0.87	2.60	7.77	0.090	0.019	0.186	14.12	2.66
1.0	0.4	0.72	1.38	6030	9.1	6.31	0.87	3.47	7.22	0.083	0.019	0.187	11.22	2.66
1.0	0.5	0.69	1.45	6030	9.1	6.57	0.87	4.33	6.68	0.077	0.020	0.190	9.45	2.66
1.0	0.6	0.65	1.54	6030	9.1	6.87	0.87	5.20	6.15	0.071	0.021	0.194	8.24	2.66
1.0	0.7	0.62	1.63	6030	9.1	7.19	0.87	6.07	5.64	0.065	0.022	0.200	7.38	2.66
1.0	0.8	0.58	1.73	6030	9.1	7.55	0.87	6.93	5.15	0.059	0.024	0.207	6.74	2.66
1.0	0.9	0.54	1.85	6030	9.1	7.96	0.87	7.80	4.67	0.054	0.026	0.216	6.24	2.66
1.0	1.0	0.51	1.98	6030	9.1	8.41	0.87	8.67	4.20	0.048	0.029	0.226	5.86	2.66

Table A4: The results of the SSS investigation ($\delta = -1.0$)

M_{2i} ($M_\odot$)	β	M_{1i} ($M_\odot$)	q_i	T_2 (K)	P_{orb} (hr)	$\dot{M}_{edd}$ (10^{20} g s^{-1})	$-\dot{M}_{2i}$ (10^{20} g s^{-1})	$\dot{M}_{1i}$ (10^{20} g s^{-1})	$\dot{M}_{1i(SNB)}$ (10^{18} g s^{-1})	γ	x_0	$f(x_0)$	t_{su} (10^2 yr)	t_{mt} (10^4 yr)
2.0	0	0.87	2.30	10080	18.2	5.44	20.37	0	9.50	0.005			-	
2.0	0.1	0.73	2.73	10080	18.2	6.24	20.37	2.04	7.36	0.004	0.011	0.146	2.41	4.23
1.8	0	0.87	2.07	9330	16.4	5.44	14.73	0	9.50	0.006			-	
1.8	0.1	0.75	2.39	9330	16.4	6.11	14.73	1.47	7.66	0.005	0.012	0.149	3.16	4.99
1.8	0.2	0.64	2.83	9330	16.4	6.99	14.73	2.95	5.96	0.004	0.013	0.157	1.85	4.99
1.6	0	0.87	1.84	8530	14.5	5.44	10.06	0	9.50	0.009			-	
1.6	0.1	0.77	2.07	8530	14.5	5.98	10.06	1.01	7.97	0.008	0.013	0.153	4.35	6.05
1.6	0.2	0.67	2.36	8530	14.5	6.65	10.06	2.01	6.52	0.007	0.013	0.157	2.51	6.05
1.6	0.3	0.58	2.76	8530	14.5	7.53	10.06	3.02	5.18	0.005	0.016	0.170	1.88	6.05
1.4	0	0.87	1.61	7650	12.7	5.44	6.56	0	9.50	0.014			-	
1.4	0.1	0.79	1.76	7650	12.7	5.86	6.56	0.66	8.28	0.013	0.014	0.159	6.23	7.36
1.4	0.2	0.72	1.95	7650	12.7	6.36	6.56	1.31	7.11	0.011	0.013	0.158	3.56	7.36
1.4	0.3	0.64	2.19	7650	12.7	6.96	6.56	1.97	6.00	0.009	0.015	0.165	2.62	7.36
1.4	0.4	0.56	2.48	7650	12.7	7.70	6.56	2.62	4.96	0.008	0.017	0.177	2.15	7.36
1.4	0.5	0.49	2.87	7650	12.7	8.65	6.56	3.28	3.99	0.006	0.021	0.195	1.88	7.36
1.2	0	0.87	1.38	6780	10.9	5.44	4.03	0	9.50	0.024			-	
1.2	0.1	0.81	1.48	6780	10.9	5.75	4.03	0.40	8.59	0.021	0.015	0.166	9.41	8.85
1.2	0.2	0.76	1.59	6780	10.9	6.09	4.03	0.81	7.71	0.019	0.014	0.161	5.31	8.85
1.2	0.3	0.70	1.71	6780	10.9	6.48	4.03	1.21	6.87	0.017	0.014	0.163	3.87	8.85
1.2	0.4	0.64	1.86	6780	10.9	6.93	4.03	1.61	6.05	0.015	0.015	0.169	3.11	8.85
1.2	0.5	0.59	2.04	6780	10.9	7.45	4.03	2.02	5.27	0.013	0.017	0.177	2.66	8.85
1.2	0.6	0.53	2.26	6780	10.9	8.08	4.03	2.42	4.53	0.011	0.020	0.189	2.36	8.85
1.2	0.7	0.48	2.53	6780	10.9	8.84	4.03	2.82	3.83	0.010	0.023	0.204	2.16	8.85
1.2	0.8	0.42	2.87	6780	10.9	9.79	4.03	3.22	3.17	0.008	0.028	0.224	2.03	8.85
1.0	0	0.87	1.15	6030	9.1	5.44	2.36	0	9.50	0.040			-	
1.0	0.1	0.83	1.20	6030	9.1	5.63	2.36	0.24	8.91	0.038	0.017	0.174	14.83	9.78
1.0	0.2	0.80	1.25	6030	9.1	5.84	2.36	0.47	8.33	0.035	0.015	0.165	8.28	9.78
1.0	0.3	0.76	1.31	6030	9.1	6.06	2.36	0.71	7.77	0.033	0.014	0.163	5.94	9.78
1.0	0.4	0.72	1.38	6030	9.1	6.31	2.36	0.94	7.22	0.031	0.015	0.164	4.72	9.78
1.0	0.5	0.69	1.45	6030	9.1	6.57	2.36	1.18	6.68	0.028	0.015	0.166	3.97	9.78
1.0	0.6	0.65	1.54	6030	9.1	6.87	2.36	1.41	6.15	0.026	0.016	0.170	3.47	9.78
1.0	0.7	0.62	1.63	6030	9.1	7.19	2.36	1.65	5.64	0.024	0.017	0.175	3.11	9.78
1.0	0.8	0.58	1.73	6030	9.1	7.55	2.36	1.89	5.15	0.022	0.018	0.181	2.84	9.78
1.0	0.9	0.54	1.85	6030	9.1	7.96	2.36	2.12	4.67	0.020	0.020	0.189	2.63	9.78
1.0	1.0	0.51	1.98	6030	9.1	8.41	2.36	2.36	4.20	0.018	0.022	0.198	2.47	9.78

Table A5: The results of the SSS investigation ($\delta = -2.0$)

M_{2i} ($M_\odot$)	β	M_{1i} ($M_\odot$)	q_i	T_2 (K)	P_{orb} (hr)	$\dot{M}_{edd}$ (10^{20} g s^{-1})	$-\dot{M}_{2i}$ (10^{20} g s^{-1})	$\dot{M}_{1i}$ (10^{20} g s^{-1})	$\dot{M}_{1i(SNB)}$ (10^{18} g s^{-1})	γ	x_0	$f(x_0)$	t_{su} (10^2 yr)	t_{mt} (10^4 yr)
2.0	0	0.87	2.30	10080	18.2	5.44	20.37	0	9.50	0.005			-	
2.0	0.1	0.73	2.73	10080	18.2	6.24	20.37	2.04	7.36	0.004	0.011	0.146	2.41	4.23
1.8	0	0.87	2.07	9330	16.4	5.44	14.73	0	9.50	0.006			-	
1.8	0.1	0.75	2.39	9330	16.4	6.11	14.73	1.47	7.66	0.005	0.012	0.149	3.16	4.99
1.8	0.2	0.64	2.83	9330	16.4	6.99	14.73	2.95	5.96	0.004	0.013	0.157	1.85	4.99
1.6	0	0.87	1.84	8530	14.5	5.44	10.06	0	9.50	0.009			-	
1.6	0.1	0.77	2.07	8530	14.5	5.98	10.06	1.01	7.97	0.008	0.013	0.153	4.35	6.05
1.6	0.2	0.67	2.36	8530	14.5	6.65	10.06	2.01	6.52	0.007	0.013	0.157	2.51	6.05
1.6	0.3	0.58	2.76	8530	14.5	7.53	10.06	3.02	5.18	0.005	0.016	0.170	1.88	6.05
1.4	0	0.87	1.61	7650	12.7	5.44	6.56	0	9.50	0.014			-	
1.4	0.1	0.79	1.76	7650	12.7	5.86	6.56	0.66	8.28	0.013	0.014	0.159	6.23	7.36
1.4	0.2	0.72	1.95	7650	12.7	6.36	6.56	1.31	7.11	0.011	0.013	0.158	3.56	7.36
1.4	0.3	0.64	2.19	7650	12.7	6.96	6.56	1.97	6.00	0.009	0.015	0.165	2.62	7.36
1.4	0.4	0.56	2.48	7650	12.7	7.70	6.56	2.62	4.96	0.008	0.017	0.177	2.15	7.36
1.4	0.5	0.49	2.87	7650	12.7	8.65	6.56	3.28	3.99	0.006	0.021	0.195	1.88	7.36
1.2	0	0.87	1.38	6780	10.9	5.44	4.03	0	9.50	0.024			-	
1.2	0.1	0.81	1.48	6780	10.9	5.75	4.03	0.40	8.59	0.021	0.015	0.166	9.41	8.85
1.2	0.2	0.76	1.59	6780	10.9	6.09	4.03	0.81	7.71	0.019	0.014	0.161	5.31	8.85
1.2	0.3	0.70	1.71	6780	10.9	6.48	4.03	1.21	6.87	0.017	0.014	0.163	3.87	8.85
1.2	0.4	0.64	1.86	6780	10.9	6.93	4.03	1.61	6.05	0.015	0.015	0.169	3.11	8.85
1.2	0.5	0.59	2.04	6780	10.9	7.45	4.03	2.02	5.27	0.013	0.017	0.177	2.66	8.85
1.2	0.6	0.53	2.26	6780	10.9	8.08	4.03	2.42	4.53	0.011	0.020	0.189	2.36	8.85
1.2	0.7	0.48	2.53	6780	10.9	8.84	4.03	2.82	3.83	0.010	0.023	0.204	2.16	8.85
1.2	0.8	0.42	2.87	6780	10.9	9.79	4.03	3.22	3.17	0.008	0.028	0.224	2.03	8.85
1.0	0	0.87	1.15	6030	9.1	5.44	2.36	0	9.50	0.040			-	
1.0	0.1	0.83	1.20	6030	9.1	5.63	2.36	0.24	8.91	0.038	0.017	0.174	14.83	9.78
1.0	0.2	0.80	1.25	6030	9.1	5.84	2.36	0.47	8.33	0.035	0.015	0.165	8.28	9.78
1.0	0.3	0.76	1.31	6030	9.1	6.06	2.36	0.71	7.77	0.033	0.014	0.163	5.94	9.78
1.0	0.4	0.72	1.38	6030	9.1	6.31	2.36	0.94	7.22	0.031	0.015	0.164	4.72	9.78
1.0	0.5	0.69	1.45	6030	9.1	6.57	2.36	1.18	6.68	0.028	0.015	0.166	3.97	9.78
1.0	0.6	0.65	1.54	6030	9.1	6.87	2.36	1.41	6.15	0.026	0.016	0.170	3.47	9.78
1.0	0.7	0.62	1.63	6030	9.1	7.19	2.36	1.65	5.64	0.024	0.017	0.175	3.11	9.78
1.0	0.8	0.58	1.73	6030	9.1	7.55	2.36	1.89	5.15	0.022	0.018	0.181	2.84	9.78
1.0	0.9	0.54	1.85	6030	9.1	7.96	2.36	2.12	4.67	0.020	0.020	0.189	2.63	9.78
1.0	1.0	0.51	1.98	6030	9.1	8.41	2.36	2.36	4.20	0.018	0.022	0.198	2.47	9.78

Table A5: The results of the SSS investigation ($\delta = -2.0$)

β	M_{1i} ($M_\odot$)	q_i	$\dot{M}_{edd}$ (10^{20} g s^{-1})	$-\dot{M}_{2i}$ (10^{20} g s^{-1})	$\dot{M}_{1i}$ (10^{19} g s^{-1})	$\dot{M}_{1i(SNB)}$ (10^{18} g s^{-1})	γ	x_0	$f(x_0)$	t_{su} (10^3 yr)	t_{mt} (10^5 yr)	λ
0	0.87	1.15	5.44	0.87	0	9.50	0.11			-		
0.1	0.83	1.20	5.63	0.87	0.87	8.91	0.10	0.002	0.058	12.07	2.66	22.0
0.2	0.80	1.25	5.84	0.87	1.73	8.33	0.096	0.001	0.055	6.74	2.66	39.4
0.3	0.76	1.31	6.06	0.87	2.60	7.77	0.090	0.001	0.054	4.83	2.66	55.0
0.4	0.72	1.38	6.31	0.87	3.47	7.22	0.083	0.001	0.055	3.84	2.66	69.2
0.5	0.69	1.45	6.57	0.87	4.33	6.68	0.077	0.001	0.056	3.23	2.66	82.2
0.6	0.65	1.54	6.87	0.87	5.20	6.15	0.071	0.002	0.057	2.82	2.66	94.2
0.7	0.62	1.63	7.19	0.87	6.07	5.64	0.065	0.002	0.058	2.53	2.66	105.1
0.8	0.58	1.73	7.55	0.87	6.93	5.15	0.059	0.002	0.061	2.31	2.66	115.1
0.9	0.54	1.85	7.96	0.87	7.80	4.67	0.054	0.002	0.063	2.14	2.66	124.2
1.0	0.51	1.98	8.41	0.87	8.67	4.20	0.048	0.002	0.066	2.01	2.66	132.2

Table A6: The time-scale ratio $\lambda = t_{mt} / t_{su}$ for $m_{2i} = 1.0$, $\delta = -1.0$, $P_{spin,i} = 3600$ s and $B_i = 10^4$ G

β	M_{1i} ($M_\odot$)	q_i	$\dot{M}_{edd}$ (10^{20} g s^{-1})	$-\dot{M}_{2i}$ (10^{20} g s^{-1})	$\dot{M}_{1i}$ (10^{19} g s^{-1})	$\dot{M}_{1i(SNB)}$ (10^{18} g s^{-1})	γ	x_0	$f(x_0)$	t_{su} (10^3 yr)	t_{mt} (10^5 yr)	λ
0	0.87	1.15	5.44	0.87	0	9.50	0.11			-		
0.1	0.83	1.20	5.63	0.87	0.87	8.91	0.10	0.014	0.161	24.15	2.66	11.0
0.2	0.80	1.25	5.84	0.87	1.73	8.33	0.096	0.012	0.152	13.49	2.66	19.7
0.3	0.76	1.31	6.06	0.87	2.60	7.77	0.090	0.012	0.150	9.68	2.66	27.5
0.4	0.72	1.38	6.31	0.87	3.47	7.22	0.083	0.012	0.151	7.69	2.66	34.5
0.5	0.69	1.45	6.57	0.87	4.33	6.68	0.077	0.013	0.153	6.47	2.66	41.1
0.6	0.65	1.54	6.87	0.87	5.20	6.15	0.071	0.013	0.156	5.65	2.66	47.0
0.7	0.62	1.63	7.19	0.87	6.07	5.64	0.065	0.014	0.161	5.06	2.66	52.5
0.8	0.58	1.73	7.55	0.87	6.93	5.15	0.059	0.015	0.167	4.62	2.66	57.5
0.9	0.54	1.85	7.96	0.87	7.80	4.67	0.054	0.017	0.174	4.28	2.66	62.1
1.0	0.51	1.98	8.41	0.87	8.67	4.20	0.048	0.018	0.182	4.02	2.66	66.1

Table A7: The time-scale ratio $\lambda = t_{mt} / t_{su}$ for $m_{2i} = 1.0$, $\delta = -1.0$, $P_{spin,i} = 1000$ s and $B_i = 10^5$ G

β	M_{1i} ($M_\odot$)	q_i	$\dot{M}_{edd}$ (10^{20} g s^{-1})	$-\dot{M}_{2i}$ (10^{20} g s^{-1})	$\dot{M}_{1i}$ (10^{19} g s^{-1})	$\dot{M}_{1i(SNB)}$ (10^{18} g s^{-1})	γ	x_0	$f(x_0)$	t_{su} (10^4 yr)	t_{mt} (10^5 yr)	λ
0	0.87	1.15	5.44	0.87	0	9.50	0.11			-		
0.1	0.83	1.20	5.63	0.87	0.87	8.91	0.10	0.004	0.087	4.47	2.66	5.9
0.2	0.80	1.25	5.84	0.87	1.73	8.33	0.096	0.003	0.082	2.50	2.66	10.6
0.3	0.76	1.31	6.06	0.87	2.60	7.77	0.090	0.003	0.081	1.79	2.66	14.8
0.4	0.72	1.38	6.31	0.87	3.47	7.22	0.083	0.003	0.081	1.42	2.66	18.7
0.5	0.69	1.45	6.57	0.87	4.33	6.68	0.077	0.003	0.083	1.20	2.66	22.2
0.6	0.65	1.54	6.87	0.87	5.20	6.15	0.071	0.004	0.085	1.05	2.66	25.4
0.7	0.62	1.63	7.19	0.87	6.07	5.64	0.065	0.004	0.087	0.94	2.66	28.4
0.8	0.58	1.73	7.55	0.87	6.93	5.15	0.059	0.004	0.090	0.86	2.66	31.1
0.9	0.54	1.85	7.96	0.87	7.80	4.67	0.054	0.004	0.094	0.79	2.66	33.5
1.0	0.51	1.98	8.41	0.87	8.67	4.20	0.048	0.005	0.098	0.74	2.66	35.7

Table A8: The time-scale ratio $\lambda = t_{mt}/t_{su}$ for $m_{2i} = 1.0$, $\delta = -1.0$, $P_{spin,i} = 1000$ s and $B_1 = 10^4$ G

β	M_{1i} ($M_\odot$)	q_i	$\dot{M}_{edd}$ (10^{20} g s^{-1})	$-\dot{M}_{2i}$ (10^{20} g s^{-1})	$\dot{M}_{1i}$ (10^{19} g s^{-1})	$\dot{M}_{1i(SNB)}$ (10^{18} g s^{-1})	γ	x_0	$f(x_0)$	t_{su} (10^3 yr)	t_{mt} (10^5 yr)	λ
0	0.87	1.15	5.44	0.87	0	9.50	0.11			-		
0.1	0.83	1.20	5.63	0.87	0.87	8.91	0.10	0.022	0.200	48.98	2.66	5.4
0.2	0.80	1.25	5.84	0.87	1.73	8.33	0.096	0.020	0.189	27.36	2.66	9.7
0.3	0.76	1.31	6.06	0.87	2.60	7.77	0.090	0.019	0.186	19.63	2.66	13.5
0.4	0.72	1.38	6.31	0.87	3.47	7.22	0.083	0.019	0.187	15.60	2.66	17.0
0.5	0.69	1.45	6.57	0.87	4.33	6.68	0.077	0.020	0.190	13.13	2.66	20.2
0.6	0.65	1.54	6.87	0.87	5.20	6.15	0.071	0.021	0.194	11.46	2.66	23.2
0.7	0.62	1.63	7.19	0.87	6.07	5.64	0.065	0.022	0.200	10.26	2.66	25.9
0.8	0.58	1.73	7.55	0.87	6.93	5.15	0.059	0.024	0.207	9.37	2.66	28.4
0.9	0.54	1.85	7.96	0.87	7.80	4.67	0.054	0.026	0.216	8.68	2.66	30.6
1.0	0.51	1.98	8.41	0.87	8.67	4.20	0.048	0.029	0.226	8.15	2.66	32.6

Table A9: The time-scale ratio $\lambda = t_{mt}/t_{su}$ for $m_{2i} = 1.0$, $\delta = -1.0$, $P_{spin,i} = 500$ s and $B_1 = 10^5$ G

β	M_{1i} ($M_\odot$)	q_i	$\dot{M}_{edd}$ (10^{20} g s^{-1})	$-\dot{M}_{2i}$ (10^{20} g s^{-1})	$\dot{M}_{1i}$ (10^{19} g s^{-1})	$\dot{M}_{1i(SNB)}$ (10^{18} g s^{-1})	γ	x_0	$f(x_0)$	t_{su} (10^4 yr)	t_{mt} (10^5 yr)	λ
0	0.87	1.15	5.44	0.87	0	9.50	0.11			-		
0.1	0.83	1.20	5.63	0.87	0.87	8.91	0.10	0.006	0.108	9.08	2.66	2.9
0.2	0.80	1.25	5.84	0.87	1.73	8.33	0.096	0.005	0.102	5.07	2.66	5.2
0.3	0.76	1.31	6.06	0.87	2.60	7.77	0.090	0.005	0.101	3.64	2.66	7.3
0.4	0.72	1.38	6.31	0.87	3.47	7.22	0.083	0.005	0.101	2.89	2.66	9.2
0.5	0.69	1.45	6.57	0.87	4.33	6.68	0.077	0.005	0.103	2.43	2.66	10.9
0.6	0.65	1.54	6.87	0.87	5.20	6.15	0.071	0.006	0.105	2.12	2.66	12.5
0.7	0.62	1.63	7.19	0.87	6.07	5.64	0.065	0.006	0.108	1.90	2.66	14.0
0.8	0.58	1.73	7.55	0.87	6.93	5.15	0.059	0.006	0.112	1.74	2.66	15.3
0.9	0.54	1.85	7.96	0.87	7.80	4.67	0.054	0.007	0.116	1.61	2.66	16.5
1.0	0.51	1.98	8.41	0.87	8.67	4.20	0.048	0.008	0.122	1.51	2.66	17.6

Table A10: The time-scale ratio $\lambda = t_{mt}/t_{su}$ for $m_{2i} = 1.0$, $\delta = -1.0$, $P_{spin,i} = 500$ s and $B_1 = 10^4$ G

Bibliography

[1] Abada-Simon M., Bastian T.S., Bookbinder J.A., Aubier M., Bromage G., Dulk G.A. & Leacheux A. 1995, LNP, 454, 268

[2] Abada-Simon M., Bastian T.S., Horne K. & Bookbinder J.A. 1995a, in Buckley D.A.H., Warner B., eds, ASP Conf. Ser. Vol. 85. Proc. Cape Workshop on Magnetic Cataclysmic Variables. Astron Soc. Pac., San Francisco, p.355

[3] Abada-Simon M., Lecacheux A., Bastian T.S., Bookbinder J.A. & Dulk G.A. 1993, ApJ, 406, 692

[4] Abada-Simon M., Mouchet M., Aubier M., Barrett P., de Jager O.C., de Martino D. & Ramsay G. 1998, in ESA SP-427, Proc. The Universe as seen by ISO. ESA, Paris, p.257

[5] Bastian T.S. , Dulk G.A. & Chanmugam G. 1988, ApJ, 324, 431

[6] Bath G.T., Evans W.D. & Pringle J.E. 1974, MNRAS, 166, 113

[7] Beardmore A.P., Done C., Osborne J.P. & Ishida M. 1995, MNRAS, 272, 749

[8] Beardmore A.P. & Osborne J.P. 1997, MNRAS, 290, 145

[9] Beskrovnaya N.G., Ikhsanov N.R., Bruch A. & Shakhovskoy N.M. 1995, in Buckley D.A.H., Warner B., eds, ASP Conf. Ser. Vol. 85. Proc. Cape Workshop on Magnetic Cataclysmic Variables. Astron Soc. Pac., San Francisco, p.364

[10] Beuermann K. 1987, Astrophys. Sp. Sci., 131, 625

[11] Beuermann K. 1988a, Adv. Sp. Res., 8, 283

[12] Beuermann K. 1988, High Energy Astronomy and Astrophysics, India University Press

[13] Beuermann K., Thomas H.-C. & Pietsch W. 1991, A&A, 246, L36

[14] Bookbinder J.A. & Lamb D.Q. 1987, ApJ, 323, L131

[15] Bowden et al. 1992, Astropart. Phys, 1, 47

[16] Bruch A. 1991, A&A, 251, 59

[17] Buckley D.A.H., Haberl F., Motch C., Pollard K., Schwarzenberg-Czemy A., Sekiguchi K. 1997, MNRAS, 287, 117

[18] Campbell C.G. 1997, Magnetohydrodynasmics in Binary Stars, Kluwer, Dordrecht

[19] Casares J., Mouchet M., Martinez-Pais I.G. & Harlaftis E.T. 1996, MNRAS, 282, 182

[20] Chanmugam G. & Frank J. 1987, ApJ, 320, 746

[21] Chanmugam G. & Ray A. 1984, ApJ, 285, 252

[22] Copeland H., Jensen J.O. & Jorgensen H.E. 1970, A&A, 5, 12

[23] Cowley A.P., Schmidtke P.C., Crampton D. & Hutchings J.B. 1990, ApJ, 350, 288

[24] Crawford J.A. & Kraft R.P. 1956, ApJ, 123, 44

[25] Cropper M. 1986, MNRAS, 222, 225

[26] Cropper M. 1990, SSRv, 54, 195

[27] D'Antona F., Mazzitelli I. & Ritter H. 1989, A&A, 225, 391

[28] de Jager O.C. 1994, ApJ, 90, 775

[29] de Jager O.C. 1995, in Buckley D.A.H., Warner B., eds, ASP Conf. Ser. Vol. 85, Proc. Cape Workshop on Magnetic Cataclysmic Variables. Astron Soc. Pac., San Francisco, p.373

[30] de Jager O.C. & Meintjes P.J. 1993, A&A, 268, L1

[31] de Jager O.C., Meintjes P.J., O'Donoghue D. & Robinson A.L. 1994, MNRAS, 267,577

[32] Done C., Osborne J.P. & Beardmore A.P. 1995, MNRAS, 276, 483

[33] Eggleton P.P. 1983, ApJ, 268, 368

[34] Eracleous M., Horne K., Robinson E.L., Zhang E.H., Marsh T.R. & Wood J. 1994, ApJ, 433, 313

[35] Eracleous M. & Horne K. 1996, ApJ, 471, 427

[36] Eracleous M., Patterson J. & Halpern J. 1991, ApJ, 370, 330

[37] Frank J., King A.R. & Lasota J.P. 1988, A&A, 193, 113

[38] Frank J., King A. R. & Raine D. 1992, Accretion Power in Astrophysics, Cambridge Univ. Press, Cambridge

[39] Frank J., King A. R. & Raine D. 2002, Accretion Power in Astrophysics, Cambridge Univ. Press, Cambridge

[40] Gansicke B.T., Beuermann K. & de Martino D. 1995, A&A, 303, 127

[41] Ghosh P. & Lamb F.K. 1978, ApJ, 223, L83

[42] Ghosh P. & Lamb F.K. 1979 a, ApJ, 232, 259

[43] Ghosh P. & Lamb F.K. 1979 b, ApJ, 234, 296

[44] Greiner J., Hasinger G. & Kahabka P. 1991, A&A, 246, L17

[45] Greiner J. 2000, NewA, 5, 137

[46] Haberl F. & Motch C. 1995, A&A, 297, L37

[47] Hamada T. & Salpeter E.E. 1961, ApJ, 134, 683

[48] Heise J., van Teeseling A. & Kahabka P. 1994, A&A, 288, L45

[49] Hellier C. 2001, Cataclysmic variable stars: how and why they vary, Springer-Praxis Publishing, Chichester

[50] Hjellming M.S. & Webbink R.E. 1987, ApJ, 318, 794

[51] Hjellming M.S., 1989, PhD thesis, Univ. Illinois

[52] Iben I. & Tutukov A.V. 1993, ApJ, 418, 343

[53] Ikhsanov N.R. 1997, A&A, 325, 1045

[54] Ikhsanov N.R. 1998, A&A, 338, 521

[55] Ikhsanov N.R. 1999, A&A, 347, 915

[56] Ikhsanov N.R. 2000, A&A, 358, 201

[57] Jackson J.D. 1975, Classical Electrodynamics, John Wiley & Sons Inc., New York

[58] Joy A.H. 1954, ApJ, 120, 377

[59] Kahabka P. & van den Heuvel, E.P.J., 1997, ARA&A, 35, 69

[60] King A.R. 1988, QJRAS, 29, 1

[61] King A.R. 1993, MNRAS, 261, 144

[62] King A.R. & Lasota J.P. 1991, ApJ, 378, 674

[63] King A.R., Schenker K., Kolb U. & Davies M.B. 2001, MNRAS, 321, 327

[64] Kippenhann R. & Weigert A. 1990, Stellar Structure and Evolution, Springer-Verlag Berlin Heidelberg, New York

[65] Kopal Z. 1959, Close Binary Systems, Chapman & Hall, London

[66] Kraft R.P., Mathews J. & Greenstein J.L. 1962, ApJ, 136, 312

[67] Kuijpers J.P. & Pringle J.E. 1982, A&A, 114, L4

[68] Kuijpers J.P., Fletcher L., Abada-Simon M., Horne K., Raadu M.A., Ramsay G. & Steeghs D. 1997, A&A, 322, 242

[69] Lamb D.Q. & Patterson J. 1983, in M. Livio and G. Shaviv (eds.), Cataclysmic Variables and Related Object', Proc. IAU Colloq. 72, 229

[70] Landau L.D. & Lifshitz E.M. 1975, The Classical Theory of Fields, 4th ed., Pergaman Press, Oxford, New York

[71] Long K., Helfang D.J. & Grabelsky D.A. 1981, ApJ, 248, 925

[72] Lubow S.H. & Shu F.H. 1975, ApJ, 198, 383

[73] Meintjes P. J. 1992, PhD thesis, PU for CHE, Potchefstroom

[74] Meintjes P. J. 2002, MNRAS, 336, 265

[75] Meintjes P. J. 2004, MNRAS, 352, 416

[76] Meintjes P.J., Raubenheimer B.C., de Jager O.C., Brink C., Nel H.I., North A.R., van Urk G. & Visser B. 1992, ApJ, 401, 325

[77] Meintjes P.J., de Jager O.C., Raubenheimer B.C., Nel H.I., North A.R., Buckley D.A.H. & Koen C. 1994, ApJ, 434, 292

[78] Meintjes P. J. & de Jager O.C. 1995, in Buckley D.A.H., Warner B., eds, ASP Conf. Ser. Vol. 85, Proc. Cape Workshop on Magnetic Cataclysmic Variables, Astron Soc. San Francisco, p.396

[79] Meintjes P. J. & de Jager O.C. 2000, MNRAS, 311, 611

[80] Mestel L., 1967, MSRSL, 55, 351

[81] Mestel L. 1968, MNRAS, 138, 359

[82] Mestel L. & Spruit H. C. 1987, MNRAS, 226, 57

[83] Morton D. 1960, ApJ, 132, 146

[84] Meyer F. & Meyer-Hofmeister E. 1983, A&A, 121, 29

[85] Okamoto I. 1974, MNRAS, 166, 683

[86] Paczynski B. 1971, ARA&A, 9, 183

[87] Pakull M.W., Ilovaisky S.A. & Chevalier C. 1985, Space Sci. Rev., 40, 229

[88] Pakull M.W., Beuermann K., Van der Klis M. & Van Paradijs J. 1988, A&A, 203, L27

[89] Patterson J. 1979, ApJ, 234, 978

[90] Patterson J. 1994, PASP, 106, 209

[91] Pearson K., Horne K. & Skidmore W. 2003, MNRAS, 338, 1067

[92] Plavec M., Ulrich R.K. & Polidan S. 1973, PASP, 85, 769

[93] Pnuman G.W. & Kopp R.A. 1971, Sol. Phys., 18, 258

[94] Prialnik D. 1986, ApJ, 310, 222

[95] Priest E.R. 1981, in Priest E.R. ed., Solar Flare Magnetohydrodynamics, Gordon & Breach, New York, p.139

[96] Pringle J.E. 1985, Interacting Binary Stars, eds. J.E. Pringle, R.A. Wade, Cambridge University Press, Cambridge

[97] Rappaport S., DiStefano R. & Smith J. 1994, ApJ, 426, 692

[98] Reinsch K. & Beuermann K. 1994, A&A, 282, 493

[99] Ritter H. 1988, A&A, 202, 93

[100] Sakurai T. 1985, A&A, 152, 121

[101] Schenker K., King A., Klob G., Wynn G. & Zhang Z. 2002, MNRAS, 337, 1105

[102] Schmidt G.D., Liebert J. & Stockman H.S. 1995, ApJ, 441, 414

[103] Schmidt G.D., Szkody P., Smith P.S., Silber A., Tovmassian G., Hoard D.W., Gansicke B.T. & de Martino D. 1996, ApJ, 473, 483

[104] Schmidt G.D. 1999, ASP Conf., 157, 207

[105] Shakura N.I. & Sunyaev R.A. 1973, A&A, 24, 337

[106] Skumanich A. 1972, ApJ, 171, 565

[107] Smale, A.P., Corbet R.H.D., Charles P.A., Ilovaisky S.A., Mason K.O., Motch C., Mukai K., Naylor T., Parmar A.N., van der Klis M. & van Paradijs J. 1988, MNRAS, 233, 51

[108] Stockman H.S., Schmidt G.D., Berriman G., Liebert J., Moore R.L. & Wickramasinghe D.T. 1992, ApJ, 401, 628

[109] Tanzi E. G., Chincarini G. & Tarenghi M. 1981, PASP, 93, 68

[110] Trumper J., Hasinger G., Aschenbach B., Brauninger H., Briel U.G., Burkert W., Fink H., Pfeffermann E., Pietsch W., Predehl P., Schmitt J.H., Voges W., Zimmermann U. & Beuermann K. 1991, Nat, 349, 579

[111] Van den Heuvel E., Bhattacharya D., Nomoto K. & Rappaport S. 1992, A&A, 262, 97

[112] Verbunt F. 1982, SSRv, 32, 379

[113] Verbunt F. 1993, ARA&A, 31, 93

[114] Verbunt F. & Zwaan C. 1981, A&A, 100, L7

[115] Wade R.A. 1982, AJ, 87, 1558

[116] Wang Y.M. 1987, A&A, 183, 257

[117] Warner B., 1995, Cataclysmic Variable Stars, Cambridge Univ. Press, Cambridge

[118] Warner B. & Wickramasinghe D.T. 1991, MNRAS, 248, 370

[119] Watson M.G. 1986, in Physics pf Accretion onto Compact Objects, eds. K.O. Mason, M.G. Watson & N.E. White, Springer-Verlag, Berlin, p.97

[120] Webbink R.F. 1977, ApJ, 211, 486

[121] Weber E.J. & Davis L.J. 1967, ApJ, 148, 217

[122] Welsh W., Horne K. & Gomer R. 1993, ApJ, 410, L39

[123] Welsh W., Horne K. & Gomer R. 1995, MNRAS, 275, 649

[124] Welsh W., Horne K. & Gomer R. 1998, MNRAS, 298, 285

[125] Welsh W., Horne K. & Oke B. 1993, ApJ, 406, 229

[126] Wickramasinghe D.T., Wu K. & Ferrario L. 1991, MNRAS, 249, 460

[127] Wynn G.A. & King A.R. 1995, MNRAS, 275, 9

[128] Wynn G.A., King A.R. & Horne K. 1995, in Buckley D.A.H., Warner B., eds. ASP Conf. Ser. Vol. 85, Proc. Cape Workshop on Magnetic Cataclysmic Variables, Astron Soc. Pacific., San Francisco, p.196

[129] Wynn G.A., King A.R. & Horne K. 1997, MNRAS, 286, 436

[130] Zinner E. 1938, Astron. Nach., 265, 345